Vertical transport methods for Deep Sea Mining

S.A. Schulte

Delft University of Technology
Section of Dredging Engineering

version 2.0 June 19, 2013

Vertical transport methods for Deep Sea Mining

Author:
Sebastiaan Schulte

Thesis Committee:
Prof. Dr. Ir. C. van Rhee
Dr. Ir. B.C. van Prooijen
Dr. Ir. G.H. Keetels
Ir. M.J.M. van den Heuvel
Ir. A. van Es

Under the authority of:
Van Oord Dredging & Marine Contractors

Abstract

Land-based mines are coping with decreasing ore grades, metal prices and demand are rising and with the success of the offshore oil & gas market in mind, mining the sea floor has once again become interesting. This young market offers a lot of new opportunities for the dredging and offshore industry, whose expertise will be required by the mining industry for operating offshore.

The feasibility study shows that deep sea mining offers interesting possibilities to Van Oord. Technical, financial, political and environmental issues will offer challenges and multimillion investments will be required to adapt existing vessels like the jumbo hoppers or the larger flexible fall pipe vessels into mining vessels. Using smaller vessels is not an option due to the open ocean conditions on most of the project locations.

A number of different deep sea mining systems were considered, varying in type of mining vessel, vertical transport method and excavation method. Their feasibility was studied for three different mining cases:

- mining phosphorite nodules from 500 m water depth;
- mining sea floor massive sulphides (SMS) from 2,000 m water depth;
- mining manganese nodules from 5,000 m water depth

Most promising of the case studies in terms of feasibility is mining phosphorites by a jumbo TSHD with a separated suction tube, because of the low threshold in both financing and technique. The alternative of mining with an ROV from a flexible fall pipe vessel seems suitable for all 3 considered working depths, making this a more all-round option for further studies.

The case studies show that feasibility not only depends on the choice for a certain mining technique, but also on mineral values, which were on record heights when the feasibility study was performed in October 2012, but are in decline again at the moment of publication of this thesis.

A comparison between the different kinds of vertical transport shows that vertical transport by mechanical bucket lifting is the most energy efficient transport system of the four compared systems. Disadvantage is the progress in winch development which will have to be achieved to meet the production targets.

The two pump systems, centrifugal and positive-displacement, have slightly lower efficiencies than mechanical lifting and have some disadvantages when used in deep water: complicated systems in case of centrifugal pumps, since a lot of them would be needed, and high pressures when using a positive displacement pump. At limited water depth these two are reasonable alternatives, as they have no problems achieving high productions, which mechanical lifting has.

The air lift system has the least efficient results, but is the only one which has an increasing efficiency for increasing water depths, while maintaining high productivity. Besides that an airlift does not have moving objects in deep water because the compressor propelling it can be on the mining vessel, which is a large practical advantage over the other three systems.

A practical disadvantage of the airlift is the annular flow regime which can occur in the top section of the riser. This flow regime does not occur when a relatively large riser diameter is used, the riser outflow is located a certain number of meters under water or when microspheres are used instead of air.

Contents

1 Introduction **1**
- 1.1 Problem definition & scope . . . 2
- 1.2 Method of approach . . . 3

2 Deep sea mining **4**
- 2.1 Mineral resources . . . 4
- 2.2 Offshore mining market . . . 10
- 2.3 Mining systems . . . 13
  - 2.3.1 Excavation systems . . . 13
  - 2.3.2 Vertical transport methods . . . 18
  - 2.3.3 Processing . . . 19
- 2.4 Environmental impacts . . . 20
  - 2.4.1 Ecological impacts . . . 21
  - 2.4.2 Socio-economic impacts . . . 23
- 2.5 Feasibility . . . 24
  - 2.5.1 Mining system selection . . . 24
  - 2.5.2 Feasibility . . . 26
  - 2.5.3 System selection . . . 27
- 2.6 Conclusion . . . 29

3 Vertical transport methods **30**
- 3.1 Centrifugal slurry pumps . . . 31
  - 3.1.1 Model . . . 32
  - 3.1.2 Performance . . . 38
- 3.2 Positive displacement pump . . . 47
  - 3.2.1 Theory . . . 49
  - 3.2.2 Model . . . 51
  - 3.2.3 Performance . . . 56
- 3.3 Mechanical lifting . . . 67
  - 3.3.1 Model . . . 67
  - 3.3.2 Performance . . . 72
- 3.4 Airlift . . . 81
- 3.5 Conclusion . . . 83

4 Airlift **84**
4.1 Theory . . . 85
4.1.1 Flow regimes . . . 86
4.1.2 Literature . . . 89
4.1.3 Model selection . . . 90
4.1.4 Experimental data . . . 91
4.2 Model . . . 92
4.2.1 Assumptions . . . 92
4.2.2 Principle . . . 93
4.2.3 Equations . . . 95
4.2.4 Calculation procedure . . . 103
4.2.5 Post-processing equations . . . 105
4.2.6 Validation . . . 111
4.3 Performance . . . 112
4.3.1 Operation . . . 113
4.3.2 Analysis . . . 119
4.4 Conclusion . . . 132

5 Conclusion & Recommendations **133**

A Validation data airlift
A.1 Weber . . .

B Matlab data
B.1 Flow charts model procedure . . .
B.1.1 Centrifugal pumps . . .
B.1.2 Positive displacement pump . . .
B.1.3 Airlift . . .
B.2 Matlab scripts . . .

C Original reports
C.1 Introduction Deep Sea Mining . . .
C.2 Vertical transport methods . . .
C.3 Airlift . . .
C.4 Buoyancy induced lift . . .

Nomenclature

α_b	Shape factor [-]
α_d	Distribution factor [-]
α_f	Stepanoff factor [-]
α_h	Hindering effects particle settling factor [-]
α_I	Inlet height factor (h_I/h) [-]
α_t	Transport factor [-]
α_u	Weight factor [-]
α_w	Workability factor [-]
α_x	Vapour quality factor [-]
β_S	Inflow concentration solids [-]
η_e	Energetic efficiency [-]
η_h	Hydraulic efficiency [-]
η_p	Pump efficiency [-]
λ	Darcy friction factor [-]
μ_G	Gas dynamic viscosity [-]
μ_L	Liquid dynamic viscosity [-]
ρ_G	Gas density [kg/m^3]
ρ_L	Liquid density [kg/m^3]
ρ_M	Mixture density [kg/m^3]
ρ_S	Solid density [kg/m^3]
$\rho_{LS,3}$	Liquid and solid density in three-phase flow [kg/m^3]

τ	Shear stress [kN/m^2]
θ	Angle [rad]
ξ_a	Acceleration pressure loss coefficient [-]
ξ_c	Friction losses in opening in- and outlet pump chamber [-]
ξ_E	Entrance pressure loss coefficient [-]
ξ_f	Length dependent pressure loss coefficient [-]
ξ_v	Length independent pressure loss coefficient [-]
A	Riser area [m^2]
A_b	Bucket area [m^2]
A_c	Area opening in- and outlet pump chamber [m^2]
A_d	Diaphragm area [m^2]
a_F	Acceleration fluid (mixture or liquid) [m/s^2]
b_i	Impeller width [m]
C_D	Drag coefficient [-]
C_G	Gas (or buoyant substance) concentration [-]
C_L	Liquid concentration [-]
C_S	Solid concentration [-]
D	Pipeline diameter [m]
D_c	Pump chamber diameter [m]
D_i	Impeller diameter [m]
D_s	Supply pipe diameter of substance [m]
d_S	Particle diameter [mm]
E_{pot}	Potential energy [kWh/kg]
E_{spec}	Specific energy [kWh/kg]
F_D	Drag force [kN]
F_p	Force on or in pump [kN]
G	Momentum [kN s]

g	Gravitational acceleration [m/s^2]
h	Water depth [m]
h_b	Bucket height [m]
h_I	Gas-inlet height [m]
j_G	Gas volumetric flux [m/s]
j_L	Liquid volumetric flux [m/s]
j_S	Solid volumetric flux [m/s]
K_L	Liquid bulk modulus [kPa]
L	Pipe length [-]
m_b	Bucket mass [kg]
m_c	Pump chamber content mass [kg]
M_M	Mixture mass flux [kg/s]
M_S	Solid production (mass flux) [ton/oh]
m_S	Solid mass [kg]
n	Polytropic index [-]
N_p	Number of pumps [-]
n_p	Pump axis revolutions [rpm]
N_r	Number of riser sections [-]
n_S	Porosity [-]
P	Power [kW]
p_I	Pressure at air inlet into the suction pipe [kPa]
p_p	Pump pressure [kPa]
p_r	Riser pressure [kPa]
p_{atm}	Atmospheric pressure [kPa]
Q_F	Fluid volumetric flow rate (flow) (mixture or liquid) [m^3/s]
Q_G	Gas (or buoyant substance) volumetric flow rate (flow) [m^3/s]
Q_L	Liquid volumetric flow rate (flow) [m^3/s]

Q_M Mixture volumetric flow rate (flow) [m^3/s]

Q_S Solid volumetric flow rate (flow) [m^3/s]

$Q_{G.atm}$ Gas volumetric flow rate (flow) under atmospheric pressure [m3/s]

R Gas constant [J/kg K]

T Temperature [K]

V_b Bucket volume [m^3]

v_b Bucket velocity [m/s]

V_c Pump chamber volume [m^3]

v_d Diaphragm velocity [m/s]

V_F Fluid volume (mixture or liquid) [m^3]

v_G Gas (or buoyant substance) velocity [m/s]

V_L Liquid volume [m^3]

v_L Liquid velocity [m/s]

v_M Mixture velocity [m/s]

V_S Solid volume [m^3]

v_S Solid velocity [m/s]

v_{tip} Tip speed pump [m/s]

x_d Diaphragm position from centerline [m]

y_b Bucket position [m]

List of Figures

2.1 Mineral resources (courtesy IHC) 5
2.2 Mineral resource location (courtesy Van Muijen) 6
2.3 Price development of minerals, corrected for inflation, in Euro per ton till October 2012 7
2.4 Development SMS Deposits (courtesy SRK Consulting) . . . 9
2.5 Deep sea mining projects (courtesy Technip) 11
2.6 Towed nodule collector and continuous line bucket system . . 14
2.7 Gemonod system and autonomous shuttles 16
2.8 Drum cutter (SMD), auxiliary cutter (IHC) and nodule collector (IKS) 17
2.9 Vessel adaptation to trailing and Gemonod system 25
2.10 Capacity excavation and vertical transport system for the three different cases 28

3.1 Effect of particle diameter d_S on the efficiency 39
3.2 Effect of pipe diameter D on the efficiency 40
3.3 Effect of concentration C_S on the efficiency 41
3.4 Energetic efficiency and power requirement for production . . 42
3.5 Factors influencing efficiency loss 43
3.6 Energetic efficiency of the centrifugal pump system over depth without workability factor 44
3.7 Energetic efficiency of the centrifugal pump system over depth including workability factor 45
3.8 Pressure in the riser system (ρ_S of 2,000 kg/m^3 / d_S of 0.05 m) 46
3.9 Schematization mining vessel with diaphragm pump 48
3.10 Schematization diaphragm pump 49
3.11 Flow diaphragm pump 50
3.12 Flow diaphragm pump 57
3.13 Mixture flow (top) and water flow (bottom) 57
3.14 Flow (top)and cumulative flow (bottom) of mixture into the mixture pipe 58
3.15 Flow fluctuation for number of chambers 58
3.16 Pressure (top) and cumulative pressure difference (bottom) . 59

3.17 Cumulative pressure difference 60
3.18 Flow and pressure fluctuation for number of chambers 60
3.19 Area diaphragm per position and velocity diaphragm over time 61
3.20 Position diaphragm in time 62
3.21 Efficiency for pressure lost over the pump 62
3.22 Variation diameter discharge pipe for efficiency 63
3.23 Influence solid concentration on efficiency 63
3.24 Relation production and efficiency / power consumption . . . 64
3.25 Efficiency over water depth 64
3.26 Pressure development over the mining system for mining manganese nodules from a water depth of 5,000 m 65
3.27 Pressure development over the mining system for mining SMS deposits from a water depth of 1,500m 66
3.28 Mechanical lifting alternatives 67
3.29 Effect of winch force F_{wi} on the efficiency 73
3.30 Effect of bucket volume V_b on the efficiency 74
3.31 Effect of drag coefficient C_D on the efficiency 75
3.32 Effect of bucket shape factor α_b on efficiency 75
3.33 Effect of bucket weight factor α_u on efficiency 76
3.34 Effect of porosity n_S on efficiency 76
3.35 Effect of stability velocity limit $v_{b.max.s}$ on efficiency 77
3.36 Low stability limit 78
3.37 No stability limit 78
3.38 Low stability limit 78
3.39 No stability limit 78
3.40 Effect of water depth h on efficiency 80
3.41 Efficiency over water depth 81
3.42 Pressure in the pipeline of an airlift with the air inlet halfway for a solid density of 2,000 kg/m^3 and a particle diameter of 0.05 m 82

4.1 Airlift (Wikipedia) 84
4.2 Schematization airlift 85
4.3 Flow regimes 86
4.4 Different flow regimes in riser 87
4.5 Flow regime map relating the different fluxes (superficial velocities) 88
4.6 Principle of airlift model 93
4.7 Flow scheme airlift model 104
4.8 Flow regime map relating the different fluxes 109
4.9 Validation Weber data 111
4.10 Efficiency and production for varying air flux 112
4.11 Variation in efficiency over working depth 113

4.12 Power and efficiency for different productions (and related gas flows) . . . 114
4.13 Concentration, density and velocity distribution along the riser 115
4.14 Pressure distribution along the riser . . . 116
4.15 Taitel's map with flow regimes for the riser . . . 117
4.16 Flow regimes in the upper 1,000 m of the riser . . . 117
4.17 Power and efficiency for different productions (and related gas flows) . . . 118
4.18 Flow regimes in the upper 1,000 m of the riser . . . 119
4.19 Schematized slug flow transport . . . 123
4.20 Flow regime changes in the upper 500 m of the riser with outflow at minus 10 . . . 126
4.21 Flow regime changes in the upper 500 m of the riser, for both air and helium . . . 128
4.22 Microspheres enlarged by microscope and regular size . . . 130
4.23 Power and efficiency for different productions (and related gas flows) . . . 131

B.1 Flow scheme centrifugal pumps model . . .
B.2 Flow scheme PD-pump model . . .
B.3 Flow scheme airlift model . . .

List of Tables

2.1 Overview mineral resources over depth 5

A.1 Measurement data Weber (1) . . . . . .
A.2 Measurement data Weber (2) . . . . . .

Chapter 1

Introduction

Land-based mines are coping with decreasing ore grades, metal prices and demand are rising and with the success of the offshore oil & gas market in mind, mining the sea floor has once again become interesting. This young market offers a lot of new opportunities for the dredging and offshore industry, whose expertise will be required by the mining industry for operating offshore.

This thesis hopes to offer an introduction into the subject of deep sea mining (DSM), including a more detailed investigation into the possibilities for vertical transport of resources from sea floor to surface. Interesting subjects within deep sea mining are:

- the resources which can be mined, including their location, mineral and metal content, value and water depth at which they occur;
- the deep sea mining market as it exists at the moment: which projects are ongoing, which parties are involved and who are stakeholder;
- techniques for mining the resources, like which methods are used for excavating the resources and bringing them to the surface, what part of the operations take place offshore and for what do the resources have to be transported to the shore, and how;
- the environmental impacts of deep sea mining, both social-economic as ecological;
- the feasibility of deep sea mining projects.

As there is no exact definition of the water depth at which mining is called deep sea mining, and therefore the difference between regular offshore mining and deep sea mining is debatable, the introduction will try to give a view that is as broad as possible.

For the technical and feasibility part of this study, deep sea mining is limited to the operations that are not (yet) done by conventional dredging or mining techniques, which means working depths of 200 m and deeper.

A more thorough study will be made regarding the vertical transport techniques which can be used during DSM operations, in particular buoyancy induced lifting like airlifting. The alternatives to be considered at first are:

- hydraulic lifting by multiple centrifugal slurry pumps;
- hydraulic lifting by a positive displacement pump;
- pneumatic lifting by airlift;
- mechanical lifting by a single bucket lift.

The methods will be modelled and compared on basis of their energetic efficiency, and practical and theoretical limitations due to occurring pressures and velocities.

Of these 4 alternatives the airlift variant is chosen for further research, since the simple model of an airlift is not sufficient to make a good comparison to the other 3 alternatives. The simple model already shows an improving efficiency for airlift with increasing water depth, and the lack of moving parts at the sea floor make it an interesting alternative.

An existing model of the airlifting technique is coded, extended and adapted to be used for simulations in deep sea mining circumstances. With this adapted model a performance study of the airlift will be performed. To avoid practical problems like changing flow regimes also alternative substances will be used instead of air.

1.1 Problem definition & scope

The main question this thesis will try to answer is:

"Which vertical transport system is most suitable for deep sea mining operations?"

To do so first a selection is made of the relevant resources and their parameters, based on the feasibility study. This feasibility study considers the costs and revenues of the entire operation from mining to selling the metals, but will focus on the activities that take place offshore: excavating, vertical transport, separation, offloading and shore transport.

1.2 Method of approach

This report consists of three parts, which have been four separate reports, but are put together in this thesis. The four separate (unpublished) reports also give an overview of the subjects as described in this thesis, and can be found in the Appendix C as reference. Their titles are:

- Deep Sea Mining: Opportunity for ingenuity
- Vertical transport: A comparative study of methods
- Vertical transport methods: Airlift
- Vertical transport methods: Buoyancy induced transport

Each report will correspond to a chapter in this thesis, with exception of airlifting and buoyancy induced lifting, which are put together. The first real chapter (chapter 2) gives a broad introduction into deep sea mining. Resources, the deep sea mining market, techniques and environmental issues are described per paragraph, and a feasibility study is made from the point of view of Van Oord Dredging & Marine Contractors.

The results of the feasibility study is used as input for the comparison of vertical transport methods and the more advanced research into the airlift and its alternative. In the comparative study in chapter 3 four systems are considered: centrifugal pumps, positive displacement pumps, airlift and mechanical lifting. Per model the functioning and the theory is described, including the theoretical and practical limitations, and a basic simplified model is build, which is used to study the performance and the energetic efficiency.

In the fourth chapter, regarding the airlift, first the functioning and basic theory is given, including a literature study, selection of the model principle and of relevant validation data. The model itself is described by first explaining the principle and the assumptions used, after which the relevant equations and calculation procedure are given and the model is validated.

A performance study is then done with the model, based on the parameters from the feasibility study. In an attempt to prevent the practical problems occurring during airlifting the air is replaced by other buoyant substances, like microspheres, in the last part of the chapter.

Based on the first chapters the main question of the thesis will be answered, and recommendations will be done for further studies.

Chapter 2

Deep sea mining

Mining the deep sea has been of interest to the mining industry since the 1960s, when J.L. Mero declared in his book that the sea floor contained almost endless supplies of certain metals. Limited technology and decreasing metal prices made commercial exploitation impossible at that time, but with the development of technology and metal prices mining the deep sea once again has gained the attention of both industry and governmental organisations.

2.1 Mineral resources

The almost endless supply of metals which J.L. Mero mentioned were manganese nodules, poly-metallic nodules which can be found at depths of up to 6,000 m, where they lie on the sea floor. Other mineral resources were already being mined from the sea floor at that time, but at a completely different depth: divers were diving to about 20 meter in their search for diamonds.

Again the border between deep sea mining and regular offshore mining is hard to distinguish, and for that reason this paragraph will elaborate on all valuable mineral resources in which the mining industry has shown interest, with the exception of simple aggregates like sand and gravel.

Name	Contains	Deposit type	Depth (m)
Mineral sands	Sn,Fe,Au,Ag,Pt,Cr,Ti,Zr	Sand	20-50
Diamonds	Diamonds	Sand	20-300
Phosphorite	Phosphate (P2O5)	Sand&Nodules	200-600
Manganese crust	Mn, Cb, Ni, Cu, REY	Rock	400-4,000
Gas hydrates	Methan (CH4)	Nodules	500-2,000
SMS deposits	Au, Ag, Cu, Zn, Pb	Rock	1,500-5,000
Metalliferous sulf.	Au,Ag,Cu,Zn,Cr,Ti,Zr,Re	Sand	2,000-3,000
Deep sea muds	REY	Sand	3,500-6,000
Manganese nodules	Mn, Cb, Ni, Cu, REY	Nodules	4,000-6,000

Table 2.1: Overview mineral resources over depth

Table (2.1) gives an overview of the mineral resources which can be found offshore and the form and water depth at which they can be found. A more detailed description of some of the minerals can be found later in this chapter.

Figure (2.1) gives an image of some of these resources, including a schematized water depth and economical attractiveness to mine, from the point of view of IHC Mining.

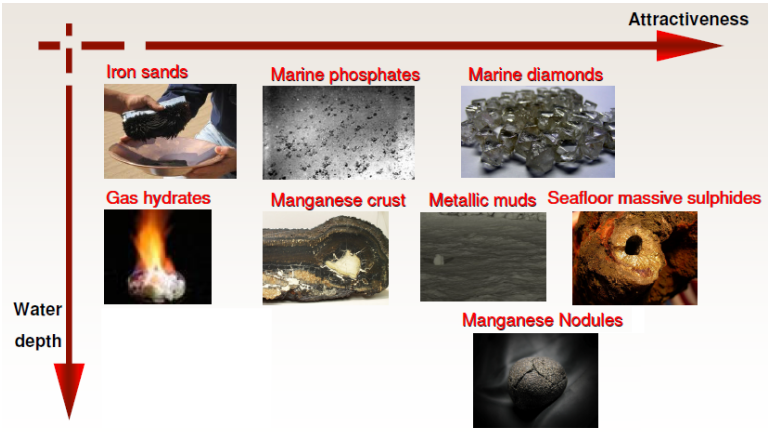

Figure 2.1: Mineral resources (courtesy IHC)

An overview of the location at which every resource can be found is hard to give, since a lot of exploring is still ongoing. With figure (2.2) Van Muijen (van Muijen, 2007) tries to give an overview of most of these minerals and their location.

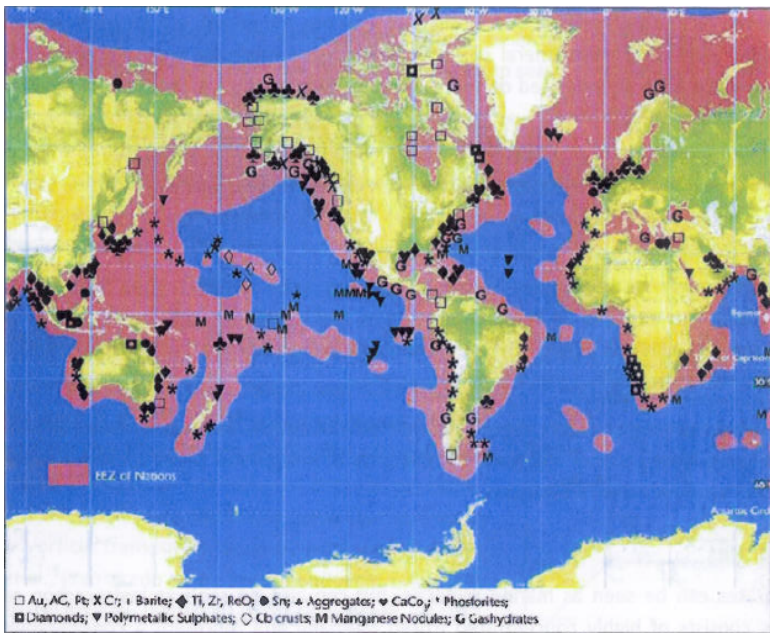

Figure 2.2: Mineral resource location (courtesy Van Muijen)

Until now the mineral resources that are mined offshore in a commercially feasible way, heavy mineral sands (tin) and diamonds, can be found at limited water depths up to 300 m. The current research into phosphorite mining is a logical next step when it comes to water depth, while the interest in iron sands originates from the fact that the mineral resource seems to be cheaper to win offshore than onshore.

The interest in the mineral resources which can be found at greater depths, SMS deposits and manganese nodules, is only justified by the high prices of the minerals. However, these mineral prices fluctuate a lot, and most deposits have not been explored thoroughly enough to make a good estimate of the mineral contents. Using some average value of the mineral content and the market prices of the minerals an overview can be given of the development of the price over the years in figure (2.3) until October 2012.

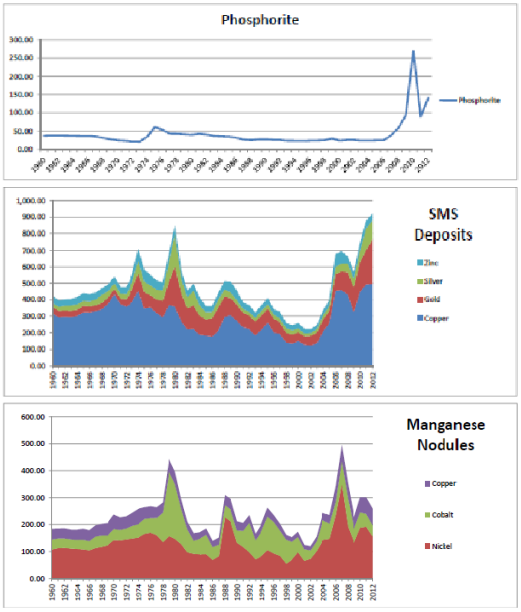

Figure 2.3: Price development of minerals, corrected for inflation, in Euro per ton till October 2012

The figure, made for phosphorites, SMS deposits and the most important minerals in manganese nodules, shows the fluctuation over the last 50 years, in particular the peaks in the 1970s causing the first deep sea mining boom, and in the most recent decade (USGS, 2013) causing the current interest in DSM.

The reason only copper, nickel and cobalt are included in the calculation of the manganese nodule value is that of the other minerals some can be found plentiful in land-based mines and / or the demand is small in comparison. The best example is manganese: the content of around 25% manganese in the nodules is interesting for mining, but there are also large land-based supplies with 30%+ manganese content, while the market demand for manganese is limited.

A similar thing can be said for gas hydrates: the alternative sources of (in particular shale) gas from both on- and offshore (under the sea floor) sources is massive, causing the gas hydrates to be a resource that is not yet feasible to explore.

A more detailed description of all the mineral resources mentioned earlier is given in Appendix C.1. The three most interesting ones were used in the feasibility study and are described in more detail here:

Phosphorites

Phosphorite is a sedimentary rock which contains a high amounts of phosphate. The main use of phosphate is fertilizers. Phosphorite is won across the globe in land-based mines in countries like China, Morocco, South-Africa and the United States (USGS, 2013). The land-based mines are estimated to not run out of phosphate for another 300 years at current rate of consumption, but these estimates differ a lot.

Due to high demand and limited producers market prices are relatively high and an alternative for the current phosphate winning could be the phosphorites which can be found on the ocean bottom in varying forms. In New Zealand Boskalis and Chatham Rock Phosphate are in the preparatory phase of a mining operation of nodular phosphorites, at a water depth of 400 m, 450 km offshore. In Namibia plans exist to mine phosphorite sand at depths of 250 m. The nodules have a diameter of 1 to 4 cm while the sand has a size of 0.25 to 2 mm.

Manganese nodules

In the 1970s and 80s a lot of research and test projects involving the deep sea mining of manganese modules was done. These poly-metallic nodules typically have a size of 5 - 10 cm, contain a lot of water (they have a wet density of 2,000 kg/m^3 and dry density of 1,400 kg/m^3) and contain i.a. manganese, cobalt, nickel, copper and rare earth elements & yttrium, and can be found on abyssal plains at depths of 3.5 - 6 km.

The rising prices of cobalt and nickel in the 70s were the reason behind the sudden interest in deep sea mining. When the prices dropped again in the mid-80s, due to the amount of land-based mines which commenced production and the emergence of other metals which were cheaper to use, the interest in mining manganese nodules vanished. Recently these nodules again have caught the interest of the market because of the rising prices of copper and nickel.

Sea floor massive sulphides

Contrary to the phosphorite deposits, sea floor massive sulphides (SMS) are high-grade deposits of multiple metals, i.a: gold, silver, copper, lead and zinc. These deposits can be found in so-called 'back-arc basins' and mid-ocean ridges. Mid-ocean ridges are caused by tectonic plates moving away from each other. Back-arc basins are formed when oceanic slabs of thick crusts are sub-ducted beneath a tectonic plate moving in the opposite direction and can generally be found behind island arcs at a depth of 1,500 to 5,000 m.

At these places hydrothermal vents are formed. Through cracks in the sea floor cold water is able to flow hundreds of meters into the crust where it is heated and enriched with minerals. Through similar cracks the water flows out again at which point the dissolved minerals solidifies again after contact with the cold water, forming the 'black-smoker' chimneys (with a height up to 30 m) around the outflow.

After a while the chimney structure collapses and the process repeats itself in the near surrounding, causing a layer of several meters of collapsed chimney structures, rich of minerals, as is schematized in figure (2.4) (SRK-Consulting, 2010).

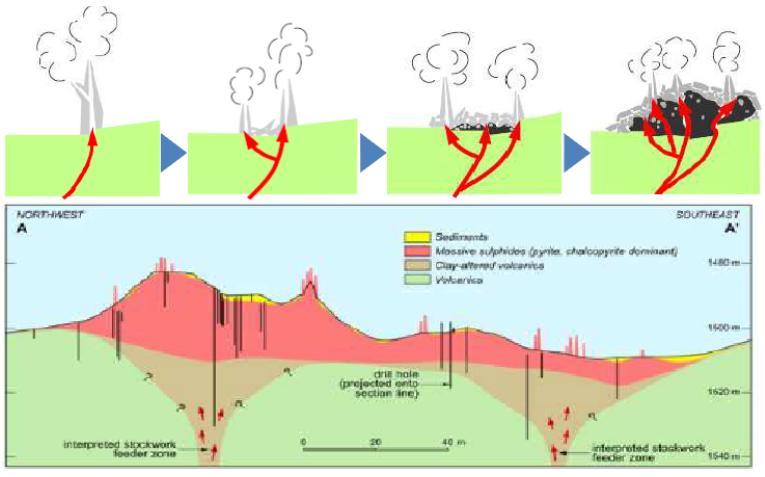

Figure 2.4: Development SMS Deposits (courtesy SRK Consulting)

2.2 Offshore mining market

The offshore mining market can be separated in minerals, stakeholders and projects. The first one has already been elaborated a bit in the previous chapter and for more details regarding mineral contents, concentrations, values and global production of the minerals is referred to the original report in Appendix C.1.

A more extensive elaboration of the roles of stakeholders can be found in this appendix as well, but they can roughly be divided in:

- the government, which is governing the area in which the mining will take place;
- the concession holder, the party or governmental organisation which has a contract with the responsible government for exploration and exploitation of the minerals;
- the mining subcontractors and suppliers, which are responsible for a part of the exploration or exploitation operation, like estimating the resources, supplying or engineering the equipment, researching the mining process and its environmental consequences or actually executing the mining operation on behalf of the concession holder;
- third parties, like environmental organisations, current users of the (surrounding) area and the consumers of the mined resources.

On different locations around the world there are projects going on, involving various mineral resources and parties. Figure (2.5) tries to give an overview of the most interesting projects which are ongoing or were ongoing till recent. The three most interesting ones will be explained in more detail here, as the feasibility studies is based on these projects. For the other projects is referred to the original deep sea mining report which can be found in Appendix C.1.

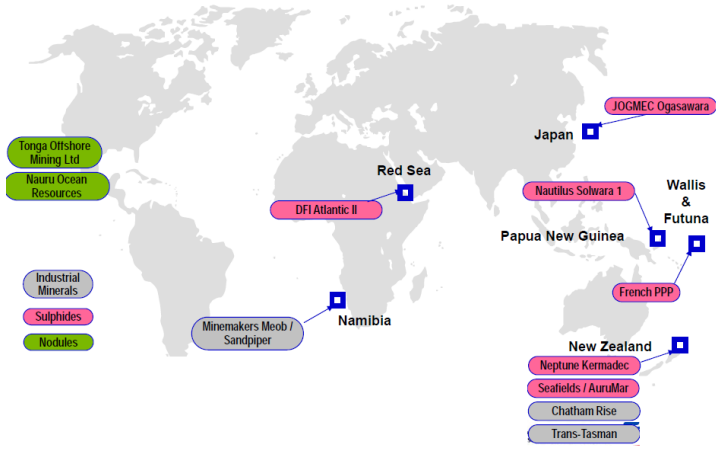

Figure 2.5: Deep sea mining projects (courtesy Technip)

Clarion-Clipperton zone

The most explored area for DSM prospects until now is probably the Clarion-Clipperton Fracture zone, which is located in the Pacific Ocean. Resource content of the area is estimated on 34 billion ton of manganese nodules spread over 9 million km^2. More than 10 different consortia hold concessions in this area and are currently exploring and mapping the area.

In the 70s and 80s there already was a peak in the interest in deep sea mining, especially concerning manganese nodules in this area. A few trial runs were done by (combinations of) contractors before the plans were largely abandoned again because of declining metal prices.

About 500 tons of nodules were collected by the combination OMA in 1977 and 1978, using a combination of towed collectors and airlifting. Another consortium, OMI, mined about 800 tons at 5,500 m water depth using a ROV on a flexible pipe which was connected to a pumping system on a rigid pipe. The other combinations, OMCO and AFTERNOD, did not manage to mine any minerals.

Solwara I

This project is a project of Nautilus Minerals and is located in the Bismarck Sea near Papua New Guinea. Nautilus plans to mine a SMS deposit at a depth of 1,600 m. The deposit is estimated to consist of about 2 million ton of minerals, containing 5,0 g/t of gold, 23 g/t silver, 7,2% copper and 0,4% zinc. Similar deposits have been found near this projects location for subsequent mining projects.

Nautilus is currently in the process of buying the equipment to mine the resources themselves. The equipment consists of 3 subsea mining tools which are connected by flexible pipes to a submerged positive displacement pump which pumps the resources over 1,600 m through a stiff pipe to the vessel. On the vessel the resources will be de-watered and loaded onto barges, which will transport the resources to the shore for further processing. Production was supposed to start in 2013, but this was delayed because of contractual issues with the government of Papua New Guinea.

Chatham Rise

This nodular phosphorite mining project is located in the exclusive economic zone (EEZ) of New Zealand 450 km offshore of Christchurch. Concession holder is Chatham Rock Phosphate and the resources are estimated on 100 million ton of phosphate. Water depth is between 300 and 400 m. Density of the nodules is about 16% in a sediment layer of 0.5 m.

The project will be executed by Boskalis and is supposed to start in 2015. Boskalis is planning to use a trailing suction hopper dredger (TSHD) with an extended (and partially flexible) suction tube to dredge the nodules. The TSHD will transport the minerals to the shore where they will be offloaded and processed.

2.3 Mining systems

One of the biggest challenges in deep sea mining lies in excavating the resources and lifting them over a vertical distance of 100 to 10,000 meter. To accomplish this challenge a number of varying mining systems has been designed. In the first paragraphs the different mining systems are described, and split up based on their excavation method, although some combinations between the systems could be possible.

Further elaboration on the vertical transport alternatives and the onboard processes during deep sea mining can be found in the other two paragraphs.

2.3.1 Excavation systems

The are three excavation systems which will be considered: the trailing system, the Gemonod system and the mechanical system. Within every system there are numerous variations, and the separation is only based on the main principle of excavation.

Trailing system

The trailing system is similar to the suction system of regular trailing suction hopper dredgers. The vessel pulls a drag head over the sea bottom while an underwater pump pumps the mixture of water and solids up to the ship. Jet nozzles on the drag head can be used to loosen the soil and ease the mixture process. An alternative to the normal draghead is a collector unit, used in a similar way as a crawler but without an propulsion system.

Difference between the regular TSHD and the trailing system could lie in the pipe segment between underwater pump and vessel, which is rigid in case of the TSHD and flexible for the so-called RoRo-vessel, which has a flexible pipeline on a reel, connecting vessel and drag head. This flexibility makes it possible to roll off the pipe and thus increase the working depth of the drag head.

Advantage of the system is that using a trailing drag head with jets and underwater pump is well known within dredging companies and existing TSHDs can be converted into this type of mining vessel, saving the high capital investment costs for building a new mining vessel.

The drag head itself that can be used for deep sea mining will probably be hardly any different from the normal drag heads used in dredging and can be equipped with jets. Differences lie in the different pump, pipe and hoisting systems attached to the drag head. Lengthening the suction tube with a flexible pipe instead of a rigid one is one of the solutions to make the suction tube deep-sea proof. The underwater pump would have to be adapted to pump over a longer (vertical) distance and the hoisting system should be able to lift the drag head to greater depths.

A different advantage of converting a TSHD is that the vessel already contains a storage area including (basic) de-watering and transshipping equipment. Disadvantages are the limited precision and cutting power of the drag head and the high pulling forces. Because of the forces working on the suction tube a completely rigid system, as is used in TSHDs, is impractical from a certain depth down.

In a similar way to a drag head of a TSHD the Japanese research institute DOMA performed tests in limited water depths with a towed nodule collecting device, as is schematized in figure (2.6). A different alternative could be to use the continuous line bucket system, which can be seen in the same figure.

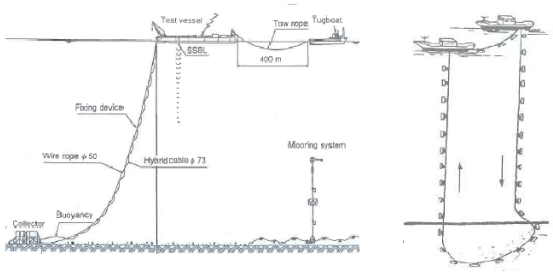

Figure 2.6: Towed nodule collector and continuous line bucket system

The continuous line bucket system was used in 1970 in test trials to mine manganese nodules at water depths of 4,000 m, according to A.M. Post (Post, 1983). The system consists of buckets connected to a wire which is trailed by one or multiple vessels over the sea floor. The vertical process is done by rotating the wire between vessel(s) and bottom, unloading the buckets when they reach the vessel and loading the buckets by trailing them over the bottom.

Advantages of this system are its simplicity. Disadvantage is the lack of cutting power, poor precision, controllability and that the wires might get entangled, either to itself or to bottom structures like wrecks or chimneys.

Gemonod system

The Gemonod system consists of one or multiple ROV-units at the sea bottom (so-called crawlers), flexible pipes which connect the crawlers to a buffer (and a possible crusher) and a rigid pipe between buffer and mining vessel. An example is given in figure (2.7).

The collector is, opposite to on the trailing system, self propelling. The data to control the unit and the energy come from the vessel through cables parallel to the suction pipe. Because of the self propelling collector the mining vessel does not have to move much during the mining operation and the precision of mining is superior to the trailing system.

A pumping system in the crawler pumps the excavated mineral resources to the buffer. The buffer stabilizes the concentration of the mixture in the riser which is pumped up to the vessel. In some cases, for example when there is a certain particle diameter required before it can be pumped up, a crusher is added to the buffer.

From the buffer the mixture is pumped up through a rigid pipe, the riser. This can be done by slurry pumps, airlifts, positive displacements pumps or other alternatives, which will be the subject of next paragraph. On the mining vessel there has to be a deployment system similar to that of fall-pipe or oil-drilling vessels to lift the mining system, and a de-watering plant to separate the water from the mineral resources.

Biggest disadvantages of this system are that it is a relatively complicated system of which not much is known yet, especially not about the cutting process at great depths and the vertical transport over greater distance. Another disadvantage are the high investment costs to build such a system.

Advantage is the bigger precision than the trailing system and the fact that the ship does not have to move during mining operation. At first glance this system seems more suitable for greater water depths.

In the paste this system (and variations to this one) were used in trial tests for mining manganese nodules. Also De Beers is using a ROV-unit in diamond mining, with a flexible pipe to connect the ROV directly to the vessel.

An alternative to the ROV which is attached to the vessel would be free flying AUVs. The autonomous shuttle system consists of a surface vessel or platform which supplies, launches and unloads the self-propelling shuttles that move to the sea floor like a submarine would, to mine the resources there. Figure (2.7) sketches the system.

Advantages are numerous: Simple maintainability, flexibility when it comes to mining depths and bathymetry of the resources and the lack of a lifting system on which all kinds of forces are working. The major downside of this system would be the high costs, both for the investment to build (multiple) shuttles and the operational costs of bringing the deposits from the sea floor to surface.

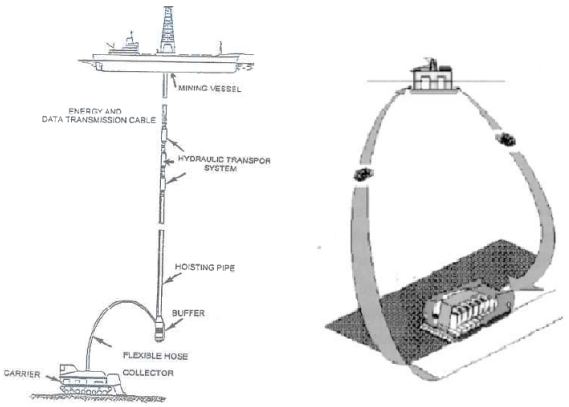

Figure 2.7: Gemonod system and autonomous shuttles

The different soil conditions and types of mineral resources are cause for a diversity in ROVs / crawlers that can be used in deep sea mining. Similarities lie in the fact that they are self-propelling, connected to a support vessel by cables to be provided with energy and guidance and have a cutter or collection tool. For horizontal movement they mostly rely on caterpillars, but there are also designs of 'walking'-equipment which have 4 or 6 spud poles.

Crawlers can be provided with a collector system and a pump to pump the mixture of water and cut solids to the vessel or a collection point. Also spud poles can be used to fix the unit during heavy cutting operations and water jets to loosen the soil. In the oil & gas industry these ROV units are generally as light weighted as possible, which in the mining industry is only useful in case of nodule mining. When soil has to be cut there are heavy loads transferred to the machine, making a higher weight preferable, typically 100 to 200 tons.

In general there are three different type of cutters that can be considered: drum cutters, auxiliary cutters and collector units. Of each of them an example is given in figure (2.8).

Drum cutters are commonly used for terrain levelling in civil works and excavating in open-pit mining and are equipped with a transverse cutting drum. Advantages are the relatively high production compared to the auxiliary cutter (land-based drum cutters have productions of more than 300 ton per hour) and the lack of need for a crusher unit since the size of the cut particles is small enough to transport right away. Also wear of the teeth is limited, improving workability. Downside is the requirement of relatively flat terrain to work on. The drum cutter is for example not fit to mine the chimney structures of the SMS deposits (alone).

An auxiliary cutter can be compared to a cutter suction unit on a cutter suction dredger (CSD), because it has one or more rotating cutter heads on a swinging boom, enabling it to move in both horizontal and vertical direction. Both production and workability (wearing of teeth) will be lower than on a drum cutter, yet rougher terrains form no problem. Alternative cutting tools like dredge wheels, backhoes, drills or simply a suction mouth could be used. The cutters can be equipped with a pump for transporting the dredged material and spud poles for stability and even propulsion.

Figure 2.8: Drum cutter (SMD), auxiliary cutter (IHC) and nodule collector (IKS)

The development of self-propelled sea floor collector units for nodules has already been going on since the 1970s. The ROVs used for nodule mining can work on relatively flat bottoms and do not have to excavate, but simply pick up the nodules spread over the sea floor. Because there is no need for a huge weight to compensate for excavation forces, the size and weight of the ROVs is a lot smaller than the ROVs used for subsea rock excavation, order of magnitude 50 tons. Limiting factor might be the carrying capacity of the subsoil, which is one of the reasons tracks might be preferable over wheels.

Mechanical mining system

The basic way of using grabs is by lowering them down until they reach the mining depth, cut the soil and lift the grab back up to the vessel. At greater water depths the efficiency of this system is really low and the grab has a limited precision and cutting power. This system could be improved by adding thrusters for the positioning and precision, while using a second system to lift the mineral resources to the vessel, which would enable the grab to keep on working at the bottom.

The second lifting system can be similar to a Gemonod system, in which the grab brings the resources to the buffer from where it is pumped up to the vessel. An alternative is using mechanical lifting, such as a bucket lift system or lifting multiple containers, similar to the one in figure (2.6).

2.3.2 Vertical transport methods

Lifting the resources from the seabed to the vessel is one of the most challenging parts of deep sea mining. The system used in normal dredging, centrifugal slurry pumps, have enough downsides when dredging at great depths to make reassessing alternative lifting systems a must.

Which lifting system is most suitable for which mining / excavation system depends on productions, transport distance and more, but all four alternatives could be applied in all the mining systems, although common sense might be used to ignore some combinations of mining systems and vertical transport methods, like mechanical lifting in combination with a draghead in shallow water.

A number of transport systems, like autonomous shuttles or capsule lifting is either considered to be very expensive (in both capital and operational costs) or needlessly complicated. The most interesting alternatives seem to be:

- hydraulic lifting by multiple centrifugal slurry pumps;
- hydraulic lifting by a positive displacement pump;
- pneumatic lifting by airlift;
- mechanical lifting by a single bucket lift.

Author's note: The subject 'vertical transport methods' will be elaborated further in chapter 3. The original description of vertical transport systems, which was used in the feasibility study, can be found in Appendix C.1.

2.3.3 Processing

Compared to the processes of excavating and lifting the remaining processes seem to be a lot less complicated. The processes can be divided into on-board processing, disposing of waste, shore-transport and further on-shore processing.

When the water-soil mixture reaches the surface it can be separated into water and solids in a de-watering installation. Further processing of the mineral resources does not seem to be viable on the mining vessel itself because of the complicated procedures and the large installation needed to process the minerals. There are some exceptions to this, in case the sediment mineral ratio is very high, like for diamonds, or if it is relatively easy to separate, like for phosphorites. But processing like splitting up the manganese nodules into manganese, cobalt and copper will have to take place on land and/or other vessels.

The remaining water and possibly sediment can simply be thrown overboard or can be brought back down to the depth from where it was mined. Since the first seems to have more environmental consequences than the second most plans for deep sea mining opt for bringing the return water back to the sea floor. To which depths the remainders are brought differs per plan and is something that has not been worked out in detail yet.

What the influence of the return water, probably still containing a number of small particles, is on the environment around the mining operation is unclear. Research institute Deltares has been doing some research into plume propagation for the Chatham Rock project, but the results are not published.

To get the mineral resources from vessel to shore there is a number of possibilities. In case of diamond mining the weight of the won resources is low enough to transport them by helicopter to the shore. The other ways would be to directly load it onto a barge after mining and separation, indirect loading of a barge from a temporary storage area on the mining vessel or storing it on the mining vessel itself and unload the vessel when it has navigated back to the shore.

The loading of the barge can be done by conveyor belts, bucket offloading or hydraulic transport. Which system is most suitable is subject to further investigation. Risks of loading the ore directly onto a barge by a conveyor belt might be the sea conditions for which barge loading is possible, while navigating back to the shore for unloading will cost valuable mining time.

2.4 Environmental impacts

While the technical challenges are very important to the deep sea market at this stage, the long-term challenge of deep sea mining is environmental. The mining, dredging and oil & gas companies get more and more aware of the importance of this subject and the necessity to work in a sustainable way. Governmental organisations implant laws and regulations to ensure the environmental issues are treated in a right way and NGOs get involved in projects in an earlier stage to cooperate in handling these issues.

Environment in this context covers more than just the direct ecological surrounding of the mining area. When considering the environmental impacts in an Environmental Impact Assessment (EIA) both the positive and negative impacts of a project on the ecological, social and economic aspects are taken into account, including alternatives for certain parts of the project and a base-line study.

The resulting report of an EIA, an Environmental Impact Statement (EIS), will also contain minimization, mitigation and monitoring measures for the remaining environmental impacts. This EIS generally forms a compulsory part of the mining license application of the concession holder to the government. So far the only known EIS for deep sea mining operations is the one made for Nautilus by Coffey, for the Solwara I project (Coffey-Natural-Systems, 2008).

Besides the ecological and socio-economic aspects during regular deep sea mining operations, which will be elaborated in the next paragraphs, there are also environmental impacts related to extreme conditions like large accidents or extreme weather. These are not described here, but can be found in Appendix C.1.

2.4.1 Ecological impacts

The ecological impacts, by a lot of people considered to be the same as environmental impacts, can for deep sea mining be divided into the impacts at the actual mining site (open deep water) and the impacts of the remaining processes, like transshipping, handling and further processing of the resources in protected shallow water and on land.

The water quality will mainly be affected at two different levels: At the bottom, around the mining operation itself, and in the top layer, where the mining vessel is located. In between leakage of the pipe or vertical transport of the equipment might have impact on the water quality too, but these will most likely be similar in effect and smaller in size than in the other two layers.

In the bottom layer the movement and work of the mining equipment will cause plumes which can consist of both sediment and small parts of the mineral resources that are mined. Similar plumes can be caused by the return water that is pumped down from the ship to the lower water layer. Sediment layers in the mining area might have to be moved from the mining location to nearby storage areas at the sea floor, leading to similar plumes.

In the top layer leakages of hydraulic fluids and lubricants can occur, while spilling during the mining or transshipping process might cause small mineral particles and sediment to end up in this layer.

Similar to the water quality, the impact on the biological environment can be split up in two layers: around the sea floor and above that. With biological environment marine life like reefs, fish and complex life forms around active hydrothermal vents are meant.

The main impact will occur at the sea floor where the actual mining operation is carried out. The loss of habitat and its associated biodiversity at this location due to mining of the top layer of the sea floor is something that cannot be prevented and not many mitigation and minimization measures are known for.

In the top layer the mining operations and corresponding water quality decrease will have influence on the animals living in this layer. Minerals might accumulate in fishes and the sediment / minerals dissolved in the water can cause smothering of the water animals.

Other ecological impacts, which in a first assessment seem to have less impact than the two mentioned earlier, are:

- air quality: the operation of a mining vessel at sea, transporting resources to the shore by barge and a handling and processing plant on land / near shore have adverse effects on the air quality of the surrounding;
- noise: similar to air quality noise will be caused by the mining operation, handling and processing plant above water. Under water the mining machines will also cause a noise;
- near shore marine environment: the movement of deep sea soil and water to the near shore environment might cause the move of deep sea flora and fauna to shallow waters. Product spillage and water run-off can also cause turbidity in this area;
- sediment: the movement of sediment before or during mining can cause changes in the quality and composition of the sediment itself, and influences the location where it is transported to;
- oceanography: changes in the bottom profile and composition because of the mining operation might have influence on the hydraulic conditions like currents and water temperatures;
- maritime safety: the continuous marine works at sea and shore traffic cause an increase in maritime traffic and the corresponding safety risks;
- offshore waste: mining productions at sea comes with waste like drill fluids, lubricants, batteries and chemicals which have to be stored and processed or transported to the shore;
- onshore soil and (ground-)water quality: similar to land-based mining operations, the processing, handling and (temporary) storage of the resources could cause contamination of the surrounding soil and (ground-)water due to leakage or dumping of chemicals and heavy metals.

Most of these impacts are not special in nature or exceptional in size compared to normal marine traffic, industry and harbour activities, do not seem to have a large impact or can be prevented and monitored by conventional methods.

An important consideration in the EIAs of deep sea mining is the comparison between the ecological effects of land-based mines and sea-based mines. Land-based mines have major adverse effects compared to deep sea mining like erosion, formation of sink holes, soil contamination and contamination of both surface and groundwater by chemicals used in the mining process and heavy metals. These, in combination with air, noise and visual pollution, also have secondary effects on the surrounding flora and fauna.

2.4.2 Socio-economic impacts

The social and economic impacts, together referred to as the socio-economic impacts, relate in case of land-based mining often to issues like land-ownership and forced movement of local inhabitants, the influence of ecological impacts like soil and water pollution on agriculture and drink water (and with that the health) of the local population, and growth of population, labour and economic activities in the surroundings due to the mining operation.

When considering deep sea mining a part of these issues is not relevant because the operations take place on open sea. Some negative impacts that could still be relevant are:

- in-migration of people towards the land-based facilities of the operating because of employment possibilities, causing disruptions in existing social structures within the local communities, tension between locals and immigrants and the reduction of employment possibilities for locals;
- disruption of other local activities like fishery, either due to contamination, disturbing fishing grounds or by taking over port facilities;
- unfair distribution of wealth / benefits, causing social inequality and disturbance;
- the abandonment of the mining area & facilities when the mining operations are done, possibly causing abrupt declines in (subsidiary) employment and adherent economic activities.

The positive effects of deep sea mining are similar to those for land-based mining, and are mainly related to the money the mining industry brings into an area, like: increased economic activity, economic benefits to authorities by taxes, economic benefits to adjacent industry and retail, business opportunities due to demand of goods and services, etc.

2.5 Feasibility

The actual deep sea mining operation will not commence before a thorough feasibility study is done. A first attempt at such a feasibility study is made at Van Oord for a wide range of possibilities, both in mining system as in resources. Goal was to identify the important factors and to make a first selection on what could be interesting and what is not.

The feasibility study is separated in 4 parts:

- the mining system selection and selection of resources to be mined, which is basically the scope of the study, which includes a description of what exactly was considered in the feasibility study;
- production estimation, what could the different considered mining systems actually produce;
- cost estimation, which costs, both capital and operational, should be incorporated in a feasibility study;
- feasibility, the balance between costs and estimated revenues.

Author's note: The original study as done at Van Oord contains a number of Van Oord vessels, their day-rates, productions, adaptation costs, etc. and a investigation of the knowledge and specialized staff Van Oord has. The report of this complete study was to be found in Appendix C.1, but is not meant for publication. This chapter will only contain a summary of the conclusions of the more extensive original feasibility study.

2.5.1 Mining system selection

To start with deep sea mining operations either new equipment will have to be procured or current equipment will have to be adapted. The specialized mining equipment on board will most likely have to be developed for the project, but the vessel itself could be an adapted existing vessel. The option with the lowest threshold for Van Oord is adapting one its existing vessels, and for that reason first is checked to what level those could be adapted for deep sea mining operations.

There is a number of different sea-going vessels within Van Oord which are considered: cutter suction dredgers (CSDs), trailing suction hopper dredgers (TSHDs), flexible fall pipe vessels (FFVs) and multi-purpose vessels (MPVs), like the ones used for installing offshore constructions like pipelines and windmills.

The vessels are compared on different criteria: seaworthiness (workability), power capacity, lifting capacity, dynamic positioning system, accommodation, survey equipment, adaptation space, storage area, offloading equipment and water separation systems. Six combinations of vessels and mining techniques are selected, the most important ones being:

- a jumbo TSHD with a trailing mining system
- a vessel with heavy lifting capabilities for a mechanical mining and lifting system
- a flexible fall pipe vessel (FFV) for a Gemonod mining system with one or more ROVs and hydraulic vertical transport

For every of the six vessels the required adaptations are described and elaborated, including (dis-)advantages, techniques which are (un-)available and an estimation of the costs of adapting the vessel. Sketches of two of these vessels (schematically adapted) are displayed in figure (2.9).

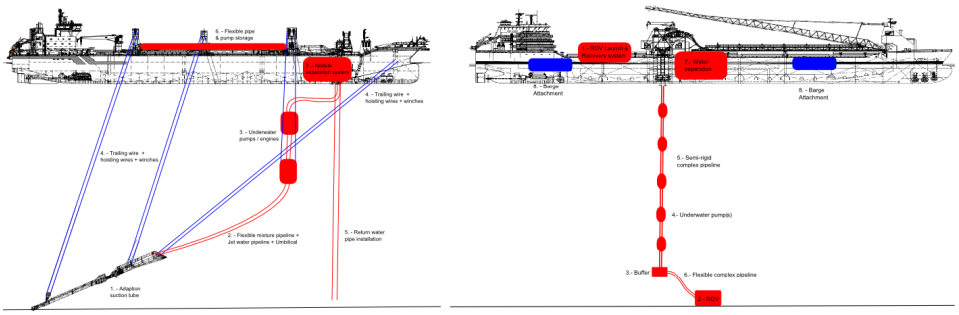

Figure 2.9: Vessel adaptation to trailing and Gemonod system

Three projects and associated resources were used as cases for the feasibility study:

- mining phosphorite nodules from 500 m water depth at Chatham Rise;
- mining sea floor massive sulphides (SMS) from 2,000 m water depth in the Bismarck Sea;
- mining manganese nodules from 5,000 m water depth in the CCZ.

Other starting points included a single mining vessel that could obtain a production of 1,500,000 ton dry resources per year, more than 250 ton pure resources per operating hour (ton/oh) and has an on-board de-watering plant and a pumping / transporting system for bringing the return water back to the sea floor.

2.5.2 Feasibility

The feasibility study as done for Van Oord shows that deep sea mining is feasible if the technical, political and environmental problems can be solved or prevented. Especially phosphorite mining with a TSHD is profitable, does not require enormous investments and is technically not that different from the current core-activity of Van Oord. Main risks would be the environmental impacts and decreasing market prices of phosphorite.

Using ROVs for phosphorite mining, similar to what the diamond miners do, would be feasible as well but would require more investment and would be different from the current activities Van Oord does. It might be interesting because instead of an expensive TSHD use can be made of a flexible fall pipe vessel, which has a lower day-rate, and separation could occur during excavation. Disadvantage would be the high amount of investments required to procure the ROV and ROV launching system.

Mining at larger depths would require a lot more investments to reach productions of 1,5M dry tons a year or more. At a smaller scale, and in calm waters, more simple approaches would suffice, but up-scaling these (by using multiple vessels) to higher productions and deep sea conditions would become very inefficient. For that reason smaller vessels with limited workability are not serious options for extensive operations, only the large trailing suction hopper dredgers and flexible fall pipe vessels are possibilities.

The SMS deposits at the Bismarck Sea are very profitable to mine, because of the high mineral prices, high concentrations and kind working conditions. Other possible locations in the world with SMS deposit mining have more difficult working conditions. The use of big and advanced ROVs to cut the rock is a necessity because of the high forces required and the difficult circumstances at the sea floor it has to operate in, requiring large investments.

For manganese nodules the feasibility is questionable. The working conditions at the surface are harsher and low concentrations of nodules in sediment require larger areas to be covered to make it profitable. Technical challenges concern particularly the enormous working depth, and with that, transport distance of minerals, return water, data, energy, etc. The ROVs used for mining operations are much smaller and more simple than its counterparts that are used in mining SMS deposits. Besides that, the development of ROVs suitable for this kind of operations is in a further stage than the ones for mining SMS deposits.

2.5.3 System selection

Mining from a FFV using the Gemonod system is the only variant feasible for all three mineral resources. This variant should be worked out more extensively. The option to use the TSHD for phosphorite mining is another variant that should be detailed out since the feasibility is larger and the investment costs lower than for the Gemonod variant. Using the vessel with heavy lifting equipment will not be considered further for now, as the only existing vessel with this equipment is not able to work in harsh conditions, although future Van Oord vessel with similar equipment might be able to.

From the mining system options considered in this deep sea mining feasibility study two variants should be worked out in more detail:

- FFV with a ROV and hydraulic lifting according to the Gemonod system;
- Jumbo TSHD with a separated suction tube, the trailing system.

Variants that were not considered in this study but could still be considered an interesting option, based on the vessel and mining system selection, are:

- FFV with a combination of a mechanical lifting system and a ROV unit
- FFV with a ROV unit with a suction head
- Jumbo TSHD with a dragged / trailing nodule picking device

Four different excavation methods have been considered in this feasibility study: A drag head, two variants of a grab and a ROV. In case of the ROV there is a difference between the nodule collectors and the rock cutter, but for the system selection this difference will be ignored since the rest of the mining system can be the same.

In figure (2.10) the productions used in the feasibility study are displayed together. The ROV is clearly the best option for all three cases, while a drag head is a serious option for mining nodules as well because of the lower investment costs and the familiarity within Van Oord with the technique. Especially at 5,000 m water depth it might be an option to combine the two somehow.

An alternative using a large grab could be considered for rock cutting, but this would require a very heavy lifting mechanism that is currently not present on one of the larger Van Oord vessels. This option will not be considered further for now.

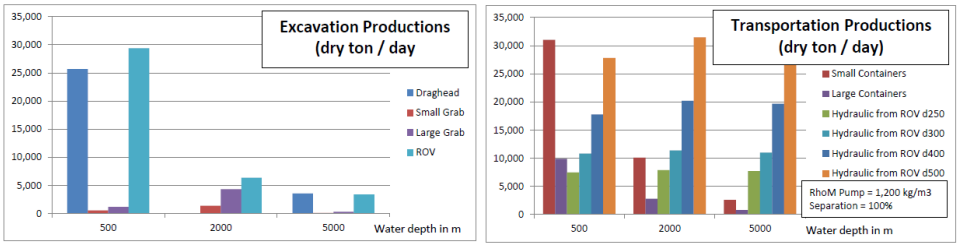

Figure 2.10: Capacity excavation and vertical transport system for the three different cases

Two variants of vertical transport were considered: hydraulic transport by centrifugal slurry pumps and mechanical lifting by containers. Within the variant of containers there also were two alternatives: continuous container lifting at an A-frame with a carrying capacity of 150 ton and normal lifting of two huge containers separately from each other by a heavy lift crane with a capacity of 500 ton. The composition of the hydraulic system differs since different amount of pumps and pump sizes were considered.

To make a comparison possible some low-diameter possibilities have been set out in figure (2.10). In both cases its assumed separation has already taken place on the sea floor and pure ore is transported. This is not valid for the alternative with a drag head at 500 m water depth, but in that variant there is no need to compare vertical transport mechanisms since the pumps needed for excavation / suction already cover most of the vertical transport.

The figure shows that the productions of mechanical transport decrease fast by decreasing water depths, and that continuous lifting (even at a smaller lift capacity) is more feasible than 'one-per-time' lifting with a heavier crane because of the higher lifting velocities that are possible. At 500 m water depth it could be a serious option if using centrifugal pumps would become difficult, but that does not seem to be the case since just 2 or 3 centrifugal slurry pumps would be required to cover that depth.

For the other two water depths it is already more difficult to use hydraulic transport since 5 to 15 centrifugal slurry pumps in series would be required. Since the production is limited by excavation, like can be seen in the figure, the continuous container lifting system would still suffice at 2,000 m and come close to the required production at 5,000 m.

A clear choice for vertical transport from water depths of 2,000 and 5,000 m cannot be made just based on productions. A more thorough research would have to be done into energetic efficiencies and practical application to determine that.

2.6 Conclusion

There is no doubt that deep sea mining offers interesting possibilities to Van Oord. It is however impossible to participate in this young industry without risks. Technical, financial, political and environmental issues as described in this chapter will offer challenges, but deep sea mining can offer work over a long term.

Multimillion investments will be required to adapt existing vessels like the jumbo hoppers or the larger flexible fall pipe vessels into mining vessels, making the decision to join the sea floor mining industry something that cannot be made without more detailed study. Using smaller vessels is not an option due to the open ocean conditions on most of the project locations.

Most promising of the studied cases in terms of feasibility is mining phosphorites by a jumbo TSHD with a separated suction tube, because of the low threshold in both financing and technique. The alternative of mining with an ROV from a flexible fall pipe vessel seems suitable for all 3 different working depths, making this a more all-round option for further studies.

The case studies show that feasibility depends a lot on mineral values, which are currently on record heights, but also on the choice for a certain mining technique. The use of bottom crawling ROVs at large water depths is most likely inevitable. When it comes to vertical transport the choice for a certain technique is not very obvious. Both centrifugal and mechanical lifting offer advantages and disadvantages, while companies like Nautilus and De Beers even use other techniques like airlifting and hydraulic lifting by a positive displacement pump.

A number of options was recommended to work out in more detail:

- case study of conversion of a jumbo hopper into a mining vessel with a separated suction tube, capable of mining nodules or sand at depths up to 500 m;
- case study of conversion of a flexible fall pipe vessel into a deep sea mining vessel capable of mining at depths between 500 and 5,000 m with one or multiple ROVs and a hydraulic riser system;
- Comparative study of the multiple possibilities in vertical transport systems over depths of 1,500 to 6,000 m.

The third option was selected to take place in this thesis, and will be elaborated in the next chapter.

Chapter 3

Vertical transport methods

One of the results of the deep sea mining feasibility study was that it was not possible to select the best vertical transport alternative for deep sea mining operations. It was recommended to perform a more thorough study regarding the vertical transport techniques which can be used at depths of over 1,500 m. The alternatives to be considered are:

- hydraulic lifting by multiple centrifugal slurry pumps;
- hydraulic lifting by a positive displacement pump;
- pneumatic lifting by airlift;
- mechanical lifting by a single bucket lift.

The methods will be described in theory, modelled and compared on basis of their energetic efficiency, and practical and theoretical limitations due for example occurring pressures and velocities.

A number of starting points for the parameters will be used in this comparative study. These points are based on the feasibility study described in the previous chapter, and give an overview of data needed to calculate the energy requirements of the transport methods. Some of these parameters are varied in the performance study to study their effect on the results.

- Targeted (minimum) solid production $M_S = 250$ ton/oh
- Liquid density for salt water $\rho_L = 1{,}030$ kg/m^3
- Solid density $\rho_S = 2{,}000$ kg/m^3 (SMS deposits) and 3,500 kg/m^3 (manganese nodules)
- Particle diameter (not crushed) $d_S = 10$ mm (SMS deposits) and 50 mm (manganese nodules)
- Water depth $h = 1{,}500$ - 6,000 m

3.1 Centrifugal slurry pumps

Centrifugal slurry pumps are the most common method for transporting material from sea floor to vessel in the dredging industry. Advantage over other types of pumps are the high efficiency, controllability of the flow and the ability to cope with abrasive flows. Multiple centrifugal pumps in series are required to transport the mixture over vertical distances of 1,500 meter or more.

A centrifugal pump is a rotodynamic pump. Rotodynamic pumps are generally used to obtain a high flow with limited pressure head. A rotodynamic pump converts the rotational kinetic energy, coming from the pump drive, to the hydrodynamic energy of a liquid flow by means of an impeller. The fluid enters the pump at the rotating axis of the impeller and is accelerated by the impeller, flowing outward into the chamber, from where it exits into the discharge pipe.

The difference between a centrifugal slurry pump used in dredging and other rotodynamic pumps lies in the large openings and limited number of blades, which allows for large particles to flow through, the simplicity of maintenance and replacement of wearing parts and the wear resistance of the parts itself. Functioning of a centrifugal slurry pump is extensively described in literature like by Van der Schrieck (van der Schrieck, 1999).

In practice there is a number of reasons why the theoretical pump curves are not met. The corrections for the frictional losses, which are velocity dependent, the entrance and impact losses of the flow and a correction for the finite number of blades, where circulation of the fluid between the blades takes place, giving a limitation on the impellers' efficiency.

These differences between theory and practice are hard to model, and for that reason the theory will be skipped in this part of the study. The most practical way to come to the efficiency of a riser system is by simply using an existing centrifugal slurry pump and scale it up or down to the right specifications according to known scaling rules.

3.1.1 Model

Modelling of the centrifugal slurry pumps is split up in 3 parts: first the behaviour of solid particles within the transport system is analysed, including their effect on the pressure loss in the riser system; then the effect of a centrifugal slurry pump on the transport system is taken into account by scaling an existing pump; and at last the energy use and the efficiency of the system are calculated.

Assumptions

A number of assumptions will be done to come to a model of a riser system consisting of centrifugal slurry pumps. Some of them are also valid for the other systems in this study. The assumptions are:

- there is no interaction between individual particles in the riser pipe, and therefore no clogging up;
- there is an endless supply of particles to the riser system in a fixed concentration;
- the workability of a single pump has a constant value, and when one pump fails the whole system fails.

The first assumption is subject to a different study done at Delft University of Technology, and is a subject of which too little is known to insert into the model here. Interaction in the form of collision between individual particles would cause a decrease in efficiency. A certain form of interaction is taken into account however, in case of the hindered terminal settling velocity of a particle, with which the velocity difference between solids and fluid will be calculated.

How the particles are supplied and in which concentration they flow in depends on the miner and the buffer system, which are different components of the mining system which will not be considered in this thesis. In practice the supply will never be in a fixed concentration.

For calculation purposes of transport by centrifugal slurry pumps in a horizontal discharge pipe in dredging operations a fixed workability value is assumed per pump. The real down- and uptime of a pump depends on a lot of factors which are accounted for by that single factor, which makes it a pretty rough estimate that can only be used in operations that last a long time, which is the case here.

Equations

The centrifugal pump model can be split up in 3 parts. First the pressure loss in the riser system is calculated for a certain production M_S. Secondly an individual pump is modelled and used to derive the pressure head it supplies and the amount of pumps which would be needed to propel the riser. Together they can be used to calculate the efficiency.

The pressure losses of the riser system $p_{r.loss}$ can be calculated using Eq. (3.1). This equation consists of a part related to the friction losses in the system, and a part for the geodetic head loss. The velocity / density term is split up in a separate term for the solids and for the liquids, which according to Shook (Shook and Bartosik, 1994) is applicable for vertical flow.

$$p_{r.loss} = (\xi_f + \xi_v\ h + \lambda \frac{h}{D})\ \frac{1}{2}\ (\rho_L\ C_L\ v_L^2 + \rho_S\ C_S\ v_S^2) + h\ g\ (\rho_M - \rho_L) \quad (3.1)$$

In this equation ξ_f is the factor for pressure losses which are independent from water depth, like inlet losses and acceleration, while ξ_v takes the water depth dependent losses into account, like the losses caused by valves which are applied every few hundred meters. Darcy friction factor λ is assumed to be of a constant value of 0.012 and forms the wall friction component of the pressure losses.

The velocity of the mixture v_M in the riser system is assumed to be equal to the velocity of the liquid v_L, which is a reasonable assumption for low solid concentrations. It can be derived from the given parameters for solid concentration C_S, solid density ρ_S, pipe diameter D (from which pipe area A follows), production M_S and the unknown transport factor α_t, using:

$$v_M = \frac{M_S}{\rho_S\ A\ \alpha_t\ C_S} \quad (3.2)$$

The transport factor α_t is used to take the difference between solid concentration C_S within the riser and delivered solid concentration $C_{S,d}$ into account, which is caused by the difference in velocity between solids and liquid. It can be calculated using Eq. (3.3).

$$\alpha_t = \frac{v_S}{v_M} = \frac{v_M\ -\ v_{S,th}}{v_M} \quad (3.3)$$

Assumed is the solid velocity v_S can be approximated by distracting the hindered terminal settling velocity $v_{S,th}$ from the mixture velocity v_M, which is reasonable when the mixture velocity and liquid velocity v_L can assumed to be equal. As both the transport factor α_t and mixture velocity v_M depend on each other the equations will have to be iterated until a constant value is reached.

To come to the hindered settling velocity $v_{S,th}$ first the terminal settling velocity of a non-spherical particle $v_{S,tn}$ is calculated. The particle which is settling in a quiescent liquid has a velocity which can be calculated using the balance between drag force (using drag coefficient C_D of 0.42) and gravity:

$$v_{S,tn} = \sqrt{\frac{4\ g\ d_S\ (\rho_S - \rho_L)}{3\ C_D\ \rho_L}} \tag{3.4}$$

The hindered terminal settling velocity $v_{S,th}$ depends on the particle Reynolds number Re_p, which itself also depends on the velocity of a particle. Iteration is required to come to a constant value. Terminal settling velocity $v_{S,tn}$ is used as the first input for calculation of the particle Reynolds number, in which μ_L is the dynamic viscosity of the liquid, in this case water:

$$Re_p = \frac{\rho_L\ v_{S,tn}\ d_S}{\mu_L} \tag{3.5}$$

The hindered terminal settling velocity $v_{S,th}$ is calculated by using Eq. (3.6), as given by Richardson & Zaki (Matousek, 2004). The dependency on the Reynold factor is expressed in the factor α_h, for which Eq. (3.7) was suggested by Wallis (Matousek, 2004). The obtained value of the hindered terminal settling velocity is then used to re-calculate the particle Reynolds number Re_p, using Eq. (3.5) again with $v_{S,th}$ replacing $v_{S,tn}$. The cycle repeats until a constant value for the hindered terminal settling velocity $v_{S,th}$ is reached.

$$v_{S,th} = v_{S,tn}\ (1 - C_S)^{\alpha_h} \tag{3.6}$$

$$\alpha_h = \frac{4.7\ (1 + 0.15\ Re_p^{0.687})}{1 + 0.253\ Re_p^{0.687}} \tag{3.7}$$

The amount of pumps N_p required to achieve a production M_S in transporting the mixture up over a vertical distance h is obtained from Eq. (3.8), with p_p being the pressure head the pump can deliver and α_f the Stepanoff factor which decreases this pressure head.

$$N_p = \frac{p_{r.loss}}{\alpha_f \; p_p} \tag{3.8}$$

To model the pressure p_p that can be delivered by a centrifugal dredge pump we use the specifications of an existing pump as input. The pump selected is a IHC HRCS 240-50-100 pump with a three blade impeller, which has a best efficiency point of 0.85, which will be used as value for the hydraulic efficiency η_h of the pump.

Water flow $Q_{L.0}$ and delivered pressure head $p_{p.0}$ related to this best efficiency point are 5.6 m^3/s and 577 kPa respectively. Original impeller diameter $D_{i.0}$ of the selected pump is 2.4 meter, related pipe diameter D_0 is 1.0 meter, while the revolutions have a value $n_{p.0}$ of 267 rpm.

Scaling rules are applied to obtain the pressure head for pumps related to a different pipe diameter:

$$p_p = p_{p.0} \; (\frac{D}{D_0})^2 \; (\frac{n_p}{n_{p.0}})^2 \tag{3.9}$$

To come to the new value for pump revolutions n_p first the new impeller diameter D_i has to be calculated, using Eq. (3.11). Maximum tip speed of the impeller v_{tip}, for a stable flow and low maintenance of the pump, is set on 34 m/s. With the newly obtained revolutions impeller diameter the revolutions are calculated:

$$n_p = \frac{60 \; v_{tip}}{\pi \; D_i} \tag{3.10}$$

$$D_i = \frac{D}{D_0} \; D_{i.0} \tag{3.11}$$

Another factor which influences the hydraulic efficiency η_h of the pump, and thus the pressure head p_p delivered by it, is the Stepanoff factor. This factor is related to the energy lost due to interaction, like collision, between the different particles in the pump and can be approximated by:

$$\alpha_f = 1 - \alpha_t \; (0.8 + 0.6 \; log(d_S)) \tag{3.12}$$

To calculate the efficiency η_e of the riser system the specific energy E_{spec} required to lift a certain amount of solids from sea floor to surface is calculated using Eq. (3.13), which is derived from dividing the power consumption of a single pump P_{pump} by the targeted production:

$$E_{spec} = N_p \ \frac{P_{pump}}{M_S} = N_p \ \frac{v_M \ A \ p_p}{M_S \ \eta_h} \tag{3.13}$$

With the energy consumed known the energy added to the solids has to be calculated: the potential energy E_{pot} in joule per kilogram. This is done by simply multiplying the solid mass m_S with the gravitational acceleration g and the height over which they are raised, divided by the same mass:

$$E_{pot} = \frac{m_S \ g \ h}{m_S} = g \ h \tag{3.14}$$

Energetic efficiency η_e is in this study defined as the difference in potential energy between the solids at sea floor and surface, divided by the energy requirement of the system. The efficiency is corrected by a factor which takes the Archimedes principle for lifting solids into account, by adding a form of the relative density into Eq. (3.15).

The efficiency of the pumps will in reality depend on the workability as well, as a higher amount of pumps will most likely cause more downtime. To take this into account in a simple way the workability factor α_w could be added per pump for which a value of 0.99 is assumed. The factor can be used to display the consequence of using more and more pumps in series in the results. The equation for the energetic efficiency η_e of the riser system becomes:

$$\eta_e = (1 - \frac{\rho_L}{\rho_S}) \ (\alpha_w)^{N_p} \ \frac{E_{pot}}{E_{spec}} \tag{3.15}$$

However, since for the other vertical transport systems workability will not be taken into account, the workability factor will not be used in the comparison between transport systems, which means that in the majority of this study a workability factor of 1,00 will be used.

Procedure

A number of steps are done to come from the equations in the last paragraph to the actual model, which will be explained in this paragraph. A number of input parameters is coded in such a way that it can be varied: water depth h, pipe diameter D, mixture concentration C_S, particle diameter d_S, solid density ρ_S and production M_S. The last three of these parameters are given in the starting points, but can be varied to see the effect.

The model consists of a number of steps:

1. The terminal settling velocity $v_{S,tn}$ of an individual particle is calculated
2. The effect of the concentration on the terminal settling velocity is taken into account, by first using $v_{S,tn}$ to calculate the Reynolds number, and in later iterations $v_{S,th}$. Using the Reynolds number and the concentration a new value of the hindered terminal settling velocity $v_{S,th}$ can be calculated, until it reaches a constant value (change in value is smaller than 10^{-3}.
3. The mixture velocity v_M is calculated, using a first assumption for transport factor α_t of 0.85. With this mixture velocity the transport factor can be calculated, which is used to re-calculate the mixture velocity. Iteration is applied until the change in transport factor is smaller than 10^{-3}. The mixture velocity is then used to calculate the pressure losses in the riser pipe.
4. Now the pressure losses are known the amount of pumps N_p can be calculated. First an existing pump is scaled up or down to the relevant diameter using the affinity rules and the Stepanoff factor, which represents a decrease in pressure build up inside the pump, is calculated. With these the amount of pumps required can be determined.
5. Both the potential energy and energy used by the lifting system can be calculated in joules per transported kilogram. Using the Archimedes-factor and a factor of the workability the energetic efficiency η_E is then calculated.

Appendix B.1.1 holds a flow chart which displays this procedure that is used to model the centrifugal slurry pump behaviour.

3.1.2 Performance

In this paragraph an attempt will be made to use the model as described in the last paragraph to come to a good design for a riser system consisting of multiple centrifugal slurry pumps. The influence of the different parameters on the design will be simulated to come to an efficient system. Starting points of the simulation are:

- solid concentration ρ_S is 2,000 and 3,500 kg/m^3;
- particle diameter d_S is 10 and 50 mm;
- pipe diameter D is 0.3 m;
- volumetric solid concentration C_S is 10%;
- production M_S is 250 ton/oh;
- water depth h is 2,000 m;
- workability factor α_w is 1.00.

During the study some parameters will be changed from the starting points to reach higher efficiencies. It should be kept in mind that the lifting system will be designed to obtain productions M_S of 250 ton/oh. If the targeted (average) production was to be higher another design for the system would have resulted from the study.

Crushing

Crushing can be defined as using mechanical energy to decrease the particle diameter d_S. In the past cycle of interest in deep sea mining this was one of the systems that gave problems, due to underestimation of forces required to crush rock under hyperbaric conditions. In this chapter the benefits of crushing to the efficiency of a riser system of centrifugal slurry pumps are analysed.

The efficiency curves for different particle diameters are displayed in figure (3.1) for both manganese nodules and SMS deposit, with particle diameters d_S of 50 mm and 10 mm respectively. Efficiency lies around 35% and 55% in case the original particle diameters for the respective resources are maintained.

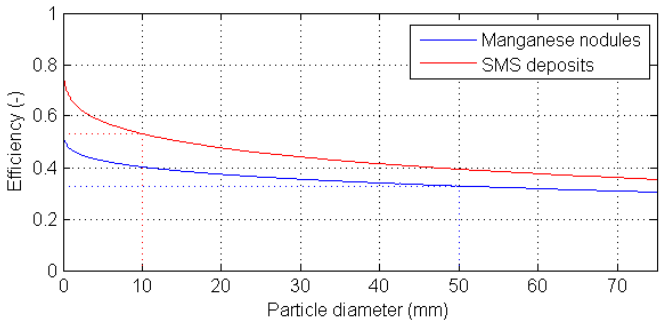

Figure 3.1: Effect of particle diameter d_S on the efficiency

Crushing could decrease the energy losses which are taken into account by the transport and Stepanoff factor. As can be seen in the figure the increase in efficiency would be around 15% if the particle diameters would be crushed to a particle diameter of 1 mm. In this calculation the energy needed for the crushing process itself is not taken into account, so the increase would be less in reality.

A decrease in fuel costs for vertical transport of around 15% might be worth wile in a later stage of development of the riser system, but will be dismissed for now. Difference between the two resources in the figure is mainly caused by the fact that for manganese nodules the system design is not yet as good as for SMS deposits. In the next paragraph this is elaborated further.

Mixture velocity

A change in mixture velocity v_M influences energy requirements in two ways: An increasing velocity decreases the energy losses caused by the velocity differences between solids and fluid (taken into account by factor α_t), while it increases the energy / pressure losses caused by friction. The mixture velocity, for a fixed production requirement M_S, can be influenced by altering either the pipe diameter D or the concentration C_S. The development of efficiency is computed for varying pipe diameters D, with the other parameters equal to the starting points. The result is displayed in figure (3.2).

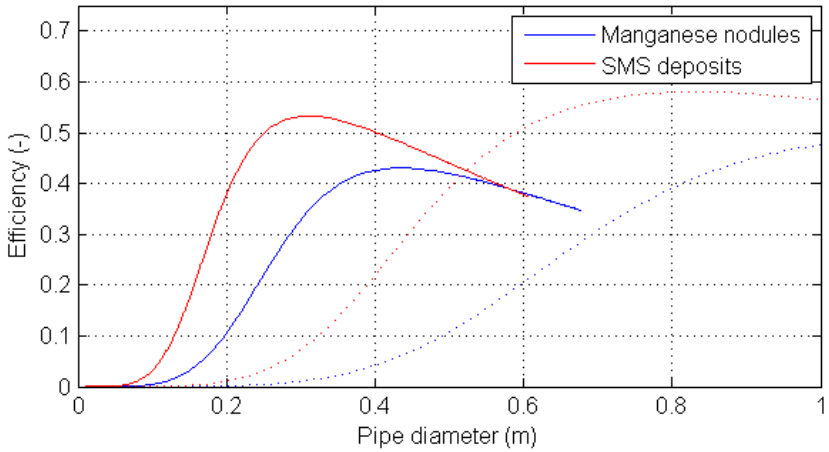

Figure 3.2: Effect of pipe diameter D on the efficiency

The steep part on the left side of the figure is caused by the increasing velocity v_M for a smaller pipe diameter D, needed to maintain a constant production M_S, which contributes to the 4th power to the pressure loss by friction. The gradual decrease right of the best efficiency point (optimum) is caused by the increase in energy required, which originates from a decreasing transport factor α_t. The figure also shows a similar (dotted) curve for a higher production M_S of 1,000 ton/oh, for which the optimum would be at a larger pipe diameter.

From the figure can be concluded that the starting point of a pipe diameter D of 0.3 m is a good first estimate for SMS deposits, but the other case study, manganese nodules, would benefit from an increase in pipe diameter D to 0.4 m. This difference in optimum explains the lower efficiency for manganese nodules in figure (3.1) for similar particle diameters. The fact the optimum is still lower for a large pipe is caused by the large particle diameter of the nodules.

Another option to vary the mixture velocity v_M is to vary the solid concentration C_S. At a constant pipe diameter D this will vary the required mixture flow Q_M to come to a certain production of solids M_S. The computation is displayed in figure (3.3) for the given starting points, with the exception that the pipe diameter D is increased to 0.4m for the manganese nodules.

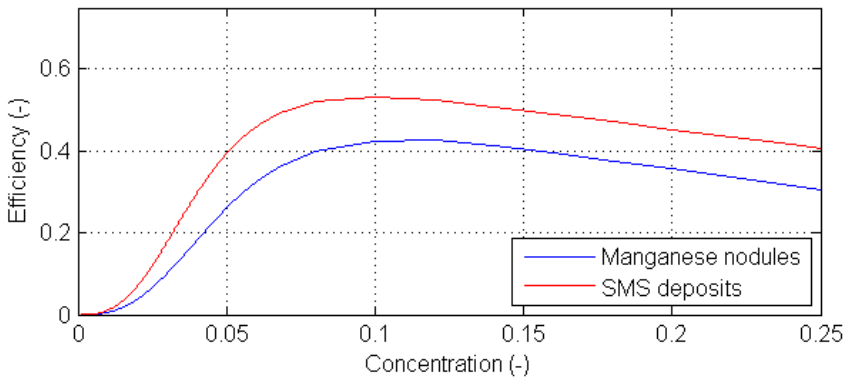

Figure 3.3: Effect of concentration C_S on the efficiency

The starting points for both solid concentrations C_S lies already at the optimum, due to the optimization with the pipe diameter. As alternative to increasing the pipe diameter D, increasing the concentration C_S is another way to reach the best efficiency point. Because higher concentrations will probably increase the possibility plugging occurs, increasing the pipe diameter has preference, but more in depth research into plugging should be done before these choices can be made permanent.

In practice the concentration will vary, but will lower the production M_S instead of increasing the energy losses, dismissing the need for a concentration value slightly above the best efficiency point.

Efficiency

The relation between efficiency, production and power consumption is displayed in figure (3.4) by varying production M_S. The targeted production of 250 ton/oh lies around the best efficiency point of the riser system, which means the parameters of the transport system do not require any further adaptation for now.

The curves are related to the parameters as used in the simulation, which means the starting points as given at the start of this paragraph, with the exception that pipe diameter D is increased to 0.4 m for mining manganese nodules.

The power consumption of circa 2 MW for lifting the targeted production over 2,000 m seems reasonable from a practical point of view. The fact that the power requirement for both resources is almost equal is caused by the increase in pipe diameter D for manganese nodules. The higher losses due to the Stepanoff factor is compensated by the lower velocity required in the riser to come to the same production.

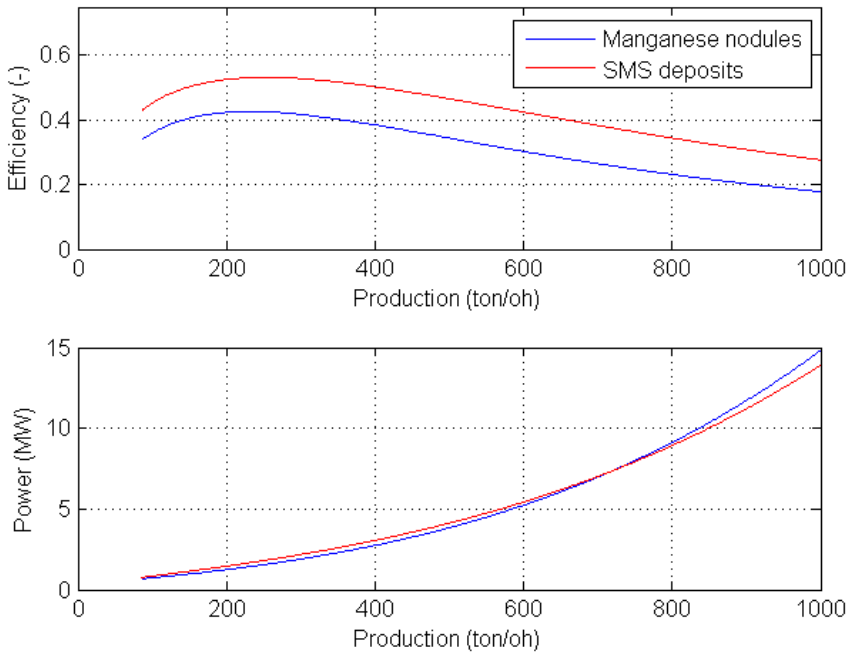

Figure 3.4: Energetic efficiency and power requirement for production

Figure (3.5) shows the causes for efficiency losses for transporting of SMS deposits from a depth of 2,000 m, with the starting points as parameters.

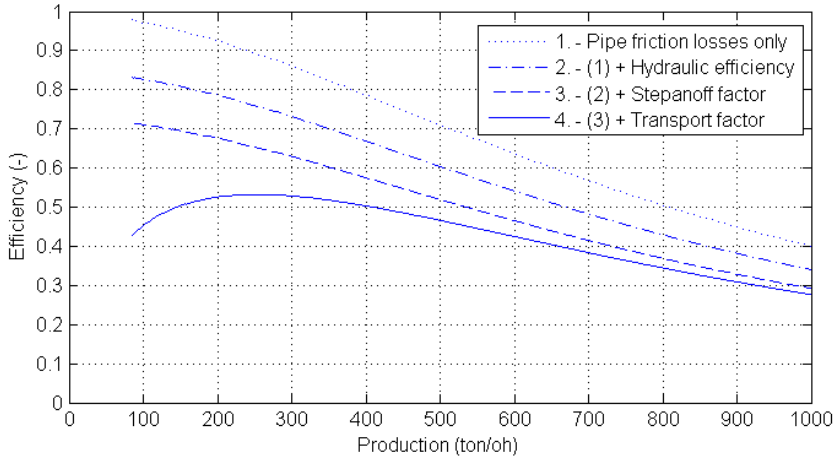

Figure 3.5: Factors influencing efficiency loss

The figure shows that both the efficiency losses due to the hydraulic efficiency of the pump and the Stepanoff factor are almost constant for varying productions. Variation in the efficiency losses are mainly caused by either the transport factor α_t or the (wall)friction losses in the riser.

The transport factor is an important factor when the productions are low, which means the velocity at which both liquid and solids flow upwards are relatively low, leading to a larger transport factor and larger efficiency losses due to the velocity difference. At higher velocities the absolute velocity difference will have the same value, but will relatively be lower in comparison to the absolute liquid velocity, leading to a smaller transport factor.

The losses due to (wall)friction are related to the velocities, as can easily be distinguished from Eq. (3.27). The effect on the efficiency loss is the opposite of to the transport factor, with higher velocities leading to higher friction losses and thus a higher efficiency loss.

Varying the water depth at which the pump works can effect the efficiency in two ways, but only the first one can be seen in figure (3.6). The figure shows that the efficiency is decreasing fast for low values of the water depth h, which does not seem very logical at first. This is caused by the fixed pipeline losses ξ_f, which is independent of depth because of acceleration and inlet losses and thus very influential at small water depths.

If the workability is neglected the efficiency is constant at water depths of a 1,000 m or more, as the figure shows:

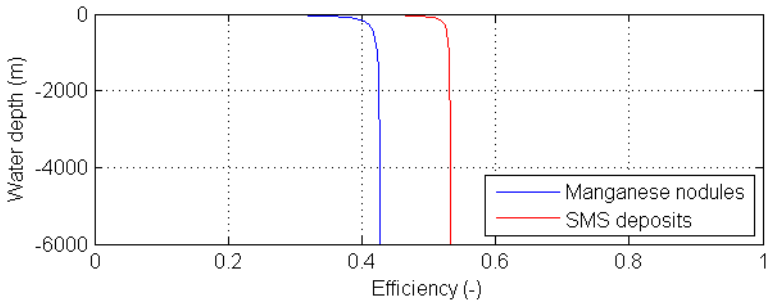

Figure 3.6: Energetic efficiency of the centrifugal pump system over depth without workability factor

The workability factor is taken into account to show the second effect of water depth on efficiency, as can be seen in figure (3.7), by changing the value from 1 to 0.99. Because multiple pumps will have to be used for increasing water depths the workability of the system as a whole will decrease. Efficiency of the riser system decreases gradually with depth as the amount of pumps required increases.

Important is to keep in mind that in this model productions do not decrease or require more energy during the downtimes of a pump, but there will be no production at all. In practise bypasses will be used to keep the system going, which would increase the overall the efficiency.

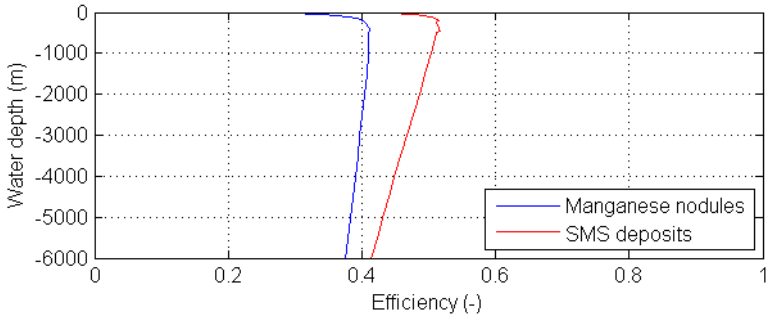

Figure 3.7: Energetic efficiency of the centrifugal pump system over depth including workability factor

Pressures

The pressure that occurs inside the pipe, and with that the difference in pressure between out- and inside the pipe, depends on the spread of the pumps over the water depth. Multiple pumps right next to each other in series are not very practical, because the pressures occurring inside the pump will become too high. Two to four pumps in series are still possible depending on generated pressure and strength of the pump casing, but in this study a gradual spread of the pumps over depth will be used.

In figure (3.8) three different pressures are displayed over water depth: the absolute water pressure; the absolute pressure in the pipe line, consisting of water pressure plus the pressure provided by pumps minus the friction losses; and the relative pressure (difference between the two other pressures). The water pressure outside the pipe is given by simply multiplying water depth h with water (liquid) density ρ_L and gravitational acceleration g and adding the atmospheric pressure p_{atm} of 0.1 MPa.

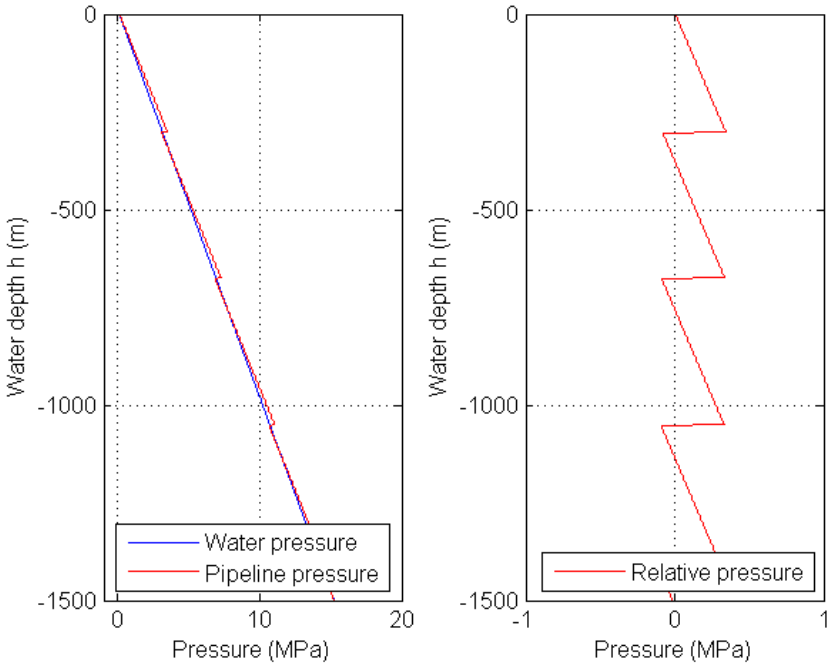

Figure 3.8: Pressure in the riser system (ρ_S of 2,000 kg/m^3 / d_S of 0.05 m)

Both the relative and the absolute pressure occurring in the pipeline are relatively low due to the gradual spread of centrifugal pumps over depth. A depth of 1,500 m is used for the computation to make the figure clear. In this case 4 pumps will be required with a power requirement of about 700 kW per pump. A larger water depth would have the same effect, but with a higher water and pipeline pressure.

3.2 Positive displacement pump

A positive displacement pump is a pump that makes a fluid move by trapping a certain volume of it in a chamber, and forcing the fluid into a discharge pipe by a displacement in or of that chamber. Within the group of positive displacement pumps there is further classification based on the mechanisms that cause the displacement:

- rotary type positive displacement, in which a rotating motion of for example an impeller causes the displacement within the fixed chamber;
- linear type positive displacement, in which a lifting device moves the chamber itself through a suction pipe;
- reciprocating type positive displacement, in which a reciprocating motion of a piston or diaphragm in a fixed chamber causes the displacement.

The reciprocating type, and then in particular the diaphragm pump, is the type which will be considered for this study.

The diaphragm pump can be further categorized based on the cause of the displacement. The diaphragm in the chamber which causes the displacement can be propelled by either a mechanical force like a motor, or by another fluid which is supplied by another pump.

In this study both types will be considered, but at different locations and simultaneously used. The first type, with a mechanical force propelling the diaphragm, is located on the mining vessel and will be used to pump water down to the second pump. The water which is pressurized and pumped down by the first pump is the fluid which propels the second pump. This second pump pumps the mixture flow of water and solids up towards the mining vessel.

A schematization of this system can be found in figure (3.9). Advantage of this system is the lack of a motor, and with that a lot of moving parts that might require maintenance, at great water depth and a nearly closed system with regard to the water movement, which is interesting for environmental reasons. Disadvantage would be the large pressure difference within the pump and between the riser and its surroundings. In practice the pump on the vessel can easily be replaced by other types of pumps, so main focus of this study will be on the underwater diaphragm pump.

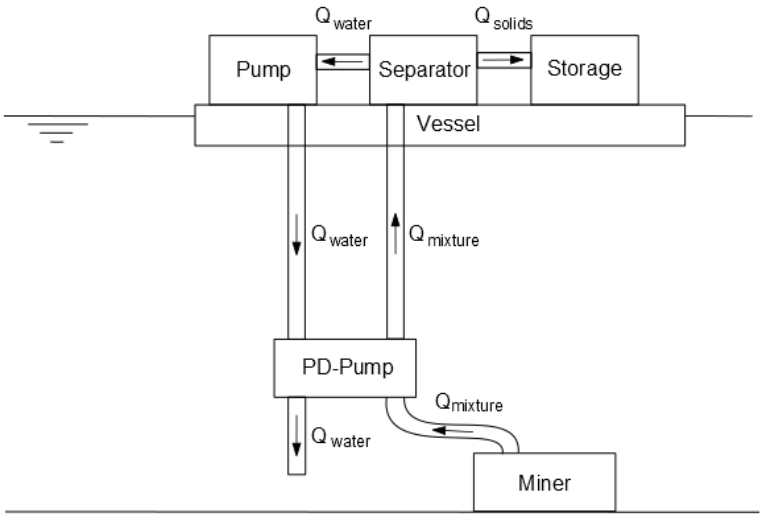

Figure 3.9: Schematization mining vessel with diaphragm pump

3.2.1 Theory

The theory on how the diaphragm pump works is explained in this paragraph. How the pump works in practice and how it is modelled will be elucidated in the next paragraph. In figure (3.10) a schematization is given of the working of the diaphragm pump. It can be split up in four phases, which repeat continuously.

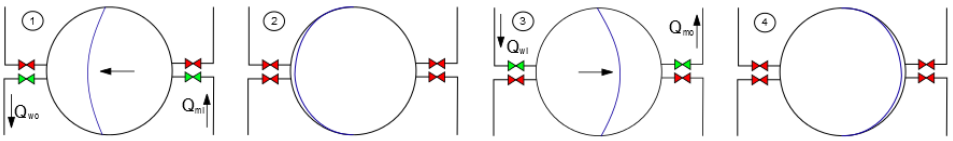

Figure 3.10: Schematization diaphragm pump

1. Mixture is pumped in from the mining unit at the sea floor into the mixture section (right side of the chamber in the figure) of the diaphragm pump. In this process the water content in the other side of the chamber is pumped out into the sea. But because the water pressure in this section of the chamber is higher than the pressure of the mixture that is pumped in, first the water will decompress and flow out, without mixture being able to flow in.

2. The diaphragm pump is completely filled with mixture and the lower valves of the pump are closed. The diaphragm is completely extended towards the water inlet. The mixture has the pressure with which it was pumped in by the pump on the mining unit.

3. The upper valves of the diaphragm pump are opened. The pressure difference between the water and the mixture column allows water to flow into the water section of the chamber again, moving the diaphragm to the right. Initially this does not cause flow of the mixture, because the pressure in the mixture column is a lot higher than the mixture pressure in the chamber, but the mixture is compressed. After the point is reached at which the mixture pressure is equal to the pressure in the mixture column the mixture starts flowing into the pipeline.

4. The diaphragm pump is completely filled with water and the valves of the pump are closed. The diaphragm is completely extended towards the mixture inlet. The water has the pressure with which it was pumped in by the pump on the surface vessel, which is a lot higher than the surrounding water pressure.

Figure (3.11) shows the theoretical change in mixture and water flow over time during the process as displayed in figure (3.10) (Miller, 1995). The losses of valve delay and (de-)compression are slightly exaggerated in time in the figure.

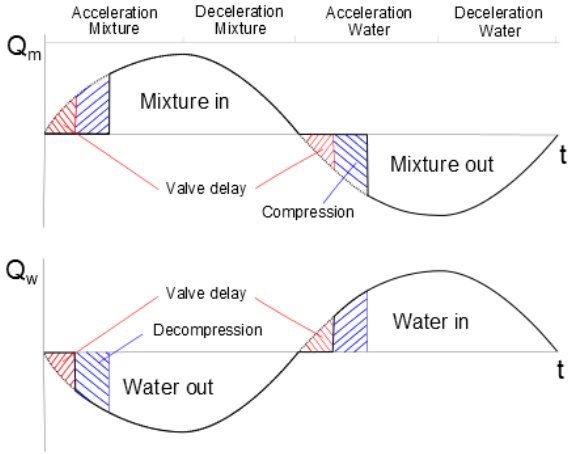

Figure 3.11: Flow diaphragm pump

At the start the chamber is completely filled with water and the valves are closed. The water inside the chamber has a higher pressure than the water outside. When the valves are opened the water starts flowing out. The valves themselves cause the first delay in flow, because the valves are not completely open instantly.

At the point when the mixture pressure which is pumped in from the miner reaches a value higher than the water pressure in the chamber, the mixture accelerates and starts flowing in. Because of the flow the difference in pressure between both sides in the chamber is decreasing, which at some point causes deceleration of the mixture flow inwards. When the velocity inward becomes zero the valves are closed again.

The mixture inside the chamber has the pressure it was pumped in with from the mining vessel. When the other valves are completely opened for the next time step, the water starts flowing in with a relatively high pressure. The mixture pressure in the riser pipe is a lot higher than the mixture inside the chamber, so the mixture will first compress when the mixture pressure inside the chamber increases. When the mixture pressures are equal to each other the mixture will start flowing out into the riser pipe. When the chamber is completely filled with water the valves close again and the cycle repeats itself.

3.2.2 Model

Assumptions

To model the underwater diaphragm pump a number of assumptions are done. These are:

- valve delay is neglected;
- compression delay is neglected;
- pressure at the in- and outlet are constant;
- pressure difference is equal for both phases;
- friction losses for in- and outflow are equal;
- change in mass of the chamber content is negligible for acceleration calculations.

The delay caused by opening the valve can be neglected, since this time period in a small diameter pipe is very short in comparison to the time required to fill the chamber. The time to fill the chamber will be more than a few seconds, while the closure time for a valve is typically between 0.01 and 0.05 seconds, at least a factor 100 smaller, which makes it indeed negligible.

The other delay, caused by decompression and compression of the fluid can be neglected as well. The compression of water can be calculated by:

$$\frac{\Delta V_L}{V_L} = \frac{\Delta p}{K_B} \tag{3.16}$$

The pressure p inside the pump at 6,000 m water depth for given concentration C_S and targeted production M_S is estimated to be around 10 MPa, which will be verified later on in this chapter. At a bulk modulus K_L for water of 2,200 MPa this leads to a decrease in volume of 0.5%, which is negligible.

The pressures at the inlet side $p_{p.in}$ and outlet side $p_{p.out}$ of the pump are not constant, but varying depending on the pressure build up by the two supply pumps and the flow through the discharge pipes. The use of multiple chambers will damp this fluctuation directly before and after the pump. The fluctuation size will be studied in more detail in a later chapter.

The friction losses over the in- and outlet of the pump are hard to determine in a theoretic way, and can best be analysed by testing them in practice. The assumption that these have a value which is equal for in- and outlet, an dependent on a constant value of the friction coefficient ξ_c, is acceptable as long as the pressure loss over the pump is low in comparison to the pressure loss of the complete system, which is the case when working at large water depths.

The change in mass of the chamber content m_c is the only assumption which could be considered questionable. The mass directly influences the acceleration of the fluid in the pump chambers and with that the flow. What the effect is on the flow should be taken into account when a more advanced model is made, but in this research an average value of the two densities, ρ_L and ρ_M, will be used for calculation of the mass.

Equations

Modelling of the diaphragm pump will be based on the balance of the force over the pump. With a constant fluid pressure on both sides of the pump a constant force will be working inwards through the openings with an area A_c. The flow into and out of the pump causes a pressure loss $p_{p.loss}$ and with that a friction force $F_{p.loss}$. The remaining force ΔF_p , which is the difference between the inlet force and the friction and outlet force, works on the fluids inside the pump and the diaphragm and can be calculated by:

$$\Delta F_p(t) = F_{p.in} - F_{p.loss}(t) - F_{p.out} = \frac{p_{p.in} - p_{p.loss}(t) - p_{p.out}}{A_c} \tag{3.17}$$

A_c is the inlet area of the chamber in this equation. When the valves are opened the velocity of the fluid inwards is 0. Since the loss in pressure depends on the velocity this also has a value of 0. At that point the remaining force ΔF_p causes an acceleration of the fluid and thus the velocity increases. This causes the pressure loss $p_{p.loss}$ to increase in time, which decreases the remaining force ΔF_p until it reaches 0. The relation between the pressure loss and fluid velocity v_F is:

$$p_{p.loss}(t) = \xi_c \frac{v_F(t)^2}{2}\rho_M + \xi_c \frac{v_F(t)^2}{2}\rho_L = \xi_c \frac{v_F(t)^2}{2}(\rho_M \ + \ \rho_L) \tag{3.18}$$

The velocity of the flow can be calculated by simply applying the second law of Newton to come to the acceleration, and then integrating it. In Eq. (3.19) the assumption of a constant mass of the fluid inside the chamber m_c is used.

$$a_F(t) = \frac{\Delta F(t)}{m_c} = \frac{\Delta F(t)}{V_c \, \frac{\rho_S + \rho_L}{2}} \tag{3.19}$$

$$v_F(t) = \int a_F(t) \; dt \tag{3.20}$$

The maximum velocity $v_{F.max}$ is reached when the remaining force ΔF, and thus the acceleration a_F, is 0. The maximum value can be calculated by:

$$v_{F.max} = \sqrt{2 \, \frac{p_{p.in} \; - \; p_{p.out}}{\xi_c(\rho_M + \rho_L)}} \tag{3.21}$$

Now the evolution of the velocity over time is known the fluid flow inwards and outwards (of either water or mixture) is determined:

$$Q_F(t) = v_F(t) \; A_c \tag{3.22}$$

The volume of the inwards flowing fluid that is inside the chamber at a certain moment can be composed by integrating the flow Q_F. So far an unlimited flow was considered, but the size of the chamber V_c is the maximum value which can be held inside the pump before the next phase commences. In some cases the maximum flow will not be reached because of this limit.

$$V_F(t) = \int_0^t Q_F(t) \; dt \tag{3.23}$$

$$V_{F.max} = V_c = \frac{1}{4}\pi D_c^2 \tag{3.24}$$

The position x_d, velocity v_d and area of the diaphragm A_d can be calculated now the development in time of the fluid volume V_F is known. Based on spherical geometry first the diaphragm position x_d in relation to the center line of the chamber is determined. Simple differentiation then leads to the velocity:

$$V_F(t) = \frac{\pi\ x_d(t)}{6}\ (x_d(t)^2\ +\ 3\ (\frac{1}{2}D_c)^2) \tag{3.25}$$

$$v_d(t) = \frac{d(x_d(t))}{dt} \tag{3.26}$$

The same spherical geometry can be used to compose the size of the diaphragm area A_d in time:

$$A_d(t) = \pi\ (x_d(t)^2\ +\ (\frac{1}{2}D_c)^2) \tag{3.27}$$

The behaviour of one diaphragm pump chamber is now modelled, and is used to get to values for the average mixture flow of the complete pumping system Q_M, which is using multiple chambers. The various pump chambers are put out of phase of each other to minimize the peaks in pressure and mixture flow.

With the pressure losses and total flow in the pump known the pressure losses along the rest of the system can be modelled. The lower part of the vertical riser, the flow of mixture into the PD-pump and flow of water into the ocean, will be neglected in these calculations since this is considered as part of the excavation system.

Equation (3.1) until Eq. (3.7) are then used, using the average value of the flow velocity, to determine the velocity of the solids in the riser system v_S, and thus the production. Efficiency η_E follows again from:

$$\eta_E = (1 - \frac{\rho_L}{\rho_S})\ \frac{E_{pot}}{E_{spec}} \tag{3.28}$$

In which E_{pot} can be calculated using Eq. (3.14) and E_{spec} can be calculated with:

$$E_{spec} = \frac{Q_F\ p_r}{M_S\ \eta_p} \tag{3.29}$$

The symbol η_p in this equation is the efficiency of the positive displacement pump on deck which delivers the pressure p_r and the flow Q_F to the riser. A constant pump efficiency η_p with a value of 0.9 will be used in the model, but the deck pump itself is not subject of this research.

Procedure

A number of steps are done to come from the equations in the last paragraph to the actual model, which will be explained in this paragraph. A number of input parameters is coded in such a way that it can be varied: water depth h, pipe diameter D, mixture concentration C_S, pressure loss over the pump $p_{p.loss}$, particle diameter d_S, solid density ρ_S and production M_S. The last three of these parameters are given in the starting points, but can be varied to see the effect.

The model consists of a number of steps:

1. the force balance over one single pump chamber is used to calculate the development of the unlimited flow inwards and outwards of the chamber;
2. the flow and the volume of the chamber are used to calculate the time required to fill the chamber, including the position and velocity of the diaphragm over time;
3. the particle settling velocities $v_{S,tn}$ and $v_{S,th}$, transport factor α_t and pressure loss in the riser p_r are calculated in a similar way to for centrifugal pumps;
4. potential energy per kilogram and required energy E_{spec} are again calculated (this time not involving Stepanoff or the workability) to come to the energetic efficiency.

Appendix B.1.2 holds a flow chart which displays this procedure that is used to model the diaphragm pump behaviour.

3.2.3 Performance

In this paragraph an attempt will be made to use the model as described in the last paragraph to come to a good design for a riser system with a positive displacement (diaphragm) pump. The influence of the different parameters on the design will be simulated to come to an efficient system. Starting points of the simulation are:

- solid concentration ρ_S is 2,000 kg/m^3;
- particle diameter d_S is 10 mm;
- production of solids M_S is 250 ton/oh;
- pipe diameter D is 0.3 m;
- volumetric solid concentration C_S is 10%;
- chamber inlet diameter D_c is 0.15 m;
- water depth h is 1,500 m;
- friction loss coefficient ϵ_c is 0.75
- pressure difference over the pump Δp is 1 MPa

These values are based on the pump procured by Nautilus to function in the Solwara deep sea mining project, and during the study some parameters will be changed from the starting points to reach higher efficiencies. Only the case study of SMS deposits is studied at first to show the effects of the different parameters.

It should be kept in mind that the lifting system will be designed to obtain productions M_S of 250 ton/oh. If the targeted (average) production was to be higher another design for the system would have resulted from the study.

Flow

For the given starting points the maximum value of the velocity and flow will not be reached, because the pump chamber will already be filled before that, as can be seen from figure (3.12).

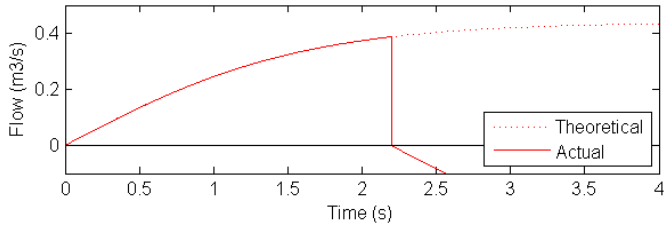

Figure 3.12: Flow diaphragm pump

The flow through one pump chamber over time is displayed in figure (3.13). The curve has similarities to (3.11), but because a constant pressure is assumed over the pump there is no deceleration. Negative values represent outflow.

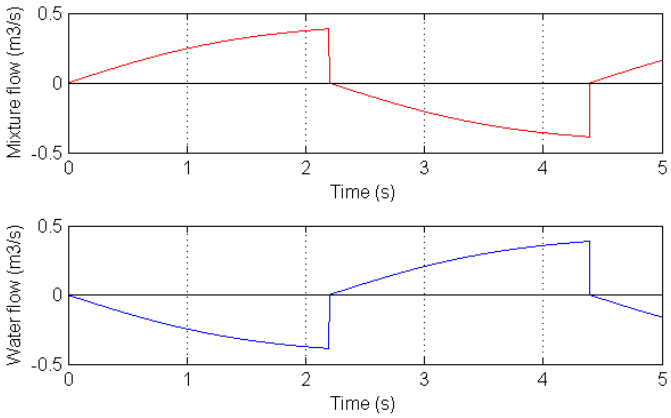

Figure 3.13: Mixture flow (top) and water flow (bottom)

The cumulative flow of mixture into the discharge pipe, for 8 pump chambers working out of phase, is displayed in figure (3.14). The use of 8 pump chambers damps the effect fluctuation of mixture flow, which prevents extra losses in pressure by deceleration and re-acceleration of the flow in the mixture pipe.

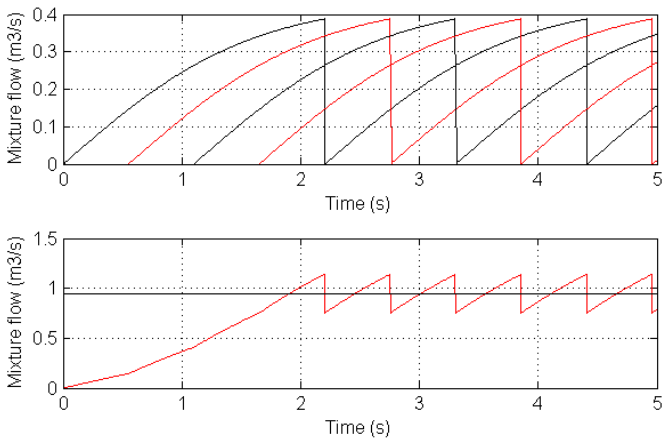

Figure 3.14: Flow (top)and cumulative flow (bottom) of mixture into the mixture pipe

The effect of the amount of pump chambers on the fluctuation in flow is set out for a number of pump chambers in figure (3.15), including a curve that displays the tendency of fluctuation decrease.

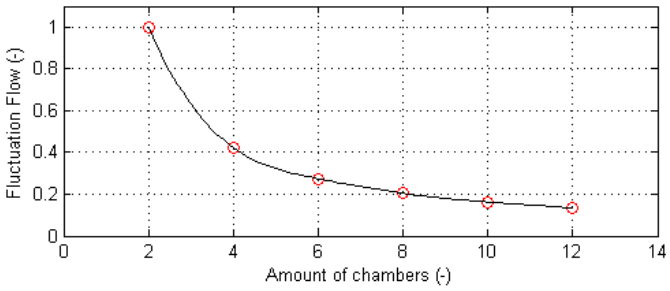

Figure 3.15: Flow fluctuation for number of chambers

For 8 pump chambers the fluctuation is around 20%, which seems to be an acceptable limit. Increasing the number of chambers to 12 would decrease the fluctuation by just 5%. Further research into the effect of the fluctuation on the pressure and velocity in the discharge pipeline would have to be done in more advanced research, but expected is the effect of the fluctuation dies out after a certain distance into the discharge pipe.

Pump pressure

The simultaneous working of the pump chambers also results in a pressure fluctuation, which was assumed to be negligible. In figure (3.16) the cumulative pressure loss required for functioning of the pump system like modelled is displayed.

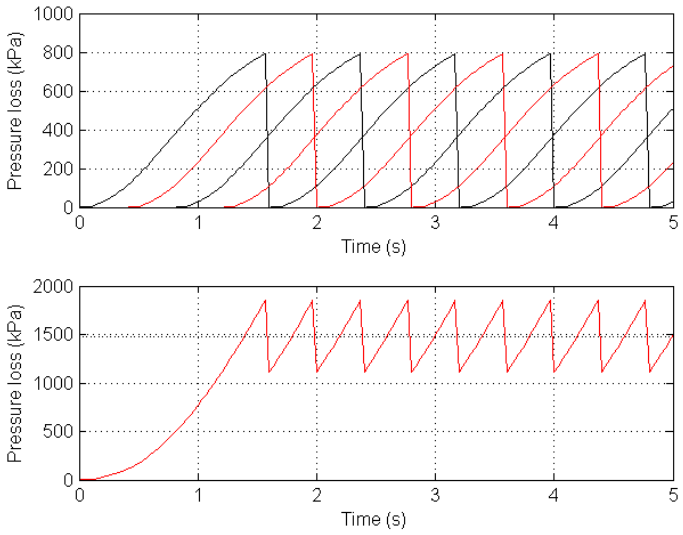

Figure 3.16: Pressure (top) and cumulative pressure difference (bottom)

The average cumulative pressure difference is 1.5 MPa, which is higher than used as input for the simulation as given in the starting points. This can be corrected by reducing the friction coefficient ξ_c to 0.45. 0.45 is a relatively low value, and whether it is realistic as friction coefficient is something which will have to be deduced from experiments and more advanced research.

As can be seen in figure (3.17) this results in a value for the pressure difference which is closer to the input factor of 1 MPa difference over the pump.

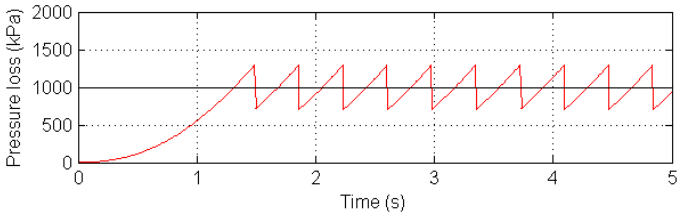

Figure 3.17: Cumulative pressure difference

In case 8 pump chambers are used the fluctuation is around 30%, as can be seen in figure (3.18). Increasing the number to 12 chambers would decrease the fluctuation by 10%. Further research into the effect of the pressure fluctuations on the pressure and velocity in the discharge pipeline would have to be done in more advanced research, but expected is, just like for the flow fluctuation, the effect of the fluctuation dies out after a certain distance into the discharge pipe.

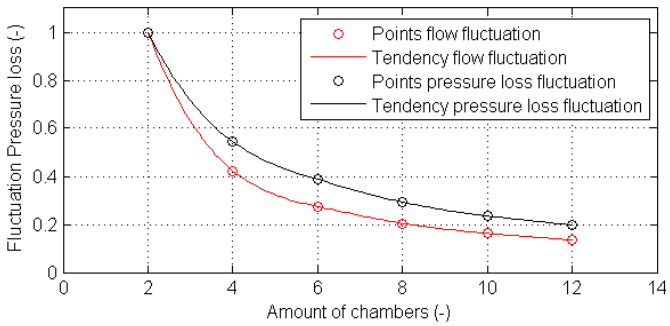

Figure 3.18: Flow and pressure fluctuation for number of chambers

Diaphragm

The diaphragm changes shape while reciprocating between the two sides of the pump chamber, as is clear from figure (3.10). The area of the diaphragm decreases from $2\pi(\frac{1}{2}D_c)^2$ in extreme position to $\pi(\frac{1}{2}D_c)^2$ when it is in the centreline of the chamber. In figure (3.19) the change in area size over position is given.

In the same figure the velocity of the diaphragm is displayed. The velocity will gradually increase at first, caused by an increasing flow into the pump. Difference between the tendency of the ingoing flow and velocity of the diaphragm originates from the fact that the chamber volume increases less per distance the closer the diaphragm approaches the centreline of the chamber.

After the centreline is reached the reverse process happens, but with a still increasing flow, until the chamber is filled.

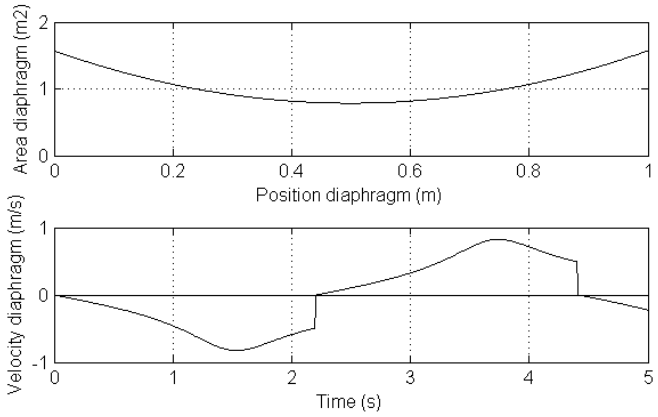

Figure 3.19: Area diaphragm per position and velocity diaphragm over time

Combing the two diagrams in figure (3.19) gives the position of the diaphragm in time. In figure (3.20) this movement can be found.

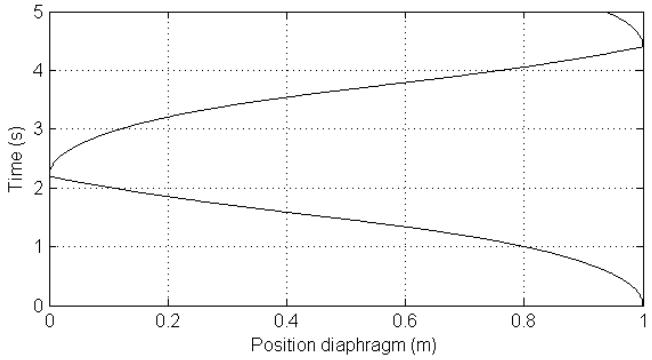

Figure 3.20: Position diaphragm in time

Efficiency

The efficiency of the system depends on more than just the pump. In figure (3.21) the efficiency is displayed for a variation of pressure losses over the pump which are used as inputs of the model. The assumed pressure difference of 1 MPa would give a very low efficiency. This is caused by the fact that a high pressure difference causes a high flow and thus a high velocity in the discharge pipeline, which makes for high friction losses.

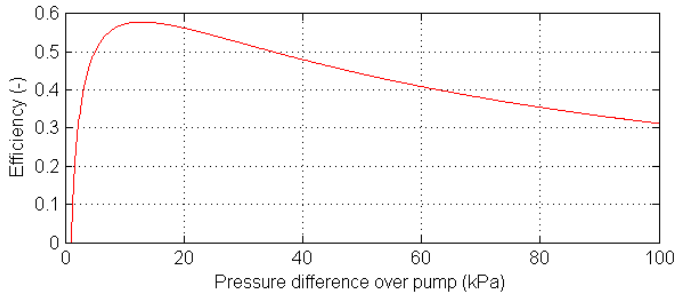

Figure 3.21: Efficiency for pressure lost over the pump

A pressure loss over the pump in the range of 10 to 30 kPa gives a more efficient system and is used to see how varying other parameters of the model could increase the efficiency, in an almost similar way as is done for centrifugal pumps, where the varying parameters were compared to the specific energy requirement.

The first parameter which is varied is the pipe diameter D, which is equal for both the discharge side transporting mixture as the supply side which transports water. A pressure loss over the pump of 20 kPa is used as input for the model.

As can be expected the diameter used earlier, 0.3 m, lies around the best efficiency point. This is a consequence of using a pressure loss of 20 kPa as input, because both are related to the flow velocity. What is more interesting is to see that a choice of a pipe diameter has a large influence on the efficiency. Decreasing the pipe diameter to 0.2 m would decrease the efficiency by a factor 2.

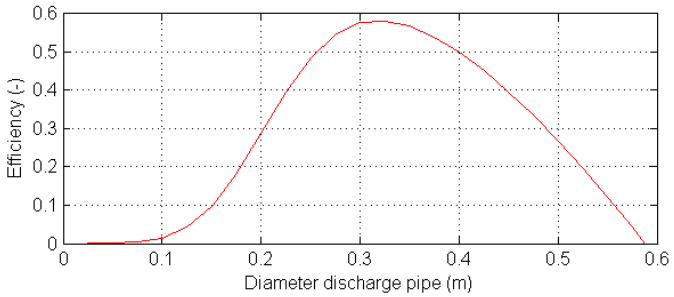

Figure 3.22: Variation diameter discharge pipe for efficiency

Another parameter which could be varied is the solid concentration C_S. In figure (3.23) the effect of varying it on the efficiency is shown. It is clear increasing the concentration would increase the efficiency, according to this model. In reality the concentration can not be increased limitless without increasing the risk of clogging up the pipeline or extra friction losses caused by interaction between the particles. An upper limit in solid concentration of 20% is assumed and used in further calculations.

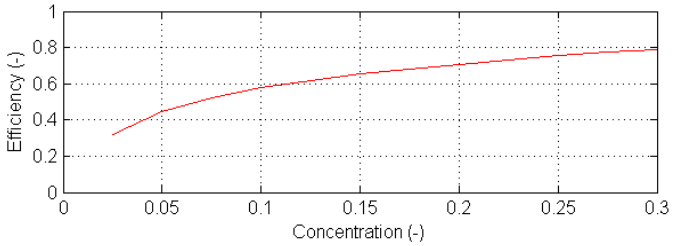

Figure 3.23: Influence solid concentration on efficiency

The relation between efficiency, production and power consumption is displayed in figure (3.24), computed for a water depth of 1,500 m. The targeted production M_S of 250 ton/oh lies around the best efficiency point which means the parameters do not require any further adaptation. The power consumption of 0.75 MW seems reasonable from a practical point of view.

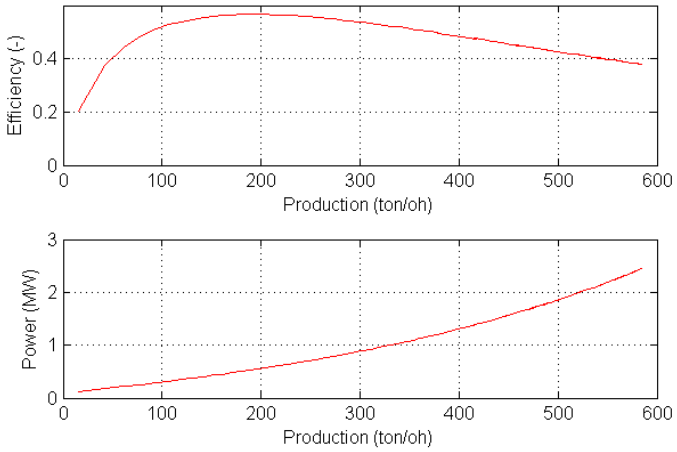

Figure 3.24: Relation production and efficiency / power consumption

Varying the water depth at which the pump works does not effect the efficiency much, as soon as the water depth is larger than 1,000 m, since both the potential energy and depth-dependent friction losses increase linearly with increasing water depth. At smaller water depths the pressure loss over the pump and the depth-independent friction losses, like losses at the inflow, influence the efficiency in a similar way as for a centrifugal pump.

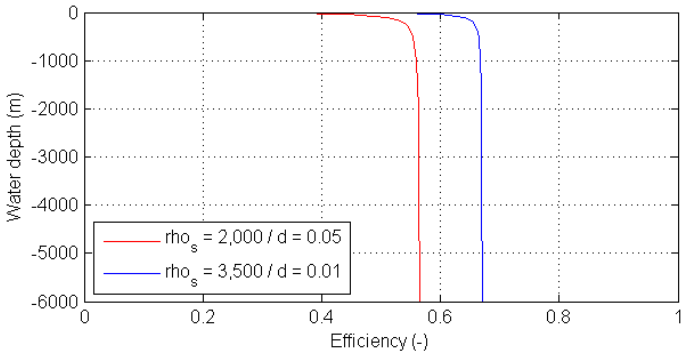

Figure 3.25: Efficiency over water depth

Pressures

The pressure in both pipelines is expected to be substantially higher for a PD-pump than for a centrifugal pump, since the PD-pump on deck will have to deliver sufficient pressure to the water to transport it down, transfers the pressure to the mixture in the diaphragm pump, and then transport the mixture up to the surface.

Figure (3.26) shows the development of pressure over the riser system, for the case of manganese nodules with a solid density ρ_S = 2,000 kg/m^3 and a particle diameter d_S of 0.05 m, with a pump at 5,000 m water depth. On the left side the pressures in the water supply pipe are shown and on the right side the pressure in the mixture discharge pipe. The two top diagrams show the absolute pressure of both the fluid inside the pipe and the outside water pressure, while the bottom diagrams show the relative pressure, the difference between the two absolute pressures.

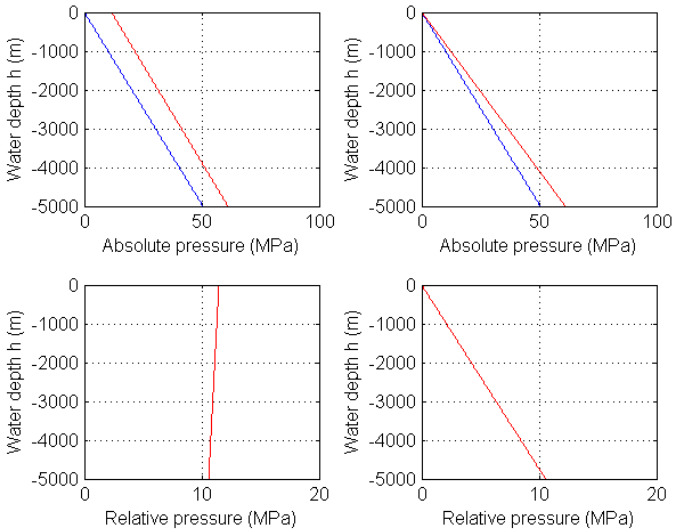

Figure 3.26: Pressure development over the mining system for mining manganese nodules from a water depth of 5,000 m

The development of the relative pressure is probably most interesting to the design of the riser system. A pressure difference of over 10 MPa requires a supply and discharge pipe which are able to handle these high pressures. Valves within the diaphragm pump will also have to cope with these pressures.

These pressures are occurring during normal operations. Peak values because of internal waves caused by valve closure might be a lot larger and should be subject to more advanced research and modelling.

The other case study, mining SMS deposits with a solid density of $\rho_S =$ 3,500 kg/m^3 and a particle diameter d_S of 0.01 m, gives even higher pressures during normal operations when the pump is applied at 5,000 m. The relative pressure would roughly be doubled. In reality the resources to which this case study relates are not found on water depths of more than 2,000 m and at that depth the values for the relative pressure are below the values found for the first case study at 5,000 m depth.

Figure (3.27) displays the results of the pressure over a the riser system for the case study, $\rho_S =$ 3,500 kg/m^3 and a particle diameter d_S of 0.01 m, at a pump depth of 1,500 m.

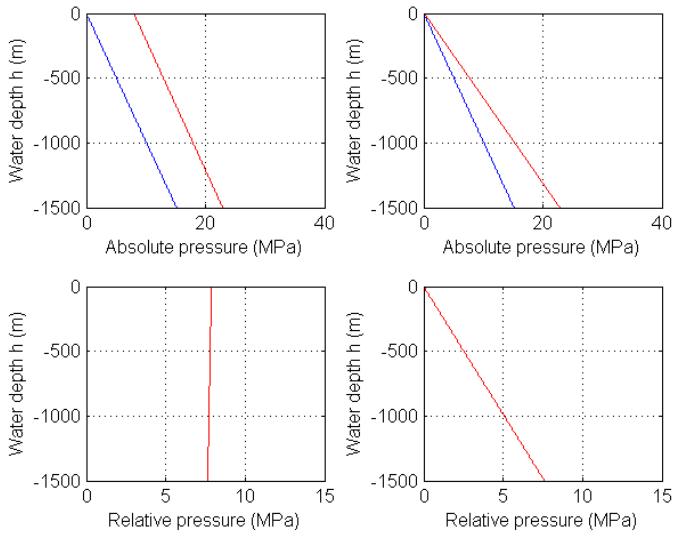

Figure 3.27: Pressure development over the mining system for mining SMS deposits from a water depth of 1,500m

3.3 Mechanical lifting

A mechanical lift is completely different from the 3 other vertical transport system mentioned in this report. Instead of converting mechanical energy somehow to flow of water, which transports the solids upwards, the mechanical energy itself is used to transport the solids upward.

The most simple way to do this is to lower a single bucket to the sea floor, fill it with solids, and lift it back up. Alternatives are using multiple buckets per lifting system or even continuous line bucket systems, like showed in figure (3.28). For sake of simplicity the single bucket lifting system will be used in this study.

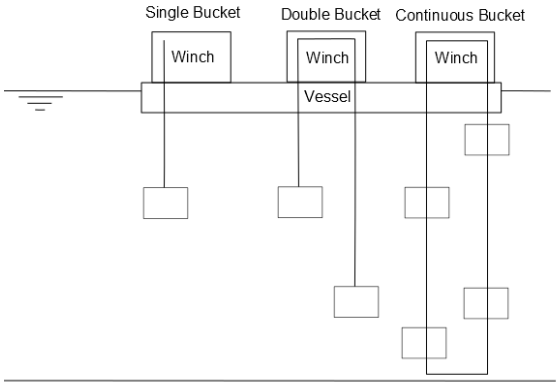

Figure 3.28: Mechanical lifting alternatives

Because it is relatively simple the theory for lifting the solids will not be described extensively.

3.3.1 Model

Assumptions

A number of assumptions are made to come to a model:

- no leakage of solids along the way up;
- buckets are emptied under water;
- period of deceleration in the bucket movement neglected.

The first assumption could become a demand of environmental permits on the deep sea mining lift, making some kind of cover necessary for the bucket.

Emptying the buckets under water might seem needlessly complicated, but it prevents the problem of rising the bucket above the water, where it requires a lot more lifting power and stability. Alternatively another type of lift could be added in the last few meters for extra lifting force and stability. Maximum lifting capacity will increase by a factor $\frac{\rho_S}{\rho_L}$ because the extra lifting power is no longer necessary over the entire vertical.

The deceleration, but perhaps also the acceleration period can be neglected, since the time it takes to do so is just a small fraction of the total lifting time. For now the acceleration period will still be taken into account, because it is larger than the deceleration period and relatively easy to model.

Equations

The force working on the bucket is used to model mechanical lifting. The force balance differs depending on the phase (upward movement of downward movement) the bucket is in. The mass of the bucket varies as well, between $m_{b.f}$ on the way upwards when it is full and $m_{b.e}$ downwards when it is assumed to be completely empty.

Upward the remaining force is calculated by Eq. (3.30), with $m_{b.f}$ used to compose gravitational force F_z, while Eq. (3.31) calculates the force in the downward movement, using $m_{b.e}$ as the bucket mass. The force coming from the winch is F_{wi} in this equation.

$$F_{r.f} = F_{wi} - F_z - F_D \tag{3.30}$$

$$F_{r.e} = F_z - F_D \tag{3.31}$$

To calculate the gravitational force F_z the bucket has to be designed. The bucket itself has a volume V_b. The bucket can, however, not be filled for a 100% with solids since there is porosity n_S between the solids. To come to the solid volume V_S equation 3.32 is used, neglecting the wall thickness of the bucket:

$$V_S = (1 - n_S)\ V_b \tag{3.32}$$

The weight of the bucket has to be split in a full bucket weight $m_{b.f}$ and an empty bucket weight $m_{b.e}$. The choice is made to model the weight of the empty bucket as an percentage of the submerged maximum bucket content mass m_S. The percentage is expressed in a factor α_u, making the equation of the bucket masses:

$$m_{b.f} = m_S + m_{b.e} = m_S + \alpha_u \; m_S = (1 + \alpha_u) \; m_S \tag{3.33}$$

The mass of the bucket content, the (submerged) mass of the solids transported upwards, can be determined by Eq. (3.34). With the volume of solids V_S known the submerged density of the solids is used to come to submerged solid mass. Consequently the mass of the bucket is only applicable as long as it remains under water. Above water the bucket will have a completely different mass since both water content in the pores as the non-submerged weight of the solids have to be taken into account.

$$m_S = V_S \; (\rho_S - \rho_L) \tag{3.34}$$

The term F_D in Eq. (3.30) and (3.31) stands for the resistance term of the bucket moving through the water. This term can be calculated by Eq. (3.35), which is also known as the equation for the drag force, in which C_D is the drag coefficient.

$$F_D = \frac{1}{2} \; \rho_L \; C_D \; A_b \; v_b^2 \tag{3.35}$$

The maximum obtainable velocity of the bucket $v_{b.max.d}$ can be derived from this equation, by rewriting it as Eq. (3.36):

$$v_{b.max.d} = \sqrt{(\frac{F_r}{\frac{1}{2} \; \rho_L \; C_D \; A_b})} \tag{3.36}$$

However, this equation gives the maximum theoretical velocity of the bucket, while in practice there are other velocities used as maximum value, because of stability conditions of the load and the hoisting capabilities of the winch.

The stability velocity limit $v_{b.max.s}$ is assumed to have a fixed value independent of the bucket type and content, and to be double the size when the movement is downward, which agrees with specifications of winches used in offshore applications (Rolls-Royce, 2013).

Equation (3.36) uses the area of the bucket, which depends on the shape of the bucket. As starting point a bucket with a cube form will be used, of which the height to width/depth ratio can be adapted. To simulate this adaptation a dimensionless factor α_b is introduced to give a relation between the bucket area A_b and the bucket height h_b:

$$\alpha_b = \frac{\sqrt{A_b}}{h_b} \tag{3.37}$$

Rewriting it, for a rectangular shape, gives the bucket area and height in relation to the bucket volume V_b:

$$A_b = \sqrt[3]{(\alpha_b V_b)^2} \tag{3.38}$$

$$h_b = \sqrt[3]{\frac{V_b}{\alpha_b^2}} \tag{3.39}$$

In a similar way to the velocity and displacement calculation of the diaphragm pump the velocity and displacement of the bucket can be calculated over time, using Eq. (3.40) till (3.42), in which y_b is the location of the bucket between sea floor and surface, a_b its acceleration and v_b its velocity.

$$a_b(t) = \frac{F_r}{m_b} \tag{3.40}$$

$$v_b(t) = \int a_b(t)\ dt \tag{3.41}$$

$$y_b(t) = \int v_b(t)\ dt \tag{3.42}$$

With the mass and velocities known the time it requires to do a complete cycle t_{cycle} can be calculated and used to estimate the production. The cycle time not only includes the time required for the buck to move up- and downward, but also the emptying time of the bucket at the surface and the refill or change time at the sea floor. Production M_S is then calculated by:

$$M_S = \frac{V_S \ \rho_S}{t_{cycle}} \tag{3.43}$$

The average power consumption and peak power consumption during the cycle can be calculated by Eq. (3.44) and Eq. (3.45).

$$P_{av} = \frac{F_{wi} \ h}{t_{cycle}} \tag{3.44}$$

$$P_{max} = \frac{F_{wi} \ h}{t_{up}} \tag{3.45}$$

The winch force F_{wi} used in these calculations is the winch force that will actually be used for the lifting of the container, which might be limited by the stability velocity limit, not the maximum winch force which is available. The average value of the power consumption is then used to calculate the specific energy required to transport the solids up to the surface:

$$E_{spec} = 3600 \ \frac{P_{av}}{M_S} \tag{3.46}$$

Energetic efficiency η_E is the outcome of this model, and is in this study defined as the difference in potential energy between the solids at sea floor and surface, divided by the specific energy requirement E_{spec} that is described above. For the bucket lift the efficiency can be calculated by:

$$E_{pot} = \frac{m_S \ g \ h}{m_S} = g \ h \tag{3.47}$$

$$\eta_E = (1 \ - \ \frac{\rho_L}{\rho_S}) \ \frac{E_{pot}}{E_{spec}} \tag{3.48}$$

3.3.2 Performance

In this paragraph an attempt will be made to use the model as described in the last paragraph to come to a good design for a riser system with a positive displacement (diaphragm) pump. The influence of the different parameters on the design will be simulated to come to an efficient system. Starting points of the simulation are:

- solid concentration ρ_S is 2,000 and 3,500 kg/m^3;
- particle diameter d_S is 10 and 50 mm;
- winch force F_{wi} is 3,000 kN;
- bucket volume is 125 m^3;
- stability velocity limit is 10 m/s;
- water depth h is 1,500 m;
- bucket shape factor α_b is 1;
- bucket weight factor α_u is 0.1;
- porosity n_S is 0.3;
- drag coefficient C_D is 1.0.

It should be kept in mind that the lifting system will be designed to obtain productions M_S of 250 ton/oh. If the targeted (average) production was to be higher another design for the system would have resulted from the study.

Heavy lifting

The performance study of the vertical lift is divided in a number of sections. In the first section the two main components of the lifting system are considered: the winch force F_{wi} and the bucket volume V_b.

Important in this performance study will be which one of the two maximum bucket velocities is critical, the theoretical boundary or the stability velocity limit. For the stability limit a first assumption is made, which is 10 m/s. This is a very large value and is merely to study the effect of both the velocities. In reality 0.5 - 1 m/s is more common.

Varying the winch force gives figure (3.29). Both the effect of the stability velocity limit and the theoretical velocity limit (based on the resistance term) are clear in the figure. The stability velocity limit is the horizontal, straight part of the curves, which stops the velocity from increasing more and more for increasing winch forces. Increasing velocity also increases the friction losses during the cycle, and with that the efficiency.

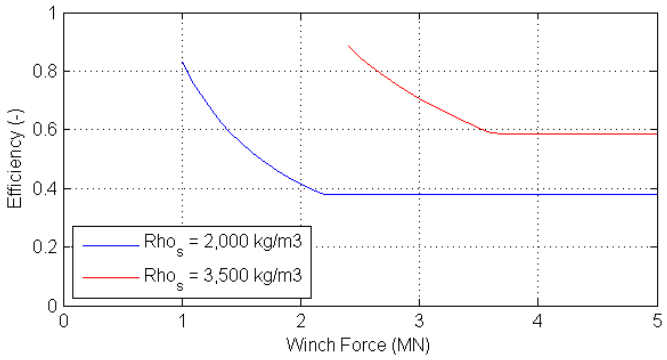

Figure 3.29: Effect of winch force F_{wi} on the efficiency

Clearly the optimum velocity from an efficiency point of view is as low as possible, which requires a winch force which is just sufficient to get the bucket to move. This would however limit the production. The winch force F_{wi} of 3,000 kN will be maintained for now.

The bucket volume influences the velocity as well. A larger bucket will be able to transport more solids and thus be heavier (higher F_z), but also generate a larger friction force. Both decrease the velocity, and with that increase the efficiency linearly, as can be seen in figure (3.30).

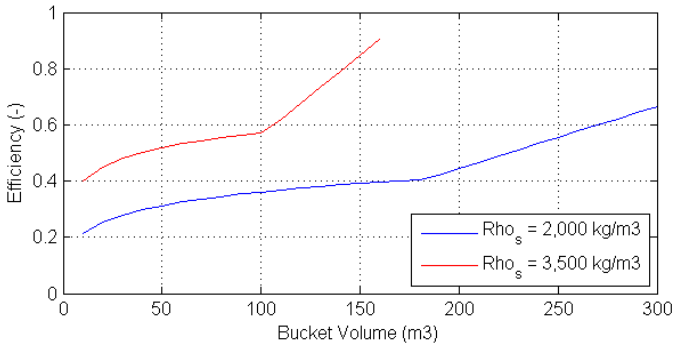

Figure 3.30: Effect of bucket volume V_b on the efficiency

The effect of the stability velocity limit can be recognized from the curved part of the lines, at low efficiencies. This is caused by decrease in solid volume V_S moved per cycle, at constant velocities. As the solid volume decreases both the production and the friction forces decrease too, but the solid volume is related linearly to the production while the friction force decrease is smaller.

Shape container

Important factors in calculation of the friction forces are dependent on the shape of the bucket. The drag coefficient C_D forms a part of Eq. (3.35). Varying the shape, to a more aerodynamic form, will decrease the drag coefficient. The cubic shape assumed now is one of the worse possible shapes from an aerodynamics point of view, so only lower values will be considered when varying.

Figure (3.31) shows the increase in efficiency for a decrease in drag coefficient and with that the drag force F_D. This is only relevant when the stability limit velocity is in effect. Without the limit the maximum velocity will increase for a decreasing drag coefficient C_D, leading to the same efficiency, as can be seen in the horizontal part of one of the curves.

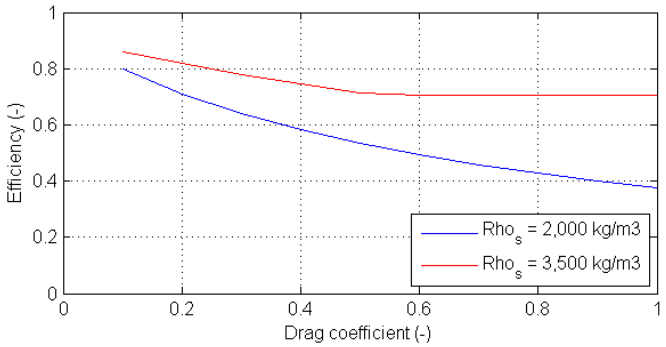

Figure 3.31: Effect of drag coefficient C_D on the efficiency

The same effect can be seen when varying the shape factor α_b. As the shape factor is increased the bucket area A_b becomes smaller and with that the friction force. If the stability limit velocity has been reached already the efficiency will increase because of that. However, if the stability limit is not reached yet, the decrease in friction will lead to an increase in velocity for a constant winch force F_{wi}, which causes the efficiency to remain the same, hence the horizontal part of the curve.

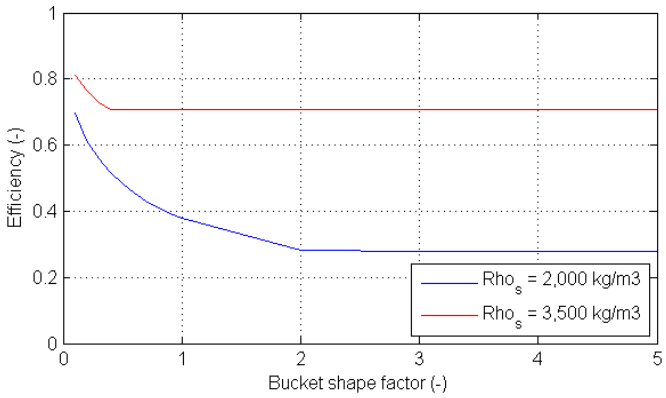

Figure 3.32: Effect of bucket shape factor α_b on efficiency

Other factors influencing the efficiency are the bucket weight factor α_u and porosity n_S. Both are varied in figures (3.33) and (3.34). The decision to keep the winch force at 3,000 kN gives a different starting point for the two case studies of $\rho_S = 3,500\ kg/m^3$ and $\rho_S = 2,000\ kg/m^3$. Like can be derived from figure (3.29): the manganese case of $\rho_S = 2,000\ kg/m^3$ already reached the stability limit velocity, while the other case did not.

The consequence of this can be seen when the bucket weight factor is varied. For the manganese case the increase in weight of the bucket itself will decrease the production, and with that the efficiency, while the velocity remains the same. In the other case the efficiency remains stable, because the lower production during the upward part of the cycle is compensated for by the faster descent, caused by the increased empty bucket weight.

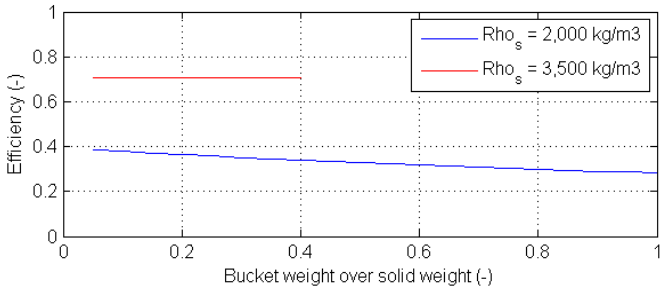

Figure 3.33: Effect of bucket weight factor α_u on efficiency

When varying the porosity n_S the effect seems similar for both: the higher the porosity, the lower the efficiency. This effect can also be deducted from the earlier variation in bucket volume V_b, both lead to lower volumes of solids and thus lower production.

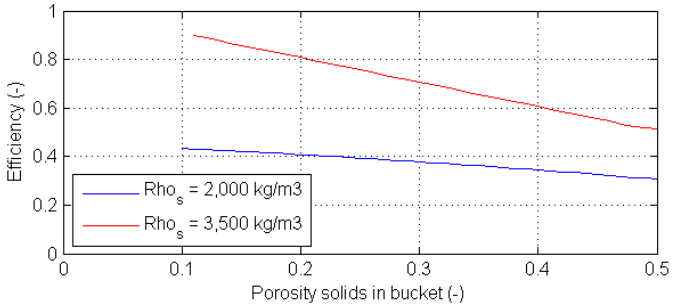

Figure 3.34: Effect of porosity n_S on efficiency

Maximum velocity

This performance study shows that the stability limit velocity $v_{b.max.s}$ has a large influence on the performance of variations of the bucket lift. In this study we assumed a value of 10 m/s, while in practice suppliers of deep sea winches advise velocities of 0.3-0.5 m/s during ascending and 0.6-1.0 m/s during descending (Rolls-Royce, 2013). However, these type of winches are often developed for one-time lifting jobs, in which safety is more important than velocity.

The effect on the efficiency for various stability limit velocities during the ascending phase can be seen in figure (3.35). The velocity in the descending phase is assumed to be double the value of the velocity during ascending phase.

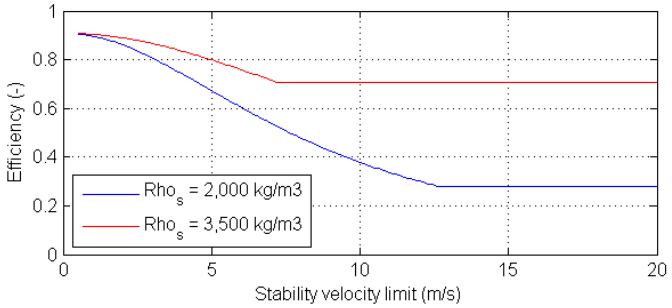

Figure 3.35: Effect of stability velocity limit $v_{b.max.s}$ on efficiency

Again is showed that the lower the velocity of the bucket, the higher the efficiency. As stated before lower velocity will most likely have a negative effect on productions. To see the consequences the two case studies are studied separately: SMS deposits with a $\rho_S = 3,500\ kg/m^3$ from 2,000 m water depth and manganese nodules $\rho_S = 2,000\ kg/m^3$ from a water depth h of 5,000 m.

Studying the first case, in which bucket volume and winch force are varied to obtain the relation between efficiency and production, gives figures (3.36) and (3.37). The first figure has a lower stability limit of 1 m/s, which is still higher than common for deep sea winches, while the second figure has no limit at all. The target production M_S of 250 ton/oh might just be obtained at this limiting velocity, making for a very efficient process.

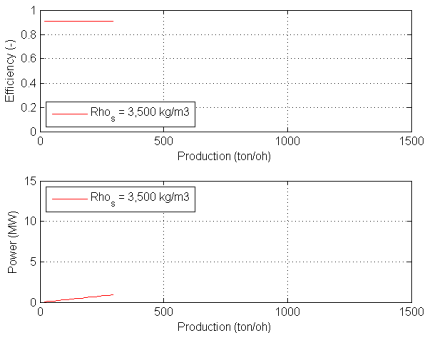

Figure 3.36: Low stability limit

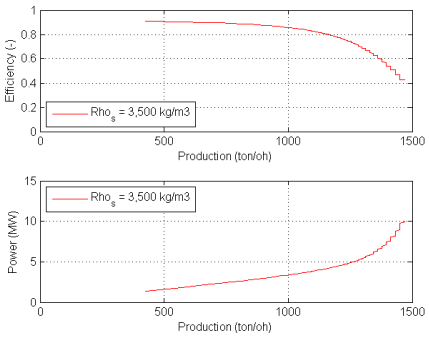

Figure 3.37: No stability limit

The second case study, $\rho_S = 2,000\ kg/m^3$ and $h = 5,000\ m$, in which again the bucket volume and winch force are varied in the same way to obtain the efficiency over production curves, gives figures (3.38) and (3.39).

The figure shows that a production M_S of 250 ton/oh can only be achieved at a very low efficiency and without a stability limit. The parameters of the lifting system will have to be adapted to achieve a more efficient system without stability problems.

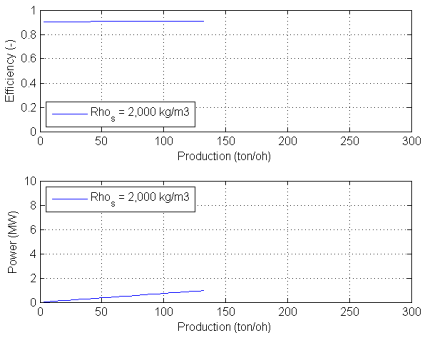

Figure 3.38: Low stability limit

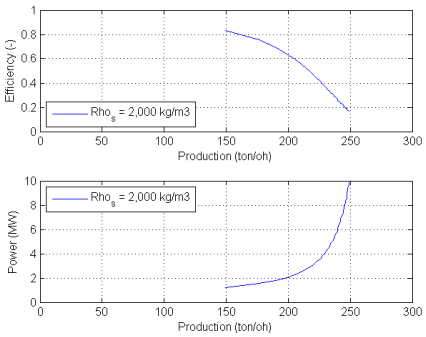

Figure 3.39: No stability limit

To achieve the targeted production M_S of 250 ton/oh at large water depths the parameters of the bucket lift are adapted. The stability limiting velocity $v_{b.max.s}$ is changed to a more realistic 2 m/s during ascending, the bucket volume V_b is increased to $250m^3$, which is a bit more than 6 by 6 by 6 meter, and the winch force F_{wi} is increased to 5,000 kN. All three values are reasonable but require more advanced study in both fluid dynamics and winch systems to see if it can be realised.

Summing up, the starting points which are changed are adapted to:

- winch force F_{wi} is 5,000 kN;
- bucket volume is 250 m^3;
- stability velocity limit is 2 m/s;
- water depth h is 1,500 - 6,000 m;

Bucket design should be subject to more detailed study, keeping in mind the method of unloading, attachment to the lifting system and drag force generated by it.

Efficiency

The resulting efficiency, including a production curve over water depth, is displayed in figure (3.40). The efficiency remains constant no matter which water depth, and is relatively high despite the unfavourable shape of the bucket. Production just reaches the target M_S at 6,000 m, but increases rapidly for decreasing water depth.

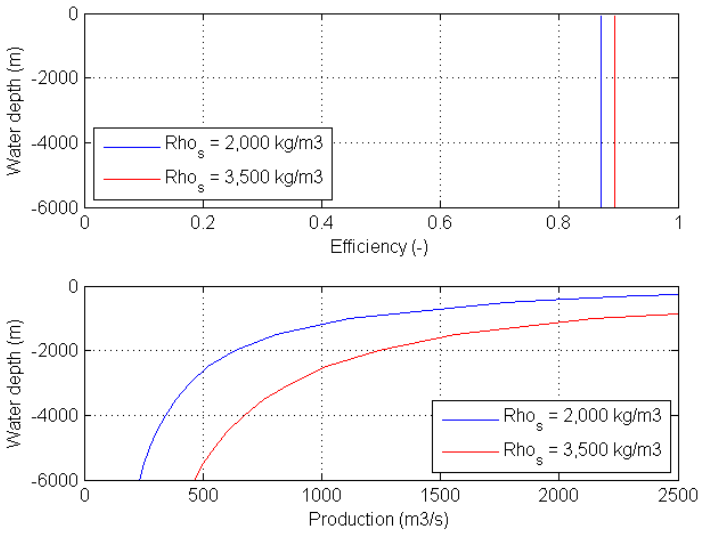

Figure 3.40: Effect of water depth h on efficiency

3.4 Airlift

This part of the study turned out to be an interesting subject for more thorough research, which will be described in the next chapter. In the original report, which can be found in Appendix C.2, Weber's (Weber and Dedegil, 1976) model was described, which was based on the balance of energy in the system. The model had already been used in an earlier study at Van Oord, although not for deep sea application, but turned out to have some disadvantages which could not be ignored, like the fact that all fluxes of the three phases (air, water, solids) had to be known.

The performance study for the airlift using Weber's model differed from the studies done for centrifugal dredge pumps and diaphragm pumps. Reason for this difference was the limited working range and the higher amount of variables which determine the efficiency η_e. Besides that Weber's model gave some questionable results for the power and efficiency curves for varying productions. A more detailed and more realistic model would have to be used to be able to vary the parameters better than with Weber's, as is done in the next chapter.

An airlift has a number of advantages: no moving parts at the sea floor, as the propulsion system is on the vessel, and no obstacles in the riser. Two other advantages of the airlift, which resulted from Weber's model, are displayed here: the increasing efficiency with increasing water depth and the low relative pressure difference between the riser and the surrounding water pressure.

Figure 3.41 shows the efficiency of the airlift for increasing water depth, which increases until a certain level when the air lift stops functioning because the air inflow is no longer sufficient to meet the targeted production M_S, according to the model.

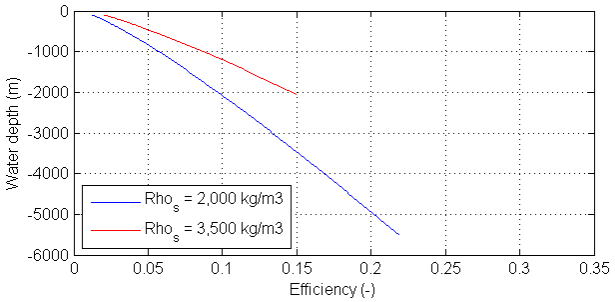

Figure 3.41: Efficiency over water depth

An airlift has a lot of variables for which it functions or not. The limitations to the working range of the airlift prevents reaching higher efficiencies. Interesting enough the higher the efficiency, the smaller the working range seems to be, which might have severe consequences in practical application. More research into this subject, and more combinations of parameters, would be interesting to see if higher efficiencies than shown in the figure can be accomplished.

In figure 3.42 the three different pressures resulting from the model are displayed over water depth for an airlift with the air inlet halfway along the pipe: The absolute water pressure, the absolute pressure in the pipe line and the relative pressure. With a maximum value of 0.5 MPA the occurring relative pressure (pressure difference between pipeline pressure and absolute pressure) is a lot lower than in case of a diaphragm pump.

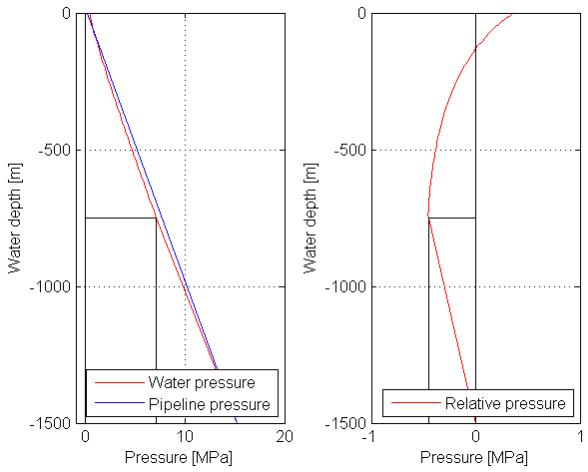

Figure 3.42: Pressure in the pipeline of an airlift with the air inlet halfway for a solid density of 2,000 kg/m^3 and a particle diameter of 0.05 m

3.5 Conclusion

A comparison between the different kind of vertical transport, based on a simplified model of the system, shows that vertical transport by mechanical bucket lifting is the most energy efficient transport system of the 4. Disadvantage is the progress in winch development which will have to be achieved to meet the production targets.

The two pump systems, centrifugal and diaphragm, have slightly lower efficiencies which do not differ much from each other, and have both their specific disadvantages over the other. Especially at limited water depth these are reasonable alternatives, as they have no problems achieving high productions.

At larger water depths other problems will arise for the pump systems, like the decreasing efficiency because of using large numbers of centrifugal dredge pumps or high pressures occurring in the riser system in case of a diaphragm pump.

The air lift system has the least efficient results, but that might be a consequence of limited investigation into the behaviour of the airlift for variable parameters. Of the 4 alternatives it is the only one which achieves increasing efficiency for increasing water depths, while maintaining high productivity.

Main recommendation would be to look into the possibilities of improving deep sea winches and their stability limits during lifting operations, and to consider other lay-outs than lifting a single bucket only.

Another recommendation is to further investigate the possibilities of an air lift system for various parameters, to see if the conclusions of this report are still valid after a more extensive performance analysis, as the airlift might still be a good alternative to mechanical lifting, especially at water depths of 4,000 to 6,000 m. This will be done in the next chapter.

Chapter 4

Airlift

Airlifting to transport solids from sea floor to surface is already in use in amongst others the offshore diamond mining industry. Main advantage of this method is the lack of moving parts under water, because the location of the propulsion system (the compressor) is on deck. Disadvantage is said to be the low efficiency and limited working range.

An airlift consists of a suction pipe (riser) from the sea floor up to the mining vessel, which contains the upward three-phase (gas-liquid-solid) flow, and an air supply tube between the air compressor on the vessel and the air-inlet somewhere along the suction pipe. In figure (4.1) an airlift is displayed schematically.

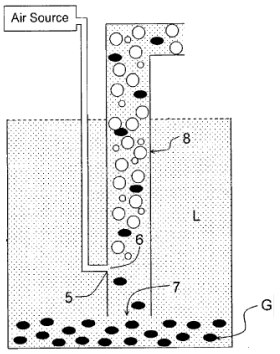

Figure 4.1: Airlift (Wikipedia)

4.1 Theory

The functioning of an airlift is explained in more detail using the steps in figure (4.2):

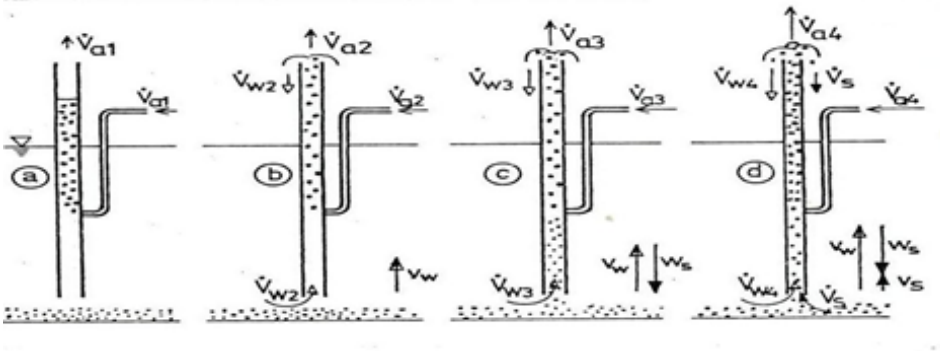

Figure 4.2: Schematization airlift

1. Air flows in at the air inlet, and rises through the fluid up to the surface. The air flow is not sufficient to let the water flow but the lower density inside the pipe and the slip between air bubbles and water makes the water level in the pipe rise above the surface level.
   $Q_a \neq 0 \;\; Q_w = 0 \;\; Q_s = 0$
2. The lower density inside the pipe and the slip between air bubbles and water caused by the higher air inflow makes the water level in the pipe rise above the level of the outlet. This is causing the water to flow through the pipe. The amount of water flow is not sufficient to pick up the solids from the sea floor. The settling velocity of the particles is smaller than the water velocity.
   $Q_a \neq 0 \;\; Q_w \neq 0 \;\; Q_s = 0$
3. Another increase in air inflow causes the water flow to increase to a sufficient level to pick up the solid particles, but not sufficient to transport them to the outlet height of the pipe. The settling velocity of the particles is equal to the water velocity.
   $Q_a \neq 0 \;\; Q_w \neq 0 \;\; Q_s = 0$
4. At this stage the amount of air insert into the pipe is sufficient to give the water velocity a value higher than the particle settling velocity, causing a flow of solids from sea floor to the pipe outlet.
   $Q_a \neq 0 \;\; Q_w \neq 0 \;\; Q_s \neq 0$

In this study, in which water depths of 1,500 to 6,000 meter are considered, the height of the pipe above the water surface is not taken into consideration, which would make the first two steps the same.

4.1.1 Flow regimes

Functioning of the airlift is in practice not as simple as it is suggested in the last paragraph. The velocity and geometry of the components of the three-phase flow (gas, liquid and solids) influence the flow regime which is occurring within the pipeline. The type of flow regime says much about the way the three components interact with each other, as will be explained in this paragraph. First the two-phase flow will be considered, leaving the third phase (solids) out of it for now.

There are 5 different flow regimes, according to Brennen (Brennen, 2005), in a two-phase flow (gas and liquid) in a vertical pipe. These 5 are displayed in figure (4.3).

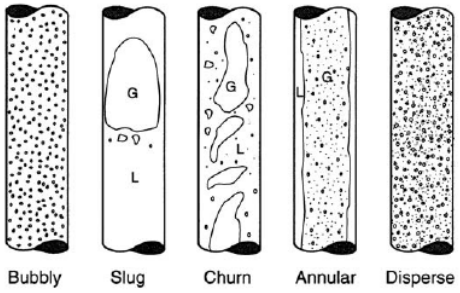

Figure 4.3: Flow regimes

The descriptions per flow regime, as cited from Thome (Thome, 2004), is:

- Bubbly / finely dispersed bubbly flow: Numerous bubbles are observable as the gas is dispersed in the form of discrete bubbles in the continuous liquid phase. The bubbles may vary widely in size and shape but they are typically nearly spherical and are much smaller than the diameter of the pipe.
- Slug / plug flow: With increasing gas void fraction, the proximity of the bubbles is very close such that bubbles collide and coalesce to form larger bubbles, which are similar in dimension to the tube diameter. These bubbles have a characteristic shape similar to a bullet with a hemispherical nose with a blunt tail end.
- Churn / froth flow: Increasing the velocity of the flow, the structure of the flow becomes unstable with the fluid travelling up and down in an oscillatory fashion but with a net upward flow. This flow pattern is an intermediate regime between slug flow and annular flow.

- Annular flow: Once the inter-facial shear of the high velocity gas on the liquid film becomes dominant over gravity, the liquid is expelled from the centre of the tube and flows as a thin layer on the wall while the gas flows as a continuous phase up the centre of the pipe.
- Mist / disperse flow: At very high gas flow rates, the annular film is thinned by the shear of the gas core on the interface until it becomes unstable and is destroyed, such that all the liquid is entrained as droplets in the continuous gas phase, inverse to the bubbly flow regime.

Different flow regimes might be occurring in deep sea airlifts. At the point where the air is inserted to the riser a bubbly flow will probably occur, since the large pressure causes a very small air bubble diameter. When rising upwards the size of the bubbles will increase with the decreasing pressure, causing slug flow from some point upward. Further up, when velocity of the air has risen more, annular and even disperse / mist flow might occur. Figure (4.4) gives a schematization of the flow regimes variation that could occur in a deep sea airlift.

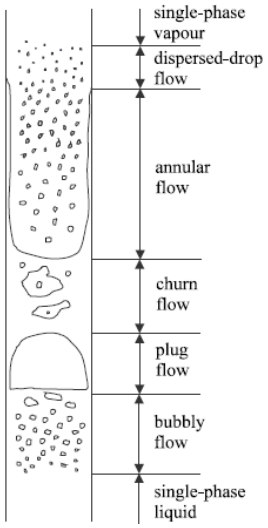

Figure 4.4: Different flow regimes in riser

A lot of attempts have been done to find the points of transition between the different flow regimes. Some publications show fitting results between theory and experimental data, but are only valid for a certain pipe diameter, as further research into the theory shows. An example of a flow regime map can be found in figure (4.5), which is made by Taitel (et al, 1980) and used by Halkyard (Halkyard and Doyle, 2007) and Nenes (et al, 2009) in their studies.

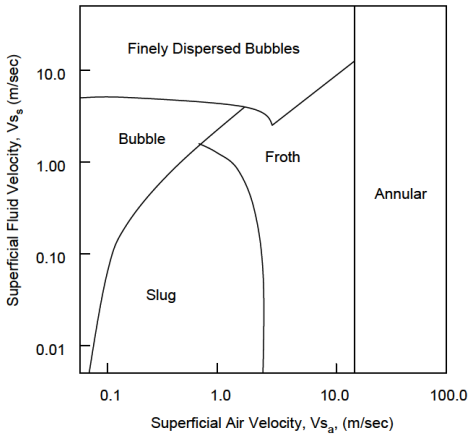

Figure 4.5: Flow regime map relating the different fluxes (superficial velocities)

This flow regime map is however based on theoretical transitions between regimes, and only confirmed by measurements done by the author himself in 2.5 and 5.0 centimetre pipes. McQuillan (McQuillan and Whalley, 1984) summarizes the transition boundary in figure (4.5) between the flow regimes in simple equations.

Differences in transport of solids in the different flow regimes has not been the subject of much research. According to Halkyard (Halkyard and Doyle, 2007) froth flow was the most efficient regime for solid transportation, while the annular regime hardly transports any solids. In other literature, like the studies by Kassab (et al, 2005) and Pougatch (Pougatch and Salcudean, 2007), no mention is made of a difference in relation between water and solids for different flow regimes.

4.1.2 Literature

The relation between the ingoing air flow under atmospheric pressure $Q_{G.atm}$ and the outgoing three phase mixture flow Q_M, of which the solid production M_S is a part, can, according to literature, be approximated by three different types of calculations / modelling:

- The momentum balance
- The energy flux (power) balance
- Multi fluid model

The momentum balance is the method most often used in theoretical studies. It uses the loss in density within the suction pipe and the friction force to calculate the difference between the mass flux times velocity (=momentum) that goes in at the suction side and the one that comes out at the discharge side. This method is used by Saito (et al, 1989), Yoshinaga (Yoshinaga and Sato, 1996), Poutgatch (Pougatch and Salcudean, 2007), Halkyard (Halkyard and Doyle, 2007), Mahrous (Mahrous, 2012) and more to model the three-phase flow in the airlift.

The calculations based on the energy flux balance use the pressure loss due friction to calculate the loss of energy flux (power) over a certain section of the suction pipe. This method is used by both Weber (Weber and Dedegil, 1976) for three-phase flow and Liang (Liang and Peng, 2004) for two-phase flow to model the airlift.

In the study of Yoshinaga the methods of Weber (energy flux), Saito (momentum) and Kawashima (empirical) are compared to each other and Yoshinaga's own model based on momentum balance, using data obtained in his own airlift tests in pipe diameters under 5 cm. The tendency of the results agree qualitatively with the model made by Saito.

A multi-fluid model is used by Yoon (et al, 2000), Hatta (et al, 1998) and Stevanovic (Stevanovic, 2007). The multi-fluid models use both the momentum and energy balance per phase (gas, liquid or solid) and model the interaction between the phases.

4.1.3 Model selection

The model as selected will have to be related to how the airlift functions in practice, which means the gas flow, expressed in gas flux j_G, into the riser is used by the operators on the vessel to control the flow, resulting in a certain production of solids transported by a certain amount of liquid, expressed in solid flux j_S and j_L respectively:

$$[\ j_L\ j_S\ ] = f(j_G,\ d_S,\ \rho_S,\ h,\ D,\ \alpha_I) \tag{4.1}$$

The input parameters which should influence the resulting solid and liquid flux are, besides gas flux j_G: the solid particle diameter d_S, the solid density ρ_S, the water depth h, riser pipe diameter D and height of the gas inlet, expressed in a factor α_I, which relates the air inlet height to the total height of the riser.

The energy flux (power) model as described by Weber (Weber and Dedegil, 1976) was used in previous chapter to model the airlift. A large disadvantage of the model however is the fact that all 3 interesting parameters, solid flux j_S, liquid flux j_L and gas flux j_G, are input parameters.

The multi-fluid model seems to be most fit for modelling an airlift, because the change in flow patterns are more simple to take into account compared to the other methods. Coding and simulating is however much more complicated than the momentum balance method, and existing publications do not show sufficient information to code it.

The momentum balance method will be used in this part of the thesis to study the performance of the airlift. Within the momentum balance method there is some variety of approaches in the existing literature. Yoshinaga's publication (Yoshinaga and Sato, 1996) is used to base the first version of an airlift model on, since the method is well documented and the authors compares their model to not only their own experimental data, but also the data of multiple other authors. Mahrous (Mahrous, 2012) based his model also on Yoshinaga's publication as well.

Yoshinaga's model can predict the liquid flux j_L related to a certain gas flux j_G and solid flux j_S. One of the adaptations to the model in this thesis is to add the inflow concentration β_S to the model, which fixes the ratio between liquid and solid flux, resulting in a model which can be simplified to:

$$[\ j_L\ j_S\ ] = f(j_G,\ d_S,\ \beta_S,\ \rho_S,\ h,\ D,\ \alpha_I) \tag{4.2}$$

The original model by Yoshinaga (Yoshinaga and Sato, 1996) can be found in the report regarding Airlift in Appendix C.3, including the validation. This model is used to make the adapted model, which is also fit for simulation of larger airlifts in deeper water. The adapted airlift model will be described in its final stage. For the order of the steps taken during the adaptation, the remaining bugs and the practical solutions to certain problems can be found in the original report regarding the airlift model.

4.1.4 Experimental data

Experiments with airlifting have been done by a number of authors, for both two-phase and three-phase flow, but mainly for short pipe lengths and/or small pipe diameters.

Weber (Weber and Dedegil, 1976) has done experiments for three-phase flow at pipe lengths h of 50 - 450 m, a diameter D of 300 mm, particle diameters d_S between 0.6 and 50 mm and solid densities of 1,100 - 2,600 kg/m^3. Saito (et al, 1989) did similar experiments, but then with smaller diameters (between 50 and 150 mm) and length (between 10 and 200 m).

Even smaller pipe diameters, of 2.6 and 4 cm, were used by Yoshinaga (Yoshinaga and Sato, 1996) for a number of tests at pipeline lengths of about 7 m, with varying particle densities and diameters. Kawashima did tests for airlifts without a suction part, so the air inlet at the same location as the solid/water inflow. The pipe diameter he used was 0.5 cm for a pipe line length of 6 m.

Two-phase flow experiments for larger pipe diameters have been done by Ohnuki in 200 mm pipes (Ohnuki and Akimoto, 1998), with the main focus on transition between flow regimes, and in 460 mm pipes (Ohnuki and Akimoto, 1995), with the main focus on method of air injection. Nenes (et al, 2009) also mentions experimental data done by Karydakis in 100 mm pipes.

For the model only the three-phase data for larger diameters is used, which is the data by Weber, which can be found in Appendix A.

4.2 Model

The adapted version of the model by Yoshinaga is described in this chapter. The original model is described extensively in the airlift report in Appendix C.3.

The adapted model is also able to simulate alternatives for gas as buoyant substance that propel the lift, the equations of the buoyancy induced lift, described more extensively in Appendix C.4 is already given in this chapter as they form part of the final model.

4.2.1 Assumptions

A number of assumptions is done in the momentum-balance model:

- steady-state;
- one dimensional, non-axial variety is neglected;
- there is no temperature variation within the riser;
- there is no spread in particle density, size or shape;
- liquid and solids are incompressible.

The steady state is the most important state of the functioning of an airlift. The start-up of an airlift will be considered in a later paragraph, when the steady state is known.

For reasons of simplicity the airlift model will be one-dimensional. There is no doubt that there is variety of the flow over the diameter of the pipe, as annular and plug flow are important examples of, but for now the one-dimensional model is complicated enough.

No temperature variation is a reasonable assumption for a deep water lift system, as the temperature surrounding the majority of the riser will be similar to the water temperature at the inflow: about 4-5 degrees Celsius.

Contrary to the temperature the particle shape, size and density do vary. At first these are left out for simplicity reasons, but they might be interesting to implement at a later stage or in further research. Incompressibility of liquid and solids is a fair assumption, as was proven in the paragraph about the diaphragm pump.

4.2.2 Principle

The principle of the airlift model is based on the momentum balance in the airlift. The left side of figure 4.6 gives a simplified display of the riser tube of the airlift. Control volume for which the momentum balance is set-up is between inflow and outflow of the riser. This volume will be split up in two parts: A two-phase section (solid and liquid only) between the riser inflow and the gas inlet, and a three-phase section (solid, liquid and air/other substance) between the gas inlet and the riser outflow.

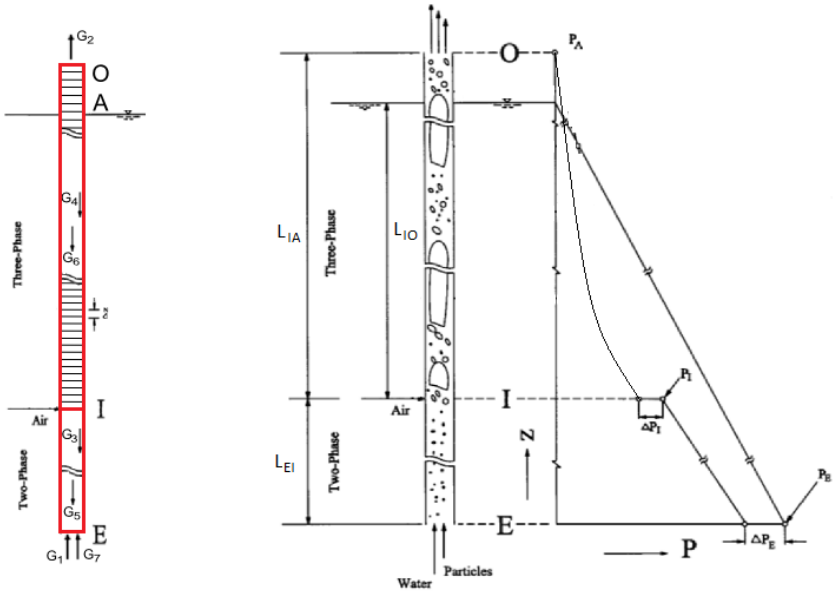

Figure 4.6: Principle of airlift model

Four different types of momenta form together the momentum balance over the control volume, as schematized by the arrows in the right side of the figure:

- the weight of the riser content, split up in a momentum caused by the weight of the two-phase section G_5 and the momentum caused by the weight of the three-phase section G_6;
- the (wall) friction, inserted into the momentum balance by a two-phase (G_3) and three-phase (G_4) component;
- the flow entering and leaving the control volume, which are taken into account by momentum G_1 and G_2 respectively;
- the hydrostatic pressure, assumed to occur at the riser inflow, which forms momentum G_7.

For the airlift, as schematized in figure (4.6), the momentum balance becomes:

$$G = A\ j_E\ \rho_E\ v_E\ -\ A\ j_O\ \rho_O\ v_O\ -\ \pi D \int_E^I \tau_2\ dz\ -\ \pi D \int_I^O \tau_3\ dz$$
$$-\ A\ g \int_E^I \rho_2\ dz\ -\ A\ g \int_I^O \rho_3\ dz + A\ g\ h\ \rho_L\ =\ 0 \quad (4.3)$$

Different symbols are used in both the figure (4.6) and in the equation as subscript. The capital letters in the subscripts which are vowels refer to a location along the riser, with E being the riser-Entrance, I the gas-Inlet, A the surface-Area and O the riser-Outflow. The capital consonants in the subscripts refer to the type of material, with S the solids, L the liquid, G the gas or other substance and M the mixture. The numbers 2 and 3 in the subscripts refer to the two-phase (solid-liquid) and three-phase (solid-liquid-gas) section respectively.

The momentum balance method requires values for gas, solids and water flow or flux for which the equation is in balance. The changing gas flow and density under different pressures causes a difference in mixture concentration and velocity over the vertical, hence the division of the upper part of the riser (the three-phase section) in small parts Δz for calculations. In the right part of figure (4.6) the pressure distribution along the vertical z of the riser is displayed.

This division is not necessary if the substance is something different than gas, like incompressible buoyant liquid or solids, or in case of two-phase flow of (incompressible) solids and liquids only.

4.2.3 Equations

Momentum

The momentum balance is split up in the 7 different terms, and then added together:

$$G = G_1 + G_2 + G_3 + G_4 + G_5 + G_6 + G_7 = 0 \tag{4.4}$$

The inflowing and outflowing terms G_1 and G_2 of the momentum balance are calculated by Eq. (4.5) and (4.6), with j being the flux of the gas (G), liquid (L) or solids (S), ρ the density and v the velocity at the entrance (E) or outflow (O).

$$G_1 = A\ (\ j_L\ \rho_L\ v_{L,E} + j_S\ \rho_S\ v_{S,E}\ ) \tag{4.5}$$

$$G_2 = -\ A\ (\ j_{G.O}\ \rho_{G.O}\ v_{G.O} + j_L\ \rho_L\ v_{L.O} + j_S\ \rho_S\ v_{S,O}\ ) \tag{4.6}$$

Both the gas flux and gas density are dependent on the pressure occurring at that depth (liquid and solids are taken as incompressible). Equation (4.7) and (4.8), which originates from a constant mass flux of gas, shows this dependency, with p_{atm} and $j_{G.atm}$ being the pressure and gas flux under atmospheric conditions and R and T the gas-constant and temperature in Kelvin.

$$\rho_G(z) = \frac{p(z)}{R\ T} \tag{4.7}$$

$$j_G(z) = j_{G.atm}\ \frac{p_{atm}}{p(z)} \tag{4.8}$$

The shear stress terms consist of the shear stress τ for the two-phase part and three-phase part of the pipeline, integrated over the length of that part and multiplied with the circumference.

To model it the equations 4.9 and 4.10 are simplified by calculating the pressure drop over the pipe sections, which consist of a length-dependent part and a fixed part for the entrance and acceleration losses. In case of the three phase flow the length-dependent wall friction factor is calculated per section with a length Δz, of which there are N_r. How to come to the pressure losses will be elaborated further in the next paragraphs.

$$G_3 = -\,\pi D \int_E^I \tau_2 \, dz = A \, (\, \Delta p_2 + \Delta p_E \,) \tag{4.9}$$

$$G_4 = -\,\pi D \int_I^O \tau_3 \, dz = A \, (\sum^{N_r} \frac{\Delta p_3}{\Delta z} \, \Delta z + \Delta p_I \,) \tag{4.10}$$

The factors which take the weight of the mixture into account are G_5 and G_6, while G_7 represents the hydrostatic pressure surrounding the pipe entrance. Equations for these terms are given by Eq. (4.11), (4.13) and (4.12), with L_{EI} and L_{EA} being the length between the entrance E and the gas inflow I or surface A. Assuming the riser entrance is located at the sea floor length L_{EA} is the same as water depth h. G_5 does not require integration over length because of its constant concentration C, while the hydrostatic pressure in G_7 is given by the weight of the water column surrounding the riser:

$$G_5 = -\,A \; g \; L_{EI} \; (\; \rho_L \; C_{L,2} + \rho_S \; C_{S,2} \;) \tag{4.11}$$

$$G_7 = A \; g \; L_{EA} \; \rho_L \tag{4.12}$$

The geodetic or gravity term of the three-phase section has to be integrated over the length of the upper section of the pipeline L_{IO}, in which the concentrations of gas C_G, liquid $C_{L.3}$ and solids $C_{S.3}$ and the gas density are varying over vertical z:

$$G_6 = -\,A \; g \int_I^O (\; \rho_G(z) \; C_G(z) + \rho_L \; C_{L.3}(z) + \rho_S \; C_{S.3}(z) \;) \; dz \tag{4.13}$$

Discretizing it for this model by splitting the upper section up in N_r parts gives:

$$G_6 = -\,A \; g \sum^{N_r} (\; \rho_G(z) \; C_G(z) + \rho_L \; C_{L.3}(z) + \rho_S \; C_{S.3}(z) \;) \; \Delta z \tag{4.14}$$

Solid and liquid concentrations

There are 5 different concentrations which are required to calculate the momentum balance: the steady concentrations of solids $C_{S.2}$ and liquid $C_{L.2}$ in the two-phase part of the riser and the varying concentrations over the vertical for gas $C_G(z)$, solids $C_{S.3}(z)$ and liquid $C_{L.3}(z)$.

The concentrations in the two-phase section will be described in this paragraph, including the relation between the solids and liquid if there is gas present, under the assumption that gas flow does not influence the solids directly. The concentrations are obtained using the volumetric fluxes and relative velocity between solids and liquid, by a function that can be schematized by:

$$[\ C_L\ C_S\ ] = f(j_L,\ j_S,\ C_G,\ d_S,\ \rho_S) \tag{4.15}$$

The original model by Yoshinaga used an empirical model by Sato to approximate the solid velocity v_S. This empirical model has as disadvantage that is was only validated for small pipe diameters. Another disadvantage is that because of this empirical model the solid velocity v_S often turned out to be larger than the liquid velocity v_L, which is quite unrealistic seeing the higher density of the solids and the fact that the shape of both solid and liquid is not taken into account.

The alternative to the empirical equation for estimating the solid velocity is coupling the solid velocity to the liquid velocity, by using the relative velocity v_r, which is a form of taking the slip-ratio into account. To estimate the value of relative velocity v_r the terminal settling velocity of particles is used.

To calculate the solid concentration C_S and liquid concentration C_L there are four parameters required: Solid flux j_S, liquid flux j_L, relative velocity v_r and the combined solid and liquid concentration C_{LS}, which is 1 in the case of the two-phase flow in the lower riser section or dependent on gas concentration C_G in case of three-phase flow in the upper section. Filling the known relations between the relative velocities and the concentrations gives:

$$v_r = v_L - v_S = \frac{j_L}{C_L} - \frac{j_S}{C_S} \tag{4.16}$$

The combined liquid and solid concentration C_{LS} can be found by simply adding the two together, as can be seen in Eq. (4.17). Inserting the equation for C_{LS} into Eq. (4.16) leads to:

$$C_{LS} = C_S + C_L = 1 - C_G \tag{4.17}$$

$$v_r = \frac{j_L}{C_L} - \frac{j_S}{C_{LS} - C_L} \tag{4.18}$$

Multiplying this equation by $C_{LS} - C_L$ and C_L, dividing it by v_r and moving everything to one side leads to Eq. (4.19), (4.20) and (4.21).

$$(C_{LS} - C_L)\ v_r = (C_{LS} - C_L)\ \frac{j_L}{C_L} - j_S \tag{4.19}$$

$$C_{LS}\ C_L\ v_r - C_L^2\ v_r = C_{LS}\ j_L - C_L\ j_L - C_L\ j_S \tag{4.20}$$

$$C_L^2 + (\frac{-C_{LS}\ v_r - j_L - j_S}{v_r})\ C_L + \frac{C_{LS}\ j_L}{v_r} = 0 \tag{4.21}$$

This equation can simply be solved using the ABC-formula (or using the function ROOT in Matlab). Of the two solutions only one has a realistic value, which should be equal to or in between zero and C_{LS}. For two-phase flow the equation can be simplified to:

$$C_L^2 + (\frac{-v_r - j_L - j_S}{v_r})\ C_L + \frac{j_L}{v_r} = 0 \tag{4.22}$$

The relative velocity v_r is assumed to be equal to the hindered settling velocity of a particle in a quiescent liquid $v_{S.th}$. Also including the form factor α_f, to take into account the fact that the solids are not spheres, the equation for hindered settling velocity of solids $v_{S.th}$, and with that relative velocity v_r, becomes (for both two-phase and three-phase flow):

$$v_r = v_{S.th} = \alpha_f \left(1 - \frac{C_S}{1 - C_G} \right)^{\alpha_h} v_{S.ts} \tag{4.23}$$

In this equation $v_{S.ts}$ is the particle settling velocity of a single spherical particle in a quiescent liquid, and can be calculated using Eq. (4.24), which originates from equalling the drag force to the gravity force on the submerged weight:

$$v_{S.ts} = \sqrt{\frac{4\ g\ d_S\ (\rho_S - \rho_L)}{3\ C_D\ \rho_L}} \tag{4.24}$$

However, when a cloud of multiple particles is settling hindering effects decrease the settling velocity. The hindered settling velocity $v_{S.th}$ depends on a varying coefficient α_h and with that on the particle Reynolds number Re_p, as suggested by Wallis (Matousek, 2004). Equation for factor α_h is:

$$\alpha_h = 4.7\ \frac{1 + 0.15\ Re_p^{0.687}}{1 + 0.253\ Re_p^{0.687}} \tag{4.25}$$

The particle Reynolds number Re_p itself also depends on the (hindered) settling velocity of a particle. Iteration is required to come to a constant value. Terminal settling velocity of a single $v_{S.ts}$ is used as the first approximation of the hindered settling velocity $v_{S.th}$ for calculation of the particle Reynolds number, by:

$$Re_p = \frac{\rho_L\ v_{S.ts}\ d_S}{\mu_L} \tag{4.26}$$

The obtained value of the hindered terminal settling velocity is used to re-calculate the particle Reynolds number Re_p and factor α_h, using Eq. (4.26) and (4.25), until a constant value for the hindered terminal settling velocity $v_{S.th}$ is reached.

Gas concentration

The concentration of gas C_G is dependent on the slip-ratio between the gas and the mixture of solid and liquids, and is given by:

$$C_G = f(j_G,\ j_S,\ j_L,\ C_S,\ C_L,\ \rho_G, \rho_S) \tag{4.27}$$

$$C_G = \frac{1}{1 + 0.4\ \frac{\rho_G}{\rho_{LS.3}}\ (\frac{1}{\alpha_x} - 1) + 0.6\ \frac{\rho_G}{\rho_{LS.3}}\ (\frac{1}{\alpha_x} - 1)\ \sqrt{\frac{\frac{\rho_{LS.3}}{\rho_G} + 0.4\ (\frac{1}{\alpha_x} - 1)}{1\ +\ 0.4\ (\frac{1}{\alpha_x} - 1)}}} \tag{4.28}$$

The concentration of gas C_G depends on the combined liquid and solid concentration, and vice versa as was described in last paragraph. The relation between the concentration and the slip-ratio $\frac{v_G}{v_{LS.3}}$ within Eq. (4.28) can be derived by writing out both velocities as:

$$v_G = \frac{Q_G}{A\ C_G} = \frac{M_M}{\rho_G}\ (\ \frac{\alpha_x}{C_G}\ ) \tag{4.29}$$

$$v_{LS.3} = \frac{Q_G}{A\ (1 - C_G)} = \frac{M_M}{\rho_{LS,3}}\ (\ \frac{\alpha_x}{1 - C_G}\ ) \tag{4.30}$$

In these equation α_x is the so-called 'vapour quality ratio', which is the ratio of the mass flux of air compared to the entire mass flux M_M of the mixture, while the $\rho_{LS.3}$ is the density of the combined solid and liquid flow:

$$\alpha_x = \frac{\rho_G\ j_G}{\rho_G\ j_G + \rho_L\ j_L + \rho_S\ j_S} = \frac{\rho_G\ j_G}{M_M} \tag{4.31}$$

$$\rho_{LS.3} = \rho_L\ \frac{C_L}{1 - C_G} + \rho_S\ \frac{C_S}{1 - C_G} \tag{4.32}$$

Combining Eq. (4.29) with Eq. (4.30) and writing it out for concentration C_G gives:

$$C_G = \frac{1}{1 + (\frac{1}{\alpha_x} - 1)\ \frac{\rho_G}{\rho_{LS.3}}\ \frac{v_G}{v_{LS.3}}} \tag{4.33}$$

The slip-ratio $\frac{v_G}{v_{LS.3}}$ can be approximated using a rewritten form of the empirical Smith's equation. The original equation by Smith, as mentioned in an Engineering Data Book (Thome, 2004), considers two-phase air-water flow. Replacing the liquid density ρ_L by combined solid and liquid density $\rho_{LS.3}$, as suggested by Yoshinaga, gives for the slip ratio:

$$\frac{v_G}{v_{LS.3}} = 0.4 + 0.6\ \sqrt{\frac{\frac{\rho_{LS.3}}{\rho_G} + 0.4(\frac{1}{\alpha_x} - 1)}{1 + 0.4(\frac{1}{\alpha_x} - 1)}} \tag{4.34}$$

Combining the two results in Eq. (4.28) for the gas concentration.

Concentration alternative substances

The model will also be able to simulate an alternative for gas in the form of buoyant solid and liquid substance, like silicone-oil or microspheres. Simulation will be a lot simpler due to the constant density and flux that will be assumed to occur over the vertical.

The concentration of the solid and liquid substance in the riser (still denoted by C_G to separate them from liquid and solid concentration C_L and C_S) will be constant over depth, as compression is negligible (max. 4-5% of the volume for silicone oil under 50 MPa pressure). Similar to the calculation of the two-phase concentrations the relative velocity $v_{r.G}$ between the substance and the water will be used to come to the substance velocity v_G, which is related to the concentration by:

$$C_G = \frac{j_G}{v_G} \tag{4.35}$$

Together with the liquid velocity which is calculated for the two-phase flow, the substance velocity is calculated using Eq. (4.36). The substance velocity is used to derive the substance concentration with Eq. (4.35), after which the two-phase concentrations and velocities are recalculated until an equilibrium is reached.

$$v_G = v_L + v_{r.G} = v_L + v_{G.ts} \tag{4.36}$$

The relative velocity in this equation is assumed to be equal to the rise velocity of the substance in quiescent water. In case of a liquid substance, which will be the water repellent silicone-oil, the bubbles will most likely be rather large. Assuming a sphere shape of the cross section and one big bubble the bubble diameter d_G is approximated by:

$$d_G = D\ \frac{j_G}{j_G + j_L + j_S} \tag{4.37}$$

The rise velocity of the liquid substance in quiescent liquid can be calculated by:

$$v_{G.ts} = \sqrt{\frac{4\ g\ d_G\ (\rho_L - \rho_G)}{3\ C_D\ \rho_L}} \tag{4.38}$$

In the same way the rise velocity for the solid particles (like microspheres) is calculated, although bubble diameter d_G is then known because of the fixed (average) size.

Pressure loss

The shear stress terms of the momentum equation are approximated by Eq. (4.9) and (4.10) using four different terms for pressure losses: Entrance and acceleration loss Δp_E, friction loss Δp_2 in the two-phase section, acceleration loss at the gas-inlet Δp_I and friction loss in the three-phase section $\frac{\Delta p_3}{\Delta z}(z)$.

The wall friction losses for the two-phase flow in the lower section of the riser, and the losses in the three-phase flow in the upper section per part Δz are calculated using a value for Darcy friction factor λ of 0.012, with Eq. (4.39) and (4.40) for two-phase and three-phase flow respectively.

$$\Delta p_2 = \lambda \, \frac{L_{EI}}{D} \, \frac{1}{2} \, q_2 \tag{4.39}$$

$$\frac{\Delta p_3}{\Delta z} = \lambda \, \frac{1}{D} \, \frac{1}{2} \, q_3 \tag{4.40}$$

In this equation q_2 and q_3 are the dynamic pressure losses, for which Shook (Shook and Bartosik, 1994) suggests to take every phase independently into account to come to the total dynamic pressure q:

$$q_2 = C_{L.2} \; \rho_L \; v_L^2 + C_{S,2} \; \rho_S \; v_S^2 \tag{4.41}$$

$$q_3(z) = C_G(z) \; \rho_G(z) \; v_G(z)^2 + C_{L.3}(z) \; \rho_L \; v_L(z)^2 + C_{S.3}(z) \; \rho_S \; v_S(z)^2 \tag{4.42}$$

Dynamic pressure q_2 is the constant value of the two-phase section of the pipeline and q_3 the one in the three-phase section which is varying over the vertical. The friction coefficients for inlet losses ξ_E and acceleration ξ_a used by Yoshinaga remain the same and thus the friction losses at entrance E and gas inlet I can be calculated by:

$$\Delta p_E = (\xi_E + \xi_a) \, \frac{1}{2} \, q_2 \tag{4.43}$$

$$\Delta p_I = \xi_a \, \frac{1}{2} \, (q_3(1) - q_2) \tag{4.44}$$

4.2.4 Calculation procedure

The momentum balance model calculates the liquid flux j_L and solid flux j_S for a given gas flux $j_{G.atm}$. Other variables that have to be known, but can be varied, are pipe diameter D, particle diameter d_S, solid density ρ_S, water depth h, particle shape factor α_f, drag coefficient C_D and gas inlet ratio α_I, which determines the position of the gas-inlet along the riser.

The procedure to calculate a value of j_L and j_S for a known value of j_G, with all the other parameters known as well, is displayed in a flow chart in figure (4.7), and is split up in 7 steps:

1. Determine the basic variables to be used in the rest of the calculation, like area A, specific density S, length of the riser sections L_{EI}, L_{IA} and L_{IO}. Divide the upper section with a length L_{IO} in N_r sections with a length Δz.

2. The bisection method will be used to find the value of j_L and associated value j_S. The upper and bottom limit used in the bisection method for j_L are 0.1 m/s and 10 m/s respectively.

3. Select a starting value for p_I for every combination of j_L and j_S, for which in this case the water pressure at the depth of the gas inlet is used as a first estimate. Calculate $p(z)$ for every node by linearly decreasing the pressure, as an first estimate, so it will be equal to the atmospheric pressure p_{atm} at the outflow. Use the pressure to calculate gas density $\rho_G(z)$ and gas flux $j_G(z)$ per node.

4. Calculate the solid and liquid concentrations at every node $C_{L.3}$ and $C_{S.3}$ of the three-phase section and in the whole two-phase section $C_{L.2}$ and $C_{S.2}$, using Eq. (4.16) till (4.26). Use the mass flux ratio as a first estimate for the concentration, so $\frac{j_S}{j_L+j_S}$ in case of $C_{S.2}$.

5. Calculate the gas concentration C_G using the values for solid and liquid concentration and Eq. (4.28) until (4.34). Reiterate step 4 and this step until the change in the gas concentration is smaller than 10^{-5}. Alternatively for solid and liquid substance Eq. (4.35) till (4.38) will have to be used.

6. Calculate the corresponding pressure losses Δp_E and Δp_2 for the two-phase section, Δp_I and $\frac{\Delta p_3}{\Delta z}(z)$ for the three-phase section and a value for the pressure just above the gas inlet p_I using Eq. (4.39) till (4.44). Use the pressure loss along the three-phase section, including the geodetic loss which is derived from the concentrations, and the new value of p_I to calculate the pressure along the vertical, which is no longer linear. Repeat steps 3 to 5 with it.

7. Calculate the momentum G for the combinations of j_L and j_S using Eq. (4.4) till (4.14). Use the bisection method to repeat step 3 to 6 to come to the value for j_L and j_S for which the momentum G is smaller than 100.

If there is no solution to the momentum balance G with a value smaller than 100 there is no solution within the selected range of j_L values or no solution at all.

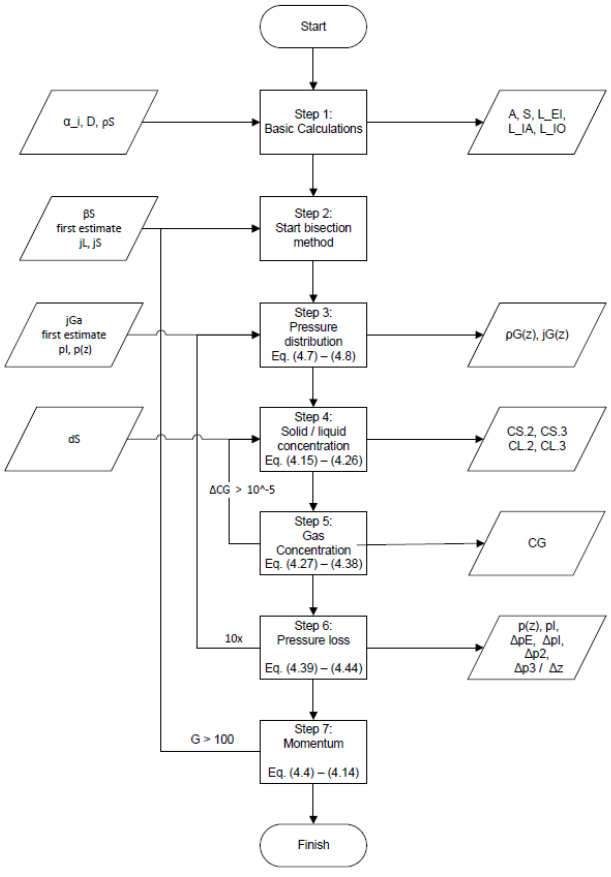

Figure 4.7: Flow scheme airlift model

4.2.5 Post-processing equations

Compression & efficiency

An important specification of an airlift is the power it consumes to come to a certain production M_s. As compressed air provides the energy which drives the water flow from sea floor to surface, it is the air compressor that provides the required energy to the lifting system. Analysing the air compressor can be used to calculate the power requirement of the riser system.

An air compressor is similar to a pump, it uses mechanical energy to increase the pressure of the fluid so it can be transported through a pipe with a certain flow. But since air, in contradiction to water, is highly compressible the compressor also reduces the volume of the air.

To compare different airlift lay-outs with different productions to each other a dimensionless parameter will be used which relates both production and power consumption for a certain water depth h: the energetic efficiency η_e. Energetic efficiency is in this study defined as the difference in potential energy (power per time-unit) between the solids at sea floor and surface, divided by the energy requirement of the system.

Energetic efficiency η_e of the entire riser system can thus be calculated by comparing these powers:

$$\eta_e = (1 - \frac{\rho_L}{\rho_S}) \frac{\Delta P_{pot}}{P_c} \tag{4.45}$$

From the equation for potential energy ($m_S\ g\ h$) the added potential power ΔP_{pot} to the solid particles, which could theoretically be re-generated by lowering the particles through the liquid over the vertical distance h, can be determined, using:

$$\Delta P_{pot} = \rho_S\ A\ j_S\ g\ h \tag{4.46}$$

The power requirement P_c for the three different compression types, and thus for transporting a certain amount of solids by airlift over a certain vertical distance h, is more difficult to calculate.

The theoretical power requirement of a compressor depends on the method which is used to model the compression. There are 3 theories of compression which are elaborated in this study:

- isothermal compression, which forms the bottom limit of power requirement, assumes a constant temperature during the process of compression and thus a transport of all generated heat to the surrounding;
- isentropic compression, which is used in design manuals of centrifugal compressors, and is an in-between form of isothermal and adiabatic compression;
- adiabatic compression, which forms the upper limit of the power requirement, assumes that there is no heat exchange at all with the surrounding, and thus the temperature rises during the process.

In most literature regarding airlifting the process of compressing is assumed to be isothermal, which means there is no change in temperature of the air during the process, but all generated heat is transported to the surrounding. Isothermal compression means the following is valid:

$$p\ V = constant = \alpha_k \tag{4.47}$$

Re-writing it would lead to $p = \frac{\alpha_K}{V}$ with α_K being the constant. The work W done to the gas with volume V between the surface and pipe inlet I can be calculated by integrating the pressure p for volume change ΔV:

$$W = \int_{V_I}^{V_{atm}} p\ dV = \alpha_k \int_{V_I}^{V_{atm}} \frac{1}{V}\ dV = \alpha_k \ln \frac{V_{atm}}{V_I} \tag{4.48}$$

Filling in $V = \frac{\alpha_k}{p}$ for both volumes and replacing α_k, using p_{atm} for the atmospheric pressure and p_I for the pressure at the air inlet along the suction pipe, leads to:

$$W = \alpha_k \ln \frac{p_I\ \alpha_k}{p_{atm}\ \alpha_k} = p_{atm}\ V_{atm}\ \ln \frac{p_I}{p_{atm}} \tag{4.49}$$

Equation 4.50 gives the isothermal power requirement of the compressor $P_{c.iso}$, which is work W per time-unit, in which $Q_{G.atm}$ is the inflow of gas under atmospheric conditions, the volume V per time-unit:

$$P_{c.iso} = Q_{G.atm}\ p_{atm} \ln \frac{p_I}{p_{atm}} \tag{4.50}$$

The power requirement of the two alternative approaches, isentropic and adiabatic compression, are harder to calculate. All three compression processes are polytropic. A polytropic process is described, with pressure p, volume V and polytropic index n, by:

$$p\ V^n = constant = \alpha_k \tag{4.51}$$

In case of isothermal compression the polytropic index n would be 1, while for adiabatic compression of air it is around 1.4. When designing a compressor it is more common to use a value for n in between the two. A value of 1.2 is used in this study to show the effect.

The power requirements of the isentropic (polytropic) process $P_{c.pol}$ and adiabatic process $P_{c.adi}$ can be calculated in a similar manner, using the different values for polytropic index n. Similar to for isothermal compression first the work W is derived, using the rewritten equation for p and integrating it:

$$p = p_{atm}\ \frac{V_{atm}}{V} \tag{4.52}$$

$$W = \int_{V_I}^{V_{atm}} p\ dV = \int_{V_I}^{V_{atm}} p_{atm}\ (\frac{V_{atm}}{V})^n\ dV = p_{atm}\ V_{atm}^n \int_{V_I}^{V_{atm}} (\frac{1}{V})^n\ dV \tag{4.53}$$

Solving the integral gives:

$$W = p_{atm}\ V_{atm}^n\ \frac{V_I^{1-n} - V_{atm}^{1-n}}{n-1} = (\frac{1}{n-1})\ p_{atm}\ V_{atm}^n\ (\frac{V_I}{V_{atm}})^{1-n} \tag{4.54}$$

Filling in $\frac{V_I}{V_{atm}} = (\frac{p_I}{p_{atm}})^{-\frac{1}{n}}$, which can be derived from Eq. (4.51), leads to:

$$W = (\frac{1}{n-1})\ V_{atm}\ p_{atm}\ ((\frac{p_I}{p_{atm}})^{\frac{n-1}{n}} - 1) \tag{4.55}$$

The total amount of power P_c required for both the isentropic (polytropic) compression $P_{c.pol}$ and the adiabatic compression $P_{c.adi}$ can then be calculated with Eq. (4.56), with only difference in the value for n.

$$P_{c.pol.adi} = (\frac{1}{n-1})\ Q_{G.atm}\ p_{atm}\ ((\frac{p_I}{p_{atm}})^{\frac{n-1}{n}} - 1) \tag{4.56}$$

In case the gas is replaced by either solid or liquids both the substances would have to be pumped down to the inlet point, where they are inserted into the riser. A pump will be required to do so. Contrary to the pumps which were compared in a previous vertical transport study the pump will not have to be able to transport large particles, which means it can be similar to the pump which transported the water down to the diaphragm pump, as was modelled in that same study.

The positive displacement pump, which will not be designed in much detail, is assumed to have a pumping efficiency η_p of 90%. Energy required for separation of the fluid will be neglected, just like attrition of the microspheres. Besides the energy losses in the PD-pump the other way in which energy is lost is by friction losses along the way. The total mechanical power required P_p to propel the PD-pump can then be estimated by:

$$P_p = \frac{Q_G \ \Delta p}{\eta_p} \tag{4.57}$$

Pressure loss Δp is the pressure loss in the substance supply system, which can be split up in the velocity dependent dynamic pressure loss and the density dependent static pressure loss, to be calculated by:

$$\Delta p = (\epsilon_E + \epsilon_a + \lambda \frac{h_I}{D_s}) \ \frac{v_{G.s}^2}{2} \ \rho_G + h_I \ g \ (\rho_L - \rho_G) \tag{4.58}$$

Substance velocity $v_{G.s}$ is the velocity in downward direction in the supply pipe. When using a solid substance the supply pipe will be used for transporting back the return water to the sea floor as well, where it will be inserted into the (a more extended) buffer at the bottom of the riser. This method of supply will make it impossible to vary the inlet height for the solid substance, unless the return water does not have to be brought back to the sea floor.

Flow regimes

Taitel mentions a number of equations for the transition in his publication, which are the lines that can be found in figure (4.8). These 5 equations are copied and used in the model, but are not derived in detail.

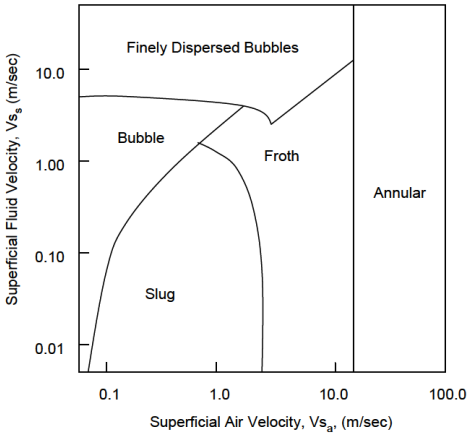

Figure 4.8: Flow regime map relating the different fluxes

Whether these are applicable perfectly to deep water riser system is something which should be tested to be certain, since the formulas are based on two-phase (air-water) tests in small diameter pipes (2.5 and 5 centimetre) with a limited riser length. Other factors which influence the results might the use of salt water and the temperature difference over depth.

The first equation is for the transition between the froth (f) flow regime and the annular (a) flow regime: $j_{G.fa}$.

$$j_{G.fa} = 3.1 \ \frac{\sqrt[4]{\sigma g(\rho_L - \rho_G)}}{\sqrt{\rho_G}} \tag{4.59}$$

In this equation σ is the surface tension of the liquid, which has a value, according to Taitel, of 0.1 N/m^2 for water. Assumed will be that a low concentration of solids will not influence this value. It is interesting to see that this equation is not dependent on liquid flux j_L and has a constant value of around 15.

The transition between the slug (s) and froth(f) flow regime is harder to determine, since it varies for different airlift geometries. An attempt is made using the factor α_{sf}, which depends on amongst others the pipe diameter D. Taitel suggests a value of about 2.24 for it.

$$j_{G.sf} = -j_L + \alpha_{sf} \sqrt{g\ D} \tag{4.60}$$

The boundary between bubbly (b) flow and slug (s) flow $j_{G.bs}$ involves the pipe diameter as well, and although Taitel only performed tests on small pipe diameters (2.5 and 5 cm) the equation for the boundary will assumed to be the same for larger pipe diameters:

$$j_{G.bs} = \frac{j_L}{3} + 0.383 \sqrt[4]{\frac{\sigma g(\rho_L - \rho_G)}{\rho_L^2}} \tag{4.61}$$

The two remaining boundaries form upper limits for the liquid flux j_L, and separate both the froth (f) and bubbly (b) flow from the dispersed bubbly (d) flow. The transition between bubbly (b) and dispersed bubbly flow is given by Eq. (4.62), which depends on pipe diameter D, and the other by Eq. (4.63):

$$j_{G.bd} = -j_L + 4\ \frac{D^{0.429}\ (\ \frac{\sigma}{\rho_L}\ )^{0.089}}{j_L^{0.072}}\ (\ \frac{\sigma g(\rho_L - \rho_G)}{\rho_L}\ )^{0.446} \tag{4.62}$$

$$j_{G.fd} = j_L \tag{4.63}$$

4.2.6 Validation

The model as coded for this research is validated based on data from the publication of Weber (Weber and Dedegil, 1976). The data itself is given in Appendix A. The problem compared to normal validations is, however, that Weber did all his experiments for different geometries of the airlift. The figure 4.9 compares the outcome of liquid flux j_L of both the model and the experiments, for a set value of gas flux $j_{G.atm}$, solid flux j_S, water depth h, inlet ratio α_I and submergence ratio of the riser α_A.

Four different types of experiments were done with varying geometries of the airlift. The resources were:

- Gravel ($\rho_S = 2575\ kg/m^3$ and $d_S = 5mm$)
- Sand ($\rho_S = 2610\ kg/m^3$ and $d_S = 0.6mm$)
- Lignite ($\rho_S = 1143\ kg/m^3$ and $d_S = 50mm$)
- Water (no solids)

Comparing the results of the model with the data from the experiments result in figure (4.9). The figure shows reasonable results of the model, especially in case of low density particles or two-phase flow (water only).

However, for five experiments the modelled liquid flux is underestimated by more than 30% in comparison to the measured liquid flux. Four of those are related to sand and have measurement number 19, 23, 24 and 25 in table (A.2) in Appendix A. These measurements have in common that, besides the fact they are related to gravel, the gas inlet is located relatively high along the riser, since the value for α_I is lower than 0.35. A similar value for the α_I does not cause large deviations in case of gravel, lignites or water.

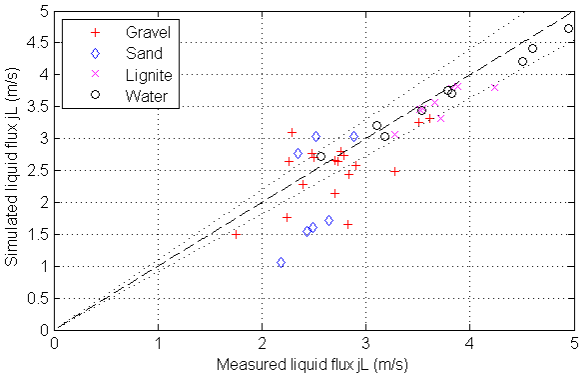

Figure 4.9: Validation Weber data

4.3 Performance

The performance of an airlift will be described in this paragraph, split in an operational part and an analytical part. The operational part will show the results that were found with the model, while the second part analyses the effects and problems associated with those results.

In the original airlift report, which can be found in Appendix C.3, a sensitivity study of the different parameters can be found as well. The most important parameter to be varied is the air flux in atmospheric conditions $j_{G.atm}$. This is also the parameter which can be still be varied when the air lift is operational.

Figure (4.10) shows the effect of varying this air flux for a certain combination of parameters. The three different efficiencies belong to the three different methods of compression for which the required power is calculated. It shows that increasing the gas flux $j_{G.atm}$ leads to an increase in production, but a decrease in efficiency.

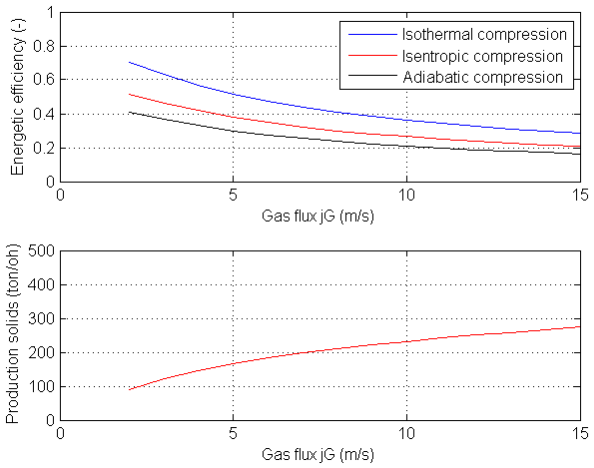

Figure 4.10: Efficiency and production for varying air flux

One of the reasons for doing a more detailed study into the behaviour of airlifting was that the Weber model showed an increasing efficiency over an increasing working depth. Figure (4.11) shows the same result for this model, with an efficiency increasing from under 10% at limited water depths to an efficiency of almost 50% in case of isothermal compression.

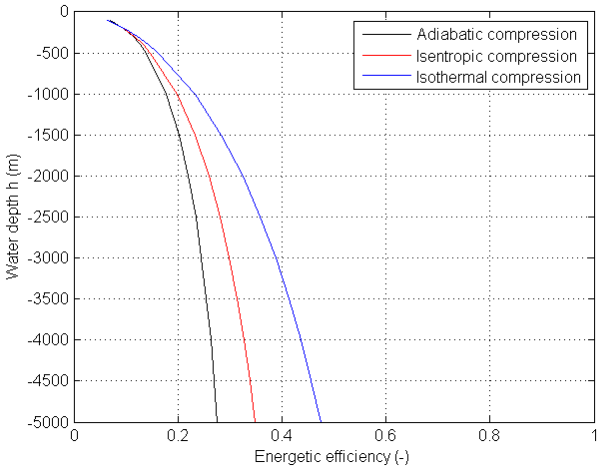

Figure 4.11: Variation in efficiency over working depth

4.3.1 Operation

Based on the parameter / sensitivity study two designs for an airlift are made. One with a high efficiency, but with the disadvantages that crushing of the solid particles would be required and that the pipe diameter would be relatively large. For this design the velocities, concentrations, occurring pressures, densities and flow regimes along the vertical will be showed.

The second one will be designed with a more practical approach. The pipe diameter will be a lot smaller while the riser is able to transport particles that are not crushed. Besides the production and efficiency the main difference between this design and the high efficiency design are pointed out.

High efficiency design

The starting points from the feasibility study were a targeted production M_S of 250 ton/oh for mining manganese nodules with a solid density ρ_S of 2,000 kg/m^3 at 5,000 m. Besides that a particle diameter d_S of 1 mm after crushing is uses in the model, a shape factor α_f of 0.7 and a drag coefficient C_D of 0.42.

The design of the airlift with the highest efficiency would have a diameter D of 1.0 m and an inflow concentration β_S of 3%, while the entrance height of the air is halfway the lift.

When the airlift is working there is still the possibility to vary the gas inflow to increase or decrease production. The bottom limit of the volumetric gas flux $j_{G.atm}$ for the given riser design is about 5 m/s, since for lower values the airlift is no longer able to transport the solids for the fixed inflow concentration β_S. The gas flux $j_{G.atm}$ of 5 m/s relates to a volumetric flow $Q_{G.atm}$ of ca. 4 m^3/s for the given diameter D of 1 m. An upper limit for the gas flux does not exist, but the production M_S moves towards an asymptotic value for increasing gas fluxes.

The effect of varying the gas flux on the production, power usage and efficiency is displayed in figure (4.12). Best efficiency point lies close to the targeted production of 250 ton/oh, which is a consequence of the search in the sensitivity study for the 'ideal' airlift. Increasing the gas flux and thus production decreases the energetic efficiency η_e somewhat. The increase in power which is necessary to provide the airlift with an increasing amount of gas flux can be seen in the bottom part of the figure.

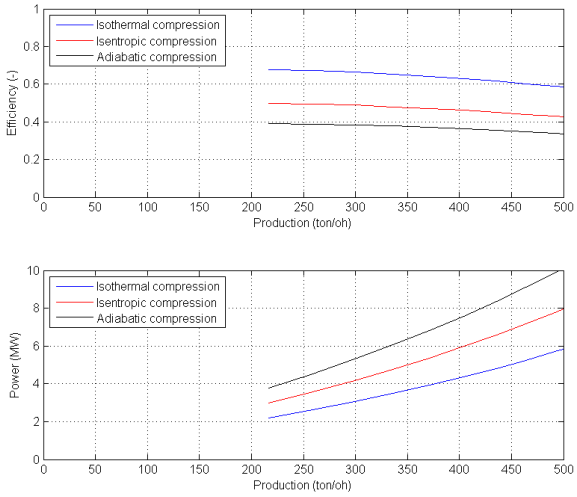

Figure 4.12: Power and efficiency for different productions (and related gas flows)

The velocities, concentrations and relative density of the mixture for the targeted production of around 250 ton/oh (for a value $j_{G.atm}$ of 6 m/s) is displayed in figure (4.13). The velocity curves for gas, liquid and solids have a similar shape, although the velocity of gas is higher than the velocity of liquid and the velocity of liquid higher than the velocity of solids at all time. This is a logical consequence of their densities.

The velocity of all three remains under the 2 m/s until the last 250 m of the riser, where they all three increase and the gas velocity reaches a value of almost 10 m/s. Because the value for the relative velocity between liquid and solids hardly depends on the velocity (only a bit through the Reynolds number) the velocity difference between the two remains the same, even in those last meters, where both reach a value of near 4 m/s.

The concentration of the gas depends partially on the value for the gas flux j_G. This value increases along the vertical with the decreasing absolute pressure. Over the last few hundred meter of the airlift the value for the gas flux increases by a factor 10, having a similar effect on the volume concentration of gas which increases from well under 10% to over 60%. Consequently the concentrations of both liquid and solids decrease.

The relative density is the density of the mixture compared to the density of the salt water with a value of 1,030 kg/m^3. Obviously the mixture density will be higher in the two-phase section of the airlift, where it is a mixture of the salt water and the heavier solids. From the location the gas flows in upward the density is lower than the water density, which is required to at least get a statical equilibrium between the heavier two-phase section and the lighter three-phase section of the riser content. The density of the mixture in the three phase section decreases over the vertical with increasing gas flow concentration C_G, reaching values of less than 400 kg/m^3 at the outflow.

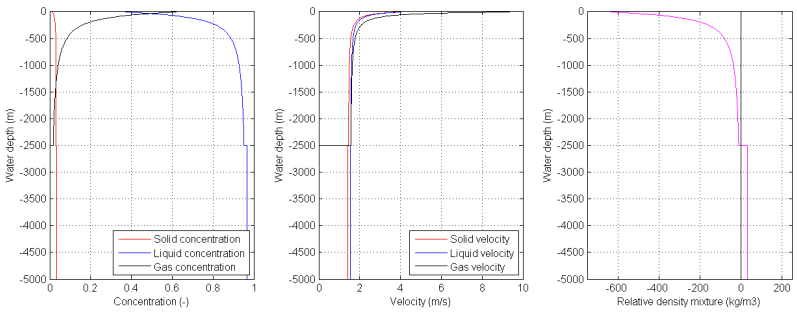

Figure 4.13: Concentration, density and velocity distribution along the riser

The pressure along the vertical has two boundary values: the atmospheric pressure p_{atm} at the outflow, which is 101.3 kPa, and the water pressure at the entrance, which is calculated by liquid density ρ_L times gravity acceleration g times water depth h. To enable the water content to flow upward the pressure within the riser has to be lower than the water pressure surrounding the riser. Figure (4.14) shows the pressure along the riser. The pressure at the gas-inlet p_I is re-calculated during the model simulation until the correct value is reached for a certain combination of parameters.

In the two-phase section of the riser the velocity will be constant and consequently the dynamic pressure loss. Since the concentration is constant as well the static (geodetic) pressure loss has a constant value too, causing a straight line from the entrance pressure to the gas-inlet pressure p_I, which is less steep than the curve of the water pressure along the same vertical.

The three-phase section has an increasing velocity and decreasing mixture density, causing respectively an increase in the dynamic pressure loss and a decrease in the static pressure loss over the vertical. At first the dynamic pressure loss dominates, causing a further increase of the absolute pressure difference (relative pressure) between the surrounding water and the riser content, up to a value of about 1 MPa. Further upwards along the vertical the decrease in static pressure loss becomes more important. The pressure value consequently decreases to the atmospheric pressure at the outflow.

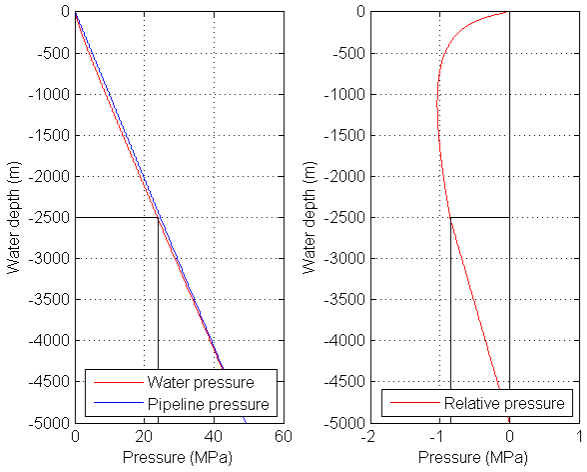

Figure 4.14: Pressure distribution along the riser

The varying pressure, the related gas flux variation along the vertical and the liquid flux j_L can be used to determine the flow types in the riser. The value for both fluxes can be plotted in Taitel's map, like given in figure (4.5). The names of all the flow regimes are not plotted in the map but can be found for reference in the original map of Taitel which is given in the theory, figure (4.14).

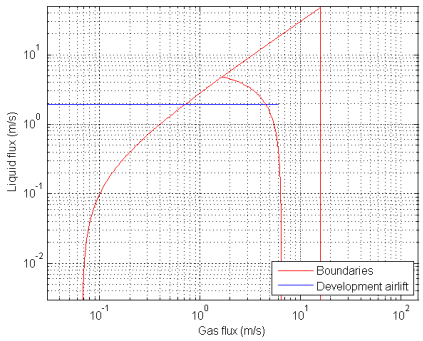

Figure 4.15: Taitel's map with flow regimes for the riser

The flow regimes occurring along the vertical of the upper part of riser are the bubbly flow, slug/plug flow and froth flow. The major part (2,370 of the 2,500 meter) of the riser will have bubbly flow, since the absolute pressure is sufficiently high to keep the gas flow low. According to Taitel's map in figure (4.15) the flow regime changes to plug/slug flow when a value of about 0.7 m/s is reached for the gas flow j_G. This takes place at a water depth of about 130 meter, as can be seen in figure (4.16).

With the decreasing pressure the gas flux keep increasing, and when a value of 15 m/s is reached (at a water depth of 20 m) the flow regime changes again, from slug/plug flow to froth flow.

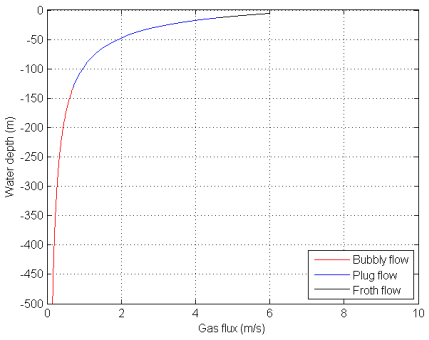

Figure 4.16: Flow regimes in the upper 1,000 m of the riser

Practical design

The pipe diameter of 1.0 meter is rather large and would lead to high capital costs. Not only for the riser itself but also for the mining vessel which will need to support the weight and handle the flow. An attempt is made to come to the same production with a smaller riser. The (crushed) particle diameter d_S which was used in the sensitivity study had a value of 1 mm. In the starting points of the feasibility study, however, a value of 50 mm was used for not-crushed particles (although larger ones occur on the sea floor as well).

The geometry of the airlift will remain almost the same as in the sensitivity study, the only parameters (besides the particle diameter) which are varied are the gas flow $j_{G.atm}$, the inflow concentration β_S and the air inlet location. The air inlet location is put all the way to the sea floor (value for α_I becomes 1), which will decrease the efficiency but increase the working range of the lift.

For a first estimate the pipe diameter is halved, to see the effect on productions and efficiencies for a varying gas flux $j_{G.atm}$. Figure (4.17) shows these, and clearly can be seen that the efficiency would be half of the original for the same production. The targeted production M_S of 250 ton/oh is reached for a gas flux of 35 m/s, which is a large increase compared to the 6 m/s which was found for the high efficiency airlift.

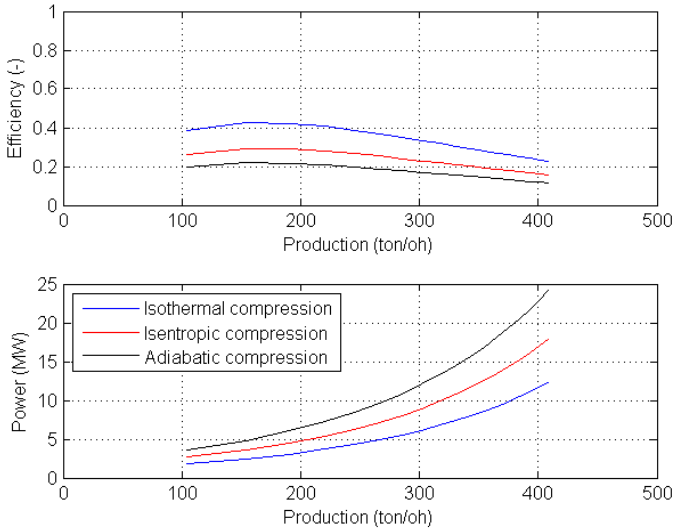

Figure 4.17: Power and efficiency for different productions (and related gas flows)

A larger disadvantage than the decreased efficiency might come from the changing flow regimes in the riser. The effect of the flow regimes is not implemented into the model, but the annular flow type might be a flow type to avoid. According to Halkyard (Halkyard and Doyle, 2007) annular flow has a limited production capacity. Figure (4.18) shows that this flow regime will be occurring in the last 40 meters of the riser.

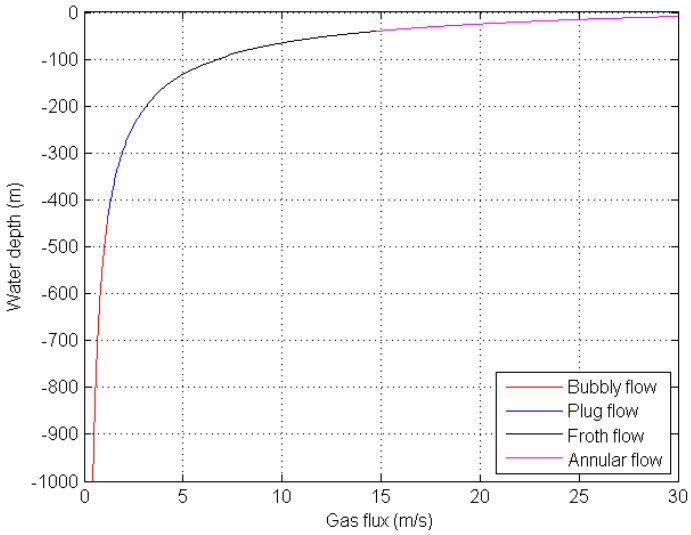

Figure 4.18: Flow regimes in the upper 1,000 m of the riser

Changing the pipe diameter D to a value of 0.75 m instead of 0.5 m would prevent the annular flow from occurring. The next paragraph will show some alternative solutions at which the pipe diameter can still be kept at 0.5 m.

4.3.2 Analysis

The analyses of the airlift will contain four main subjects: the process that takes place during the start-up of the airlift until the steady-state is reached; the air supply of the airlift; an analyses of the flow regimes, and in particular the plug/slug flow regime; and two alternatives to a large pipe diameter that prevent annular flow regimes from occurring.

Start-up

The functioning of the airlift was explained in the chapter about theory. The three steps (step 3 and 4 of the original explanation are combined) occurring during the riser start-up are:

1. Air (gas) flows in at the gas inlet, and rises through the fluid up to the surface. The gas flow is not sufficient to let the liquid flow.

2. The lower density inside the pipe and the slip between gas bubbles and liquid makes the water flow through the pipe. The amount of liquid flow is not sufficient to pick up the solids from the sea floor. The relative velocity between solids and liquid is larger than the liquid velocity.

3. At this stage the amount of air insert into the pipe is sufficient to give the water velocity a value higher than the particle settling velocity, causing a flow of solids from sea floor to the pipe outlet.

In practice the airlift will be started up slowly, by increasing the gas flux step by step by adding more power to the compressor. The boundary values for which the start-up goes to the next step can be calculated using the model. The assumption is made that the inserted (pressure dependent) gas flux will be applicable for the entire riser at once, however this in practice might take up to half an hour, as this is how long it can take for one bubble to rise over the entire vertical.

The (practical) small pipe diameter airlift with not-crushed particles was used for the example simulation. The value for $j_{G.atm}$ for which the start-up goes from first to second step is found by simulating the model with a very small solid inflow concentration (β_S is 10^{-10}). In reality this means that the lower density of the riser content compared to the surrounding water will be sufficient to compensate for the pressure losses by wall friction. A small value, like 10^{-5} m/s for the atmospheric gas flux $j_{G.atm}$, is already sufficient to make the liquid flow.

The second transition occurs when the inflow velocity liquid is higher than the particle settling velocity. The minimum value for the atmospheric gas flux needed to come to this velocity is 0.2 m/s (about 0.04 m^3/s).

Air supply

The two airlifts which were studied so far, the high efficiency airlift and the practical airlift design, have slightly different properties when it comes to the air supply. The high efficiency airlift requires an airflow $Q_{(}G.atm)$ of 4.7 m^3/s to a depth 2,500 m, where it needs to have a pressure p_I of 24 MPa. The other airlift needs an airflow $Q_{(}G.atm)$ of 6.9 m^3/s at a depth 5,000 m, with a pressure p_I of 50 MPa.

The selection of a compressor which is capable of these productions and pressures is relatively simple: only a multi-stage centrifugal compressor will be able to do something like that (et al, 2007). In one stage the compression increase can be a factor 6 max, which means at least 4 stages would be required to go from atmospheric pressure (p_{atm} is 101.3 kPa) to the required pressure p_I.

Depending on the method of compression the temperature can have changed. In case of isothermal the temperature would remain the same, but for isentropic and adiabatic compression the change in temperature can be calculated by Eq. (4.64). The temperature after isentropic compression would be 50 degree Celsius for the 'ideal' airlift and 56 degree Celsius for the alternative in case of an inflow temperature of 20 degree Celsius.

$$T_I = T_{atm} \, (\frac{p_I}{p_{atm}})^{\frac{n-1}{n}} \tag{4.64}$$

For adiabatic compression the temperatures would become 95 and 118 degree Celsius. Air at these temperatures are not impossible to handle, especially not for isentropic compression, but might even be lowered by lowering the inflow temperature by cooling it first: halving the inflow temperature would also half the outflow temperature.

The compressed flow between compressor and gas inlet of the riser will have to be able to handle a transport of 0.02 m^3/s for the 'ideal' airlift, at a pressure of 24 MPa (assuming the pressure loss can be neglected) and 0.06 m^3/s for the 'ideal' airlift, at a pressure of 50 MPa. The volumetric flux itself will not pose a problem for the hose design, nor does the pressure difference of 50 MPa or the temperature of up to 118 degree Celsius, as their all many pipe variants available will are able to cope with these properties.

The gas inlet (diffuser) into the riser can be executed in several different ways. The type of diffuser will have an influence on the gas distribution in the riser directly after the point, but the effect can most likely be neglected over the entire vertical. Guet (Guet, 2004) proposed a number of different methods for such a diffuser: a nozzle, a vertical long porous inlet and an annular porous medium.

He concluded that the smaller the initial bubbles, the higher the efficiency of the airlift. An annular porous medium was preferable for that reason, since bubbles would remain smaller as they can be generated in smaller size and / or do not run into each other right away, which would be the case for the other two diffuser types.

The use of multiple inlet points was proposed in some airlift studies as well. The advantages could be that the pressure which would need to be overcome would be lower for the second gas inlet, as the pressure along the vertical is lower than the surrounding water pressure. Disadvantage would be the higher amount of gas flow required to make the riser content have the right density on average to come to a certain production. This subject is not further studied in this thesis.

It would be more interesting if it were possible to remove a certain amount of gas along the vertical. With a lower gas content in the upper meters a flow regime change to annular flow could be prevented and the velocities in that section could remain lower, decreasing the pressure loss by wall friction. However, the methodology to do seems rather complicated and will also not be part of this thesis.

Flow regime analysis

So far we have assumed that all regimes have the same transport capabilities. This sounds reasonable for bubbly flow and perhaps froth flow, but when considering slug / plug flow some other effects might occur, while for annular flow the transport capacity might be completely different.

Annular flow is considered to be lift regime which is not able to transport solids (Halkyard and Doyle, 2007). This limitation was not build into the model yet as it would decrease the possibility to study the performance by varying parameters even further, but should be looked into in more detail now some potential designs for an airlift are found.

For slug/plug flow a more detailed analyses is made: imagine a particle being transported by an airlift and in the considered section the slug flow regime is occurring. The difference in velocity between gas, liquid and solids makes for the gas plugs to catch up with the liquid and solids constantly. When that happens the liquid flows around the plug in a small film near the wall. The solid particles have two options, either the solid-water mixture stays intact and the solids flow in the small film near the wall as well, or the particles fall through the plug into the next slug.

The first of these two options is used in the model, but the second option will be considered in this paragraph. To do so we use the high efficiency airlift as found after the parameter study as an first example. Figure (4.19) shows that slug flow occurs in the section between 130 m water depth and 20 m water depth. For this study the velocity and concentration data from the node at 100 m water depth will be used.

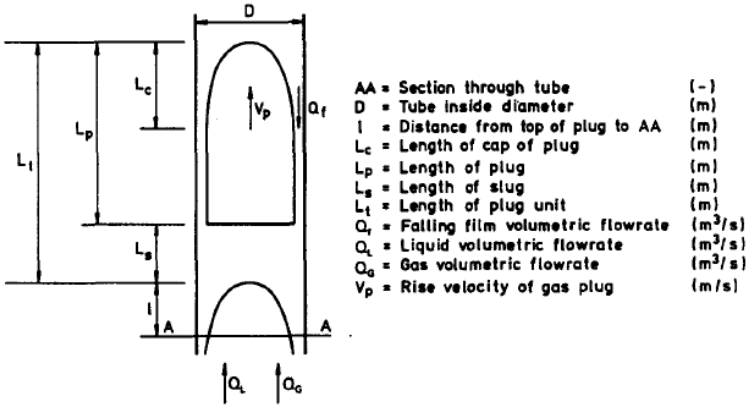

Figure 4.19: Schematized slug flow transport

McQuillan (McQuillan and Whalley, 1984) suggested a method to calculate the velocity of the slug and plug in a two-phase air water flow. However, when testing this method the results were fairly unrealistic, and for that reason a simpler approach was used.

The assumption is that the plug flow is cylindrical of shape, and covers the entire area of the riser. The length of the gas plug in comparison to the length of the liquid slug is then easily derived from the ratio between gas flux and liquid flux, which are 1.06 and 1.6 respectively at this depth, leading to a plug/slug length ratio $L_{plug} : L_{slug}$ of 1:1.51. The influence of the low concentration of solids is considered negligible.

With this ratio known the effect on one solid particle from this example is investigated. This solid particle has (on average) a hindered settling velocity of 0.11 m/s in quiescent liquid, which is equal to the relative velocity between liquid and solid particles. The relative velocity when the particle enters the plug is calculated in a similar manner: the free fall velocity of a particle with a diameter d_S of 1 mm, which is assumed to be obtained instantly, is calculated by:

$$v_{SG} = \sqrt{\frac{4\ g\ d_S\ (\rho_S - \rho_G)}{3\ C_D\ \rho_G}} = 7.13 m/s \tag{4.65}$$

The average velocity of the gas and liquid in the airlift are 3.32 and 2.45 m/s. Given the relative velocities this would lead to a negative velocity downward when the particle enters the plug. The average velocity of the solid particle can then be calculated, by simply calculating the distance it covers during its path through one slug and one plug and the amount of time it takes.

At a relative velocity of 0.11 m/s it would take the particle 13.73 seconds to travel through the slug of 1.51 m, during which it has an absolute velocity v_S of $2.45 - 0.11 = 2.34 m/s$. The relative velocity in the gas plug will be a lot higher with 7.13 m/s, causing the particle to fall through it in 0.14 second, during which it has an absolute velocity v_S of $3.32 - 7.13 = -3.81 m/s$.

Average absolute velocity for the particle becomes $2.17 m/s$, which is about 7% lower than followed from the model, where the influence of gas is neglected and the velocity is $2.45 - 0.11 = 2.34 m/s$.

For the practical airlift design it might be different. The same analyses is made for the example given in figure (4.18), where bubbly flow takes place between a water depth of 435 m and 205 m. The specifications of a water depth of 300 m will be used in the calculation.

Velocities at this depth are respectively 6.48 m/s, 5.02 m/s and 4.28 m/s for gas, liquid and solids, while gas flux j_G has a value of 1.91 m/s and liquid flux j_L 3.33 m/s, leading to a ratio between plug/slug length ratio $L_{plug} : L_{slug}$ of 1:1.74 for the given assumptions. Hindered relative velocity between solids and liquid thus has a value of 0.74 m/s, while the fall velocity of a solid particle in gas is again calculated by:

$$v_{SG} = \sqrt{\frac{4\ g\ d_S\ (\rho_S - \rho_G)}{3\ C_D\ \rho_G}} = 15.94 m/s \tag{4.66}$$

Repeating the same calculation gives an average absolute velocity of the solids of 3.94 m/s, which is only 8% lower than the model velocity of 4.28 m/s. The conclusion can be made that the plugs do have an influence on the solid velocity if the particles fall through them, and the lower the velocities the larger the influence, but it is not unreasonable to neglect for now.

The transition to annular flow might become a problem for the practical airlift. One method to prevent such transition was already described earlier in the paragraph about air supply, but the removal of gas further up the vertical seems relatively complicated and will not be investigated in this thesis.

Other alternatives could be: alteration of the pipe geometry, by creating an underwater or pressurized outflow or using alternative substances to air, like other gasses, light liquids or light solids. These will be analysed in the next two paragraphs.

Alternative geometry

First the under water outflow will be considered, which is in practice the same as a pressurized outflow for a short pipeline. In the model the boundary value for the pressure at the outflow is the atmospheric pressure $j_{G.atm}$, with a value of 101.3 kPa. To simulate an under water outflow the boundary pressure is increased by the water pressure at the new outflow depth, which can be calculated by $\rho_L\ g\ h_o$ with h_o the water depth where the outflow will be located.

A simulation is made for the practical airlift geometry to see the effect on the flux development and the flow regime changes. The outflow depth h_o is set at 10 m, which would be equal to a pressurized outflow of 101 kPa more, giving a total absolute pressure at the outflow point of 202.3 kPa.

The resulting flow regime changes in the last 500 meter of the riser are shown in figure (4.20), which can be compared to a similar plot for the original simulation in figure (4.18). As can be seen the maximum flux j_G which is reached is almost a factor two smaller than the original, which corresponds to the factor 2 increase in the pressure at the outflow point. Besides that the point at which the flow regime changes to annular flow is no longer at 40 meter below the water level, but 20 meter (10 meter under outflow point).

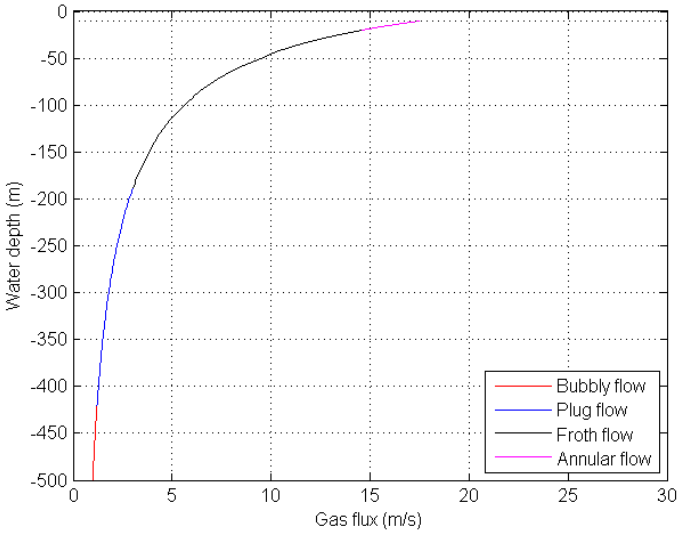

Figure 4.20: Flow regime changes in the upper 500 m of the riser with outflow at minus 10

Increasing the outflow depth to 13 meter under water level (and subsequently increasing the outflow pressure to 232.7 kPa) would decrease the gas flux at the outflow even further to a value of around 15, which would mean no transition to annular flow at all. If the outflow pressure can be increased by using some kind of pressure chamber or how the solids should be transported over the last 13 meters is not investigated further in this thesis.

Alternative substances

The buoyant substance which will replace air will need to have one important property: the density (ρ_G) has to be lower than the (salt) water density ρ_L. Other requirements could be that they should be cheap, not damaging to the environment or dangerous to any part of the operation, easy to store and transport, easy to separate from the water and solids, and not cause a chemical reaction in the process.

Using another gas to replace air will not change the fact that the flow regimes will change along the vertical. However, it might change the maximum flux near the riser outflow, where the annular flow regime takes place for the airlift.

Two gas alternatives to air are selected, both of them relatively easy and cheap to obtain and occurring in large quantities in the atmosphere: helium and argon, both noble gasses. Difference between the two is the density. Argon is higher in density than air by a factor 1.5, while helium is a factor 7 lighter than air. These two fit all the given in requirements in the start of this paragraph, except that the use of argon might lower the amount of oxygen, which could be dangerous when used in a closed environment where people work because of the risk of asphyxiation. Two other gasses, methane and carbon dioxide, are used as references.

As the required gas flux for helium turns out to be lower than for air, while efficiency and production remains the same, helium forms an interesting alternative. The problem it would have to solve, however, is the change to the annular flow regime which takes place in the upper section of the airlift.

Figure (4.21) shows the flow regime variation in the upper 500 meter of the riser, for both air (solid line) and helium (dotted line). The difference is hard to see in this figure, as the change is small. Annular flow still takes place, but only starts slightly higher along the vertical, at 30 meter under water level instead of 35.

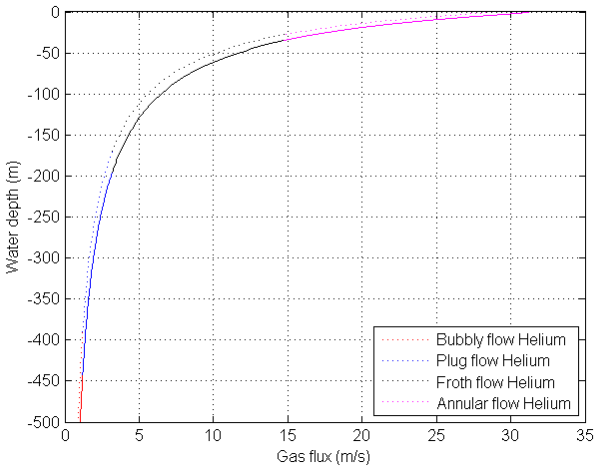

Figure 4.21: Flow regime changes in the upper 500 m of the riser, for both air and helium

The problems with the changing flow regime will not occur if either liquid of solids are used. However, compared to gas the densities of both liquids and solids are a lot higher. Finding a substance which is a lot less dense than (salt) water and still fulfils most of the other requirements is difficult.

An non-flammable alternative is silicone-oil. This is a transparent liquid which is used as hydraulic fluid or lubricant and the properties of the silicone oil are a density ρ of 816 kg/m^3 and a dynamic viscosity η of about 0.001, which is equal to water and a lot lower than most oil-type liquids. Disadvantage is that the environmental disadvantage of using this liquid remains. Furthermore the fluid is known to be water-repellent. How this would behave within the riser should be subject to testing, as this could be both an advantage (easy to separate) as an disadvantage (does not mix at all).

The production of the lift system is being limited by the riser in the simulation, and not by the supply. To determine the amount of liquid substance (silicone-oil) required to make the lift work first a variation of substance fluxes j_G is simulated to see the related productions, for exactly the same riser geometry as was used in the airlift study (with small pipe diameter and no crushing).

The model shows that the targeted production M_S of 250 ton/oh is not reached for the liquid substance, no matter how much silicone-oil is added to the system. Varying inflow concentration β_S and inlet height ratio α_I does not improve the maximum production.

The only factor which could improve the production to the required level would be the pipe diameter of the riser D. Improving D from 0.5 to 0.7 would cause an increase of the production to close to 300 ton/oh. However, at 0.7 m pipe diameter the airlift, where the liquid substance variant would be an alternative for, hardly has any flow regime problems left, making an alternative unnecessary.

A solid with a density lower than the density of salt water is not hard to find: wood, cardboard, cork, charcoal, polystyrene, etc. The low density of these materials is however based on their porosity and the high riser pressures would crush these materials, making them more dense than water. The metals lithium and potassium are less dense than water as well, but their flammability and capability to cause a chemical reaction with water ensures they are not alternatives.

An alternative could be a combination of a solid and a gas like a football or a balloon. To be able to cope with the high pressures the solid part should be very strong, like the materials which are used for building deep sea ROVs and submarines. Microspheres or microballoons are one of the materials used in this kind of application. They are also used as an filler material in foam or as thickener in adhesives.

Microspheres in general have a size of between 1 micrometre and 1 millimetre, densities between 120 kg/m^3 and 2,400 kg/m^3 and are either made of glass, ceramic or a polymer. Density not only depends on the material used, but also whether the microspheres are hollow or not. The low density microspheres able to cope with pressures of around 50 MPa (7,200 psi) are typically glass hollow microspheres with a size of around 2 micrometers and a density of 450 kg/m^3.

Although the microspheres can handle the high pressures, a possible disadvantage could be their inability to handle other forces caused by for example collision with solids. Attrition of the microspheres should be a subject to further research, if it turns out to be a serious alternative.

Figure (4.22) shows hollow microspheres which are used as filler material in adhesives and have a smaller skin than the microspheres used for the simulation.

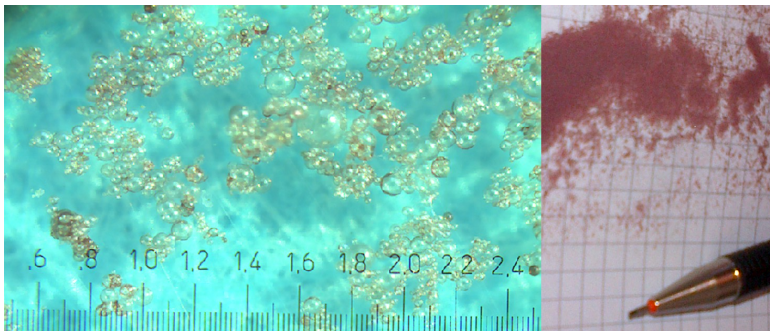

Figure 4.22: Microspheres enlarged by microscope and regular size

The supply pipe to the airlift will attempt to combine two functions: supplying a buoyant medium which will propel the lift and bringing back the water from mining vessel to sea floor, for environmental reasons. In practice it might be interesting to use two separate tubes for return water: one combining return water with microspheres and the other containing return water with tailings / sediment if present. The return water with microspheres is then added to the riser again, creating a closed system for the microspheres but keeping an semi-open system for water. In the model this separation is not (yet) present.

First a simulation is made in a similar way to the liquid substance, assuming the riser is the limiting factor. The related efficiency and power curves for the varied productions can be found in figure (4.23). Similar to the airlift the highest efficiency is achieved for the lowest flux for which the lift still functions. Based on that a value for the solid substance flux j_G of 0.6 m/s is selected, which would mean a volumetric flow of about 0.1 m^3/s of microspheres.

The maximum efficiency depends on the size of the supply pipe diameter D_s. However, the difference between a supply pipe diameter of 0.5 m (same size as the riser) and a diameter of 0.25 m is almost 40% energetic efficiency, which seems not worth it at first sight for making the pipe a factor 4 smaller. A more detailed feasibility study should be done to say it for certain, but for now a supply diameter of 0.5 m will remain to be used.

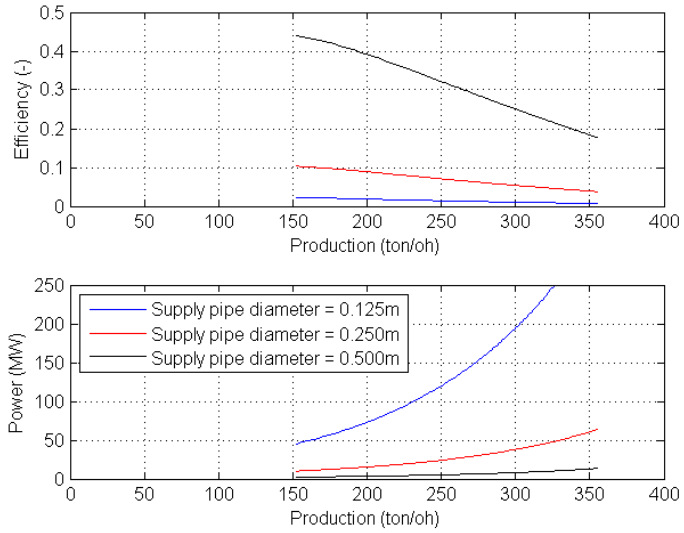

Figure 4.23: Power and efficiency for different productions (and related gas flows)

The chosen substance flux j_G of 0.6 m/s gives a production of slightly over 200 ton/oh, which is under the targeted production of 250 ton/oh. The concentration is increased to 7% to reach the targeted production M_S.

The supply pipe, which has to go all the way to the sea floor to return the water from the vessel (α_I cannot be varied in the model yet), has a pipe diameter of 0.5 m and can reach an efficiency η_E of 45%. In the pipe a combined flow of microspheres and return water will occur, with roughly the same velocity of about 3.1 m/s. The content has a density of almost 900 kg/m^3 in downward direction, consisting of a volumetric flow of 0.12 m^3/s microspheres and 0.5 m^3/s water.

In upward direction (the riser) the density of the content is 975 kg/m^3, while velocities of the microspheres, water and solid resources have values of 3.4, 3.3 and 2.7 m/s respectively.

One single microspheres will take almost an hour to go from the vessel to the sea floor and back up through the riser, making the total microsphere content of the system 360 m^3 (162 ton) of pure microspheres, which would be about 500 m^3 of microspheres when the porosity is taken into account. Attrition, losses due leaking and losses at the separation are then not even taken into account yet.

4.4 Conclusion

The original goal of this chapter was to model an airlift and compare it to the other 3 vertical transport methods that were described in chapter 3. A relatively simple model was made, and it can be concluded that for the best-case scenario of the simulation the airlift would reach efficiencies up to 50% at 5,000 m water depth, which would still be lower than the energetic efficiency of mechanical lifting. The airlift would have a size of 1 m in diameter and be able to reach the targeted production of 250 ton/oh without problems.

A more practical approach would be to use a smaller pipe diameter and not crush the particles. Disadvantages would be a lower efficiency (of 25%) and the occurrence of the annular flow regime.

Two methods to prevent annular flow regime from occurring are studied: An pressurized or under water outflow of the riser and the use of alternative substances. Lowering the outflow of the airlift to a water depth of 13 m would prevent the annular flow regime, in case of the practical approach which requires a riser diameter of just 0.5 m instead of 1.0 m.

Three different types of substances were used as alternatives to air: other gasses, buoyant liquids and buoyant solids. Both the alternative gas substances (helium and argon) and buoyant liquid (silicone-oil) were not large improvements when it comes to preventing annular flow.

The microspheres could be a more serious alternative to the other two types of substances. Main reason is the double function of the supply pipe: not only does it supply the microspheres to the lift, it also pumps the rest-water coming from the riser back down to the sea floor. The fact that an extra pipe with the same size as the riser would be needed to do this in an efficient way is a disadvantage which is not as crucial as it would seem, as such a pipe would be needed anyway to bring the return water down for environmental reasons.

Possible disadvantages could be the large amount of microspheres needed to propel the buoyancy induced lift: about 500 m^3 microspheres (bulk) at a time. Exact costs for the microspheres are not known, but the costs for replacing lost or broken microspheres might be an important factor. Besides that it can be recommended to study the attrition of the microspheres during the process first, and study the more detailed processes of separation at the mining vessel and supply to the riser at the sea floor.

Chapter 5

Conclusion & Recommendations

A number of conclusions can be made, based on the three different parts of the study altogether:

- Deep sea mining is feasible for Van Oord, especially in case of phosphorite mining. Resource prices, and to a lesser extent workability, are important factors when determining the feasibility.
- The Gemonod mining system, using ROVs, is most suitable for deep sea mining application based on the three different case studies considered in this thesis, although a trailing mining system would be preferable in case of phosphorite mining to save on capital investment costs.
- Mechanical lifting of the solids from sea floor to surface would be the most energy efficient transport system for the given case studies. To obtain the required productions the current velocity limits would have to be extended. Centrifugal pumps would be an alternative for phosphorite mining at limited water depths, especially when the trailing mining system is used.
- Centrifugal pumps and diaphragm pumps are less suitable to mine manganese nodules / at great water depth. Centrifugal pumps because of the complicated lay-out of the system and low efficiency, the diaphragm pump because of the high pressures occurring in the system.
- Airlifting is only interesting as alternative when mining manganese nodules / at great water depth. Efficiency remains lower than for mechanical mining and a relatively large riser would be required.

- Annular flow regime can cause problems when airlifting, but can be prevented by using a large pipe diameter for the riser, putting the airlift outflow 10-15 meters under water or using buoyant microspheres instead of air.

Some recommendations can be made for further study or research:

- A more detailed feasibility study should be done at Van Oord. The new study should take price development of mineral resources and costs for processing into account in more detail than was done in this thesis.
- Two case studies should be done for the design of deep sea mining vessels. The first one should be a technical design to convert one of Van Oord's flexible fall-pipe vessels into a deep sea mining vessel, which would be using the Gemonod system. The second one should be a similar design for conversion of one of Van Oord's TSHDs, to mine phosphorites at water depths up to 500 m using the trailing system. A detailed cost estimation should be included.
- The possibilities to use mechanical lifting as vertical transport mode should be explored in more detail, especially regarding the cause for the current velocity limitations of deep sea winches and the possibility to extend those limits.

Bibliography

C.E. Brennen. *Fundamentals of multi-phase flow.* 2005.

Coffey-Natural-Systems. Environmental impact statement solwara i project, 2008.

A. Nenes et al. Simulation of airlift pumps for deep water wells, 2009.

B. Guo et al. *Petroleum production engineering.* 2007.

C.H. Yoon et al. An experimental study on lab scale air-lift pump flowing solid-liquid-air three-phase mixture, 2000.

N. Hatta et al. Theoretical analysis of flow characteristics of multiphase mixtures in a vertical pipe, 1998.

S.Z. Kassab et al. Experimental and analytical investigations of airlift pumps operating in three-phase flow, 2005.

T. Saito et al. Lifting characteristics of manganese nodules by air-lift-pump on 200m vertical test plant, 1989.

Y. Taitel et al. Modelling flow pattern transitions for steady upward gas-liquid flow in vertical tubes, 1980.

S. Guet. Bubble size effect on gas lift technique, 2004.

John. E. Halkyard and Robert E. Doyle. Large scale airlift expirements for application to deep-ocean mining, 2007.

N.K. Liang and H.K. Peng. A study of airlift artificial upwelling, 2004.

A.F. Mahrous. Numerical study of solid-particles based airlift pump performance, 2012.

V. Matousek. *Dredge pumps and slurry transport.* 2004. Lecture notes OE4625, Delft University of Technology.

K.W. McQuillan and P.B. Whalley. Flow patterns in vertical two-phase flow, 1984.

John E. Miller. *The reciprocating pump*. 1995.

A. Ohnuki and H. Akimoto. An experimental study on developing air-water two-phase flow along a large vertical pipe: effect of injection method, 1995.

A. Ohnuki and H. Akimoto. Experimental study on transition of flow pattern and phase distribution in upward airwater two-phase flow along a large vertical pipe, 1998.

A.M. Post. *Deep Sea Mining and the Law of the Sea*. 1983.

K. Pougatch and M. Salcudean. Numerical modelling of deep sea air-lift, 2007.

Rolls-Royce. Fact-sheet cable traction control unit ctcu, 2013.

C.A. Shook and A.S. Bartosik. Particle-wall stress in vertical slurry flow. *Powder technology, volume 81, issue 2*, 1994.

SRK-Consulting. Offshore production system definition and cost study, 2010.

V. Stevanovic. Multi-fluid model predictions of gas-liquid two-phase flows in vertical tubes, 2007.

J.R. Thome. *Engineering databook III*. 2004.

USGS. Historical statistics for mineral and material commodities, 2013. URL `http://minerals.usgs.gov/ds/2005/140/`.

G.L.M. van der Schrieck. *Introduction to Dredging Technology*. 1999. Lecture notes CIE5300, Delft University of Technology.

H. van Muijen. Offshore dredging mining, 2007.

M. Weber and Y. Dedegil. Transport of solids according to the air-lift principle, 1976.

T. Yoshinaga and Y. Sato. Performance of an air-lift pump for conveying coarse particles, 1996.

Appendix A

Validation data airlift

A.1 Weber

The experimental data as given in table 1 of the publication by Weber (Weber and Dedegil, 1976).

Fixed data for these experiments are:

- Pipe diameter $D = 0.3$ m
- Water depth $\lambda = 0.025$
- Drag coefficient $C_D = 0.42$

Table A.1: Measurement data Weber (1)

	ρ_s	d_s	L	α_A	α_i	j_G	j_L	j_S	β_s
[-]	[kg/m^3]	[m]	[-]	[-]	[mm]	[m/s]	[m/s]	[m/s]	[-]
1	2575	5.00	279.0	0.96	0.63	2.65	2.50	0.029	0.011
2	2575	5.00	282.0	0.96	0.63	3.62	2.70	0.063	0.023
3	2575	5.00	285.0	0.96	0.64	5.43	2.29	0.080	0.034
4	2575	5.00	288.0	0.96	0.64	5.73	3.28	0.135	0.040
5	2575	5.00	294.0	0.96	0.65	3.68	2.76	0.053	0.019
6	2575	5.00	324.0	0.97	0.68	3.52	2.48	0.055	0.022
7	2575	5.00	325.9	0.97	0.68	5.62	2.79	0.117	0.041
8	2575	5.00	329.9	0.97	0.69	4.65	2.84	0.109	0.037
9	2575	5.00	332.9	0.97	0.69	3.40	2.26	0.058	0.025
10	2575	5.00	365.6	0.91	0.19	8.06	2.70	0.057	0.021
11	2575	5.00	407.6	0.94	0.28	5.29	1.75	0.079	0.043
12	2575	5.00	449.7	0.95	0.34	3.71	2.39	0.036	0.015
13	2575	5.00	451.3	0.94	0.23	7.70	2.24	0.075	0.032
14	2575	5.00	449.8	0.97	0.56	2.97	2.83	0.132	0.044
15	2575	5.00	450.3	0.97	0.56	5.19	2.90	0.077	0.026
16	2575	5.00	55.4	0.85	0.87	8.13	3.61	0.180	0.047
17	2575	5.00	55.4	0.85	0.87	5.52	3.51	0.096	0.027
18	2575	5.00	55.4	0.85	0.87	3.30	2.73	0.076	0.027

Table A.2: Measurement data Weber (2)

	ρ_s	d_s	L	α_A	α_i	j_G	j_L	j_S	β_s
[-]	[kg/m^3]	[m]	[-]	[-]	[mm]	[m/s]	[m/s]	[m/s]	[-]
19	2610	0.60	249.4	0.86	0.19	6.85	2.64	0.106	0.039
20	2610	0.60	57.3	0.88	0.90	3.57	2.88	0.078	0.027
21	2610	0.60	61.3	0.85	0.91	5.52	2.35	0.180	0.071
22	2610	0.60	61.3	0.85	0.91	6.45	2.52	0.172	0.064
23	2610	0.60	157.4	0.85	0.32	6.90	2.43	0.152	0.059
24	2610	0.60	157.9	0.84	0.32	3.11	2.18	0.073	0.033
25	2610	0.60	157.4	0.85	0.32	5.02	2.49	0.160	0.060
26	1143	50.00	451.0	0.94	0.23	8.26	3.72	0.024	0.060
27	1143	50.00	451.0	0.94	0.23	10.09	3.52	0.028	0.075
28	1143	50.00	451.0	0.94	0.23	5.83	3.28	0.016	0.048
29	1143	50.00	449.8	0.96	0.35	9.78	3.82	0.036	0.086
30	1143	50.00	449.3	0.95	0.33	7.46	3.55	0.030	0.078
31	1143	50.00	449.4	0.97	0.55	7.14	3.88	0.022	0.054
32	1143	50.00	449.3	0.97	0.55	7.03	4.24	0.021	0.047
33	1143	50.00	449.4	0.97	0.55	5.49	3.66	0.018	0.047
34			443.0	0.93	0.23	3.89	3.18		
35			443.0	0.93	0.23	5.87	3.54		
36			443.0	0.93	0.23	7.77	3.82		
37			130.0	0.94	0.96	1.41	2.57		
38			130.0	0.94	0.96	1.98	3.10		
39			130.0	0.94	0.96	2.89	3.79		
40			130.0	0.94	0.96	3.99	4.51		
41			130.0	0.94	0.96	4.60	4.60		
42			130.0	0.94	0.96	5.74	4.95		

Appendix B

Matlab data

B.1 Flow charts model procedure

B.1.1 Centrifugal pumps

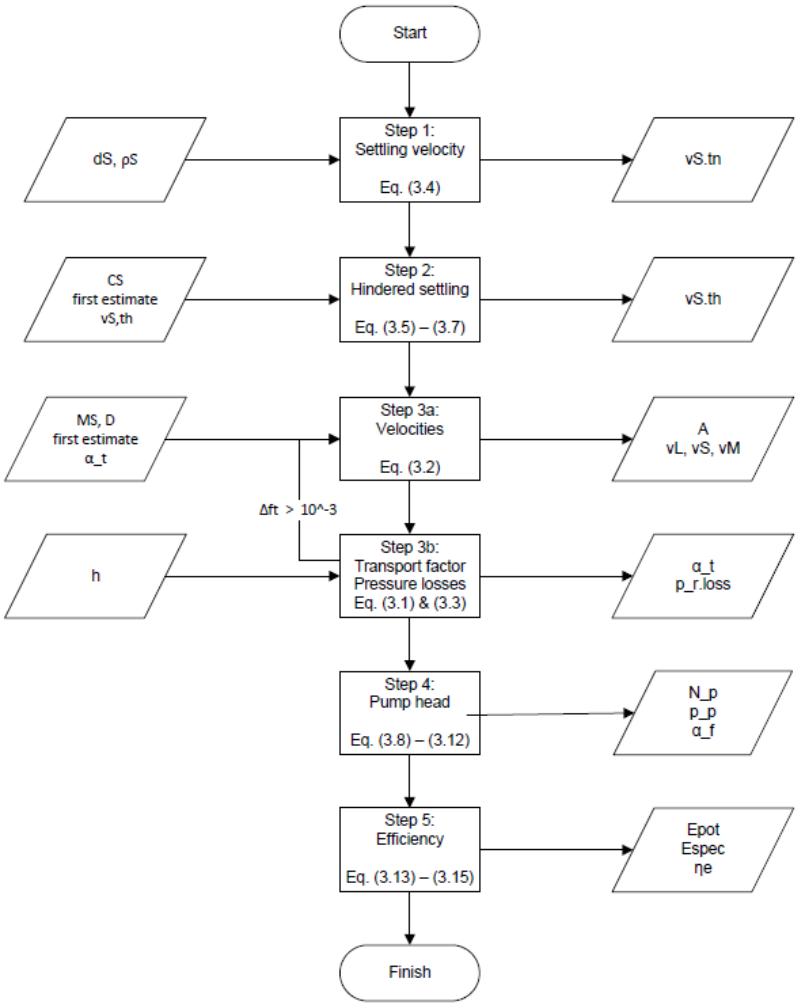

Figure B.1: Flow scheme centrifugal pumps model

B.1.2 Positive displacement pump

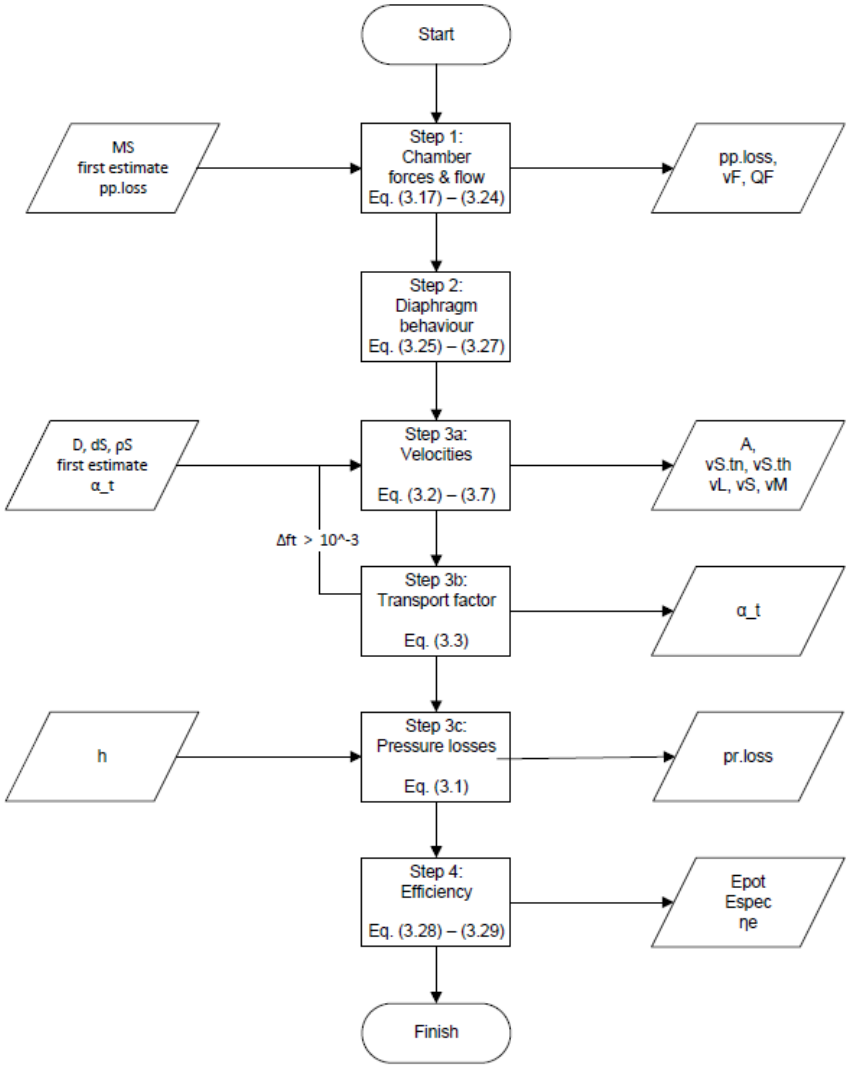

Figure B.2: Flow scheme PD-pump model

B.1.3 Airlift

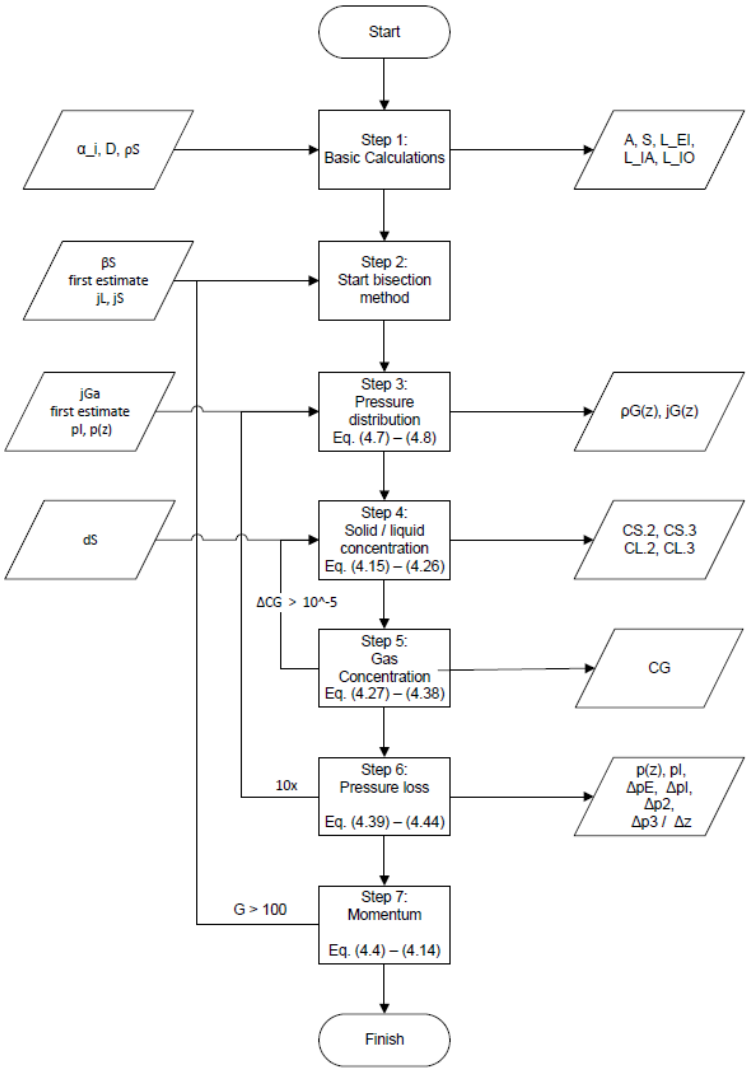

Figure B.3: Flow scheme airlift model

B.2 Matlab scripts

Author's note: Supplied digitally in separate files

Appendix C

Original reports

C.1 Introduction Deep Sea Mining

Author's note: This appendix will not be published, since it contains sensitive data of Van Oord. In case the Appendix is needed for some reason, the reader is advised to contact the author or ir. A. van Es, team-manager Research & Development at Van Oord Dredging and Marine Contractors.

-

C.2 Vertical transport methods

-

C.3 Airlift

-

C.4 Buoyancy induced lift

-